UNIVERSITA' DEGLI STUDI DI VERONA

DEPARTMENT OF

DIAGNOSTICS AND PUBLIC HEALTH

GRADUATE SCHOOL OF

LIFE AND HEALTH SCIENCES

DOCTORAL PROGRAM IN

NEUROSCIENCE, PSYCHOLOGICAL AND PSYCHIATRIC SCIENCES,

AND MOVEMENT SCIENCES

Cycle / year: XXXV/2019

TITLE OF THE DOCTORAL THESIS

BRAIN ORGANOIDS AS INNOVATIVE TOOL FOR REGENERATIVE MEDICINE

S.S.D. BIO/14

Coordinator: Prof. Michela Rimondini

Tutor: Prof. Ilaria Decimo

Co-tutor: Dr. Sissi Dolci

Doctoral Student: Dr. Alessandra Campanelli

Contents

INDEX OF FIGURES

INDEX OF TABLES

ABBREVIATIONS

BDNF	Brain derived neurotrophic factor
CA	Cornu Ammonis
CNS	Central Nervous System
CSF	Cerebrospinal fluid
DCX	Doublecortin
DG	Dentate Gyrus
EC	Entorhinal cortex
ECM	Extracellular Matrix
EGF	Epidermal growth factor
FGF	Fibroblast growth factor
GFAP	Glial Fibrillary Acid protein
GFP	Green fluorescent protein
i.p.	Intraperitoneal injection
KA1	Kainate acid 1
MAP2	Microtubule-associated protein 2
NSCs	Neural stem cells
OB	Olfactory bulb
SE	Status epilepticus
SGZ	Subgranular zone
SOX2	Sex determing region Y-box2
SVZ	Subventricular zone
Syn	Synaptophisin
TLE	Temporal Lobe Epilepsy
TUBB3	Beta3 Tubulin
vCA	ventral Cornu Ammonis
ZBTB20	Zing finger BTB domain containing 20

SOMMARIO

Per anni, studi biochimici e farmaceutici si sono concentrati sulla ricerca di terapie innovative ed efficaci per la cura di patologie che colpiscono il Sistema Nervoso Centrale (SNC). Nonostante numerosi progressi fatti in medicina e in farmacoterapia, il trattamento di tali patologie rimane ancora oggi una sfida aperta. Al giorno d'oggi, i farmaci in uso per la cura delle malattie del SNC sono poco efficaci, sono estremamente costosi e provocano molti effetti collaterali. Recentemente, lo studio di strutture tridimensionali, quali gli organoidi, ha rivoluzionato il campo della biologia dello sviluppo e delle cellule staminali e tali strutture stanno emergendo come l'ultima frontiera nella medicina rigenerativa per il trattamento di patologie associate al SNC, come l'epilessia, la malattia di Alzheimer e del Parkinson. Nello specifico, gli organoidi cerebrali sono strutture tridimensionali che ricapitolano la struttura dell'intero cervello o di regioni specifiche di esso; ad esempio, sono stati generati organoidi del proencefalo dorsale e ventrale, organoidi mesencefalici, organoidi corticali, organoidi talamici, organoidi striatali, organoidi cerebellari e organoidi ippocampali. Grazie alle loro caratteristiche sono presto diventati un eccellente modello per lo studio dello sviluppo cerebrale e di efficaci terapie per il trattamento di malattie neurologiche.

In questo scenario, **l'obiettivo generale della mia tesi di Dottorato è quello di andare a sviluppare organoidi cerebrali ippocampali funzionali che possono essere usati nella medicina rigenerativa per la cura dell'epilessia del lobo temporale.** Specificatamente, in questo lavoro di tesi miro ad **i)** aumentare la maturazione e la funzionalità neuronale negli organoidi murini cerebrali, **ii)** indurre una specifica identità regionale in senso ippocampale degli organoidi murini cerebrali e **iii)** utilizzare l'organoide cerebrale come una nuova strategia terapeutica per il trattamento dell'epilessia del lobo temporale.

Per il ***primo obiettivo*** della mia tesi di Dottorato, **abbiamo generato organoidi cerebrali** in accordo con il protocollo messo a punto nel nostro laboratorio (Ciarpella et al., 2021), usando come fonte primaria cellule neuronali staminali isolate da embrioni murini di età embrionale 14.5 e **abbiamo investigato gli effetti di i) una matrice extracellulare di derivazione vegetale, l'alginato e di ii) una selezione di molecole bioenergetiche,**

definite α5, sul differenziamento, sulla maturazione e sulla funzionalità di tali organoidi.

i) Un aspetto chiave per l'organizzazione spaziale degli organoidi è la presenza di una matrice extracellulare in grado di dare supporto strutturale e biochimico alle cellule. Tra le matrici extracellulari commercialmente disponibili, l'alginato è un polisaccaride di origine algale altamente biocompatibile e poco immunogenico in grado di supportare la maturazione funzionale dei neuroni primari e sostenere il differenziamento di cellule staminali di roditori in molte linee cellulari. I nostri risultati hanno mostrato che l'utilizzo dell'alginato come matrice extracellulare per l'organoide cerebrale promuove una riduzione della morte cellulare, fornendo così un supporto trofico all'organoide, e induce una maturazione neuronale andando ad aumentare significativamente la densità sinaptica, specialmente la componente eccitatoria.

ii) In linea con quanto riportato in letteratura, il metabolismo cellulare potrebbe rappresentare un target attrattivo per ristabilire le funzioni delle cellule neurali ed eventualmente per curare condizioni patologiche. Specificatamente, studi hanno dimostrato che il supplemento di amminoacidi a catena ramificata e di precursori del ciclo di Krebs, nel complesso definiti α5, nel terreno di coltura cellulare di cellule neuronali staminali, determina un cambiamento metabolico verso un'ossidazione fosforilativa, aumentando così l'energia metabolica e promuovendo il differenziamento e la maturazione neuronale (Bifari et al., 2020). In linea con tali dati, i nostri risultati hanno mostrato che il supplemento degli α5 nel terreno di coltura degli organoidi cerebrali induce un aumento del differenziamento, della maturazione e della funzionalità di tali organoidi. Inoltre, l'utilizzo degli α5 promuove un aumento della densità sinaptica e delle oscillazioni di flusso di calcio negli organoidi cerebrali maturi.

Il *secondo obiettivo* della mia tesi di Dottorato **è stato quello di indurre una specifica identità regionale in senso ippocampale degli organoidi cerebrali**. Nonostante i meccanismi alla base della crescita e dello sviluppo dell'ippocampo non sono del tutto chiari, è stato visto che il segnale di WNT3a, un fattore che regola lo sviluppo embrionale dell'ippocampo, gioca un ruolo chiave in tali processi. L'ippocampo è una delle regioni cerebrali altamente coinvolta nella progressione di molte malattie neurodegenerative quali l'epilessia e la malattia di Alzheimer. Pertanto, una struttura tridimensionale *in vitro*

capace di replicare il tessuto ippocampale può essere estremamente utile per studi farmacologici e per il rimodellamento di tali malattie.

Il supplemento del fattore WNT3a nel terreno di coltura degli organoidi cerebrali ci ha permesso di generare organoidi con una specifica identità regionale in senso ippocampale, specificatamente nella regione del Cornu Ammonis (CA) 3 dell'ippocampo. Infatti, i nostri risultati hanno mostrato che il supplemento di WNT3a nel terreno di coltura degli organoidi cerebrali, ha un effetto sull'intero trascrittoma degli organoidi cerebrali andando ad aumentare l'espressione di geni relativi all'ippocampo. Notevolmente, il supplemento di WNT3a promuove un aumento dell'espressione dei marcatori caratteristici della regione ippocampale del CA3 e delle oscillazioni di flusso di calcio in organoidi cerebrali maturi.

Il *terzo obiettivo* della mia tesi di Dottorato è stato quello di utilizzare l'organoide cerebrale come una nuova strategia terapeutica per il trattamento dell'epilessia. L'epilessia del lobo temporale è una delle più comuni epilessie focali caratterizzata da diversi sintomi che colpiscono principalmente l'ippocampo. Le convulsioni che si manifestano durante l'epilessia sono spesso resistenti ai farmaci antiepilettici. La resezione chirurgica del tessuto epilettogeno potrebbe rappresentare un'alternativa, ma è altamente costosa e richiede molto tempo. Pertanto, una strategia da poter esplorare per il trattamento dell'epilessia del lobo temporale è l'utilizzo di tessuti cerebrali bioingegnerizzati (organoidi cerebrali) in combinazione con microelettronica neuromorfica e intelligenza artificiale per promuovere un processo di autoriparazione dei circuiti cerebrali non funzionanti.

Come punto di partenza per l'applicazione dell'organoide nel trattamento delle malattie del SNC, abbiamo valutato gli effetti del trapianto di cellule neuronali staminali risospese o no in una soluzione di alginato, nella zona ventrale del CA3 in un modello animale di epilessia del lobo temporale. **In questo lavoro siamo stati in grado di settare un protocollo standardizzato di trapianto di cellule neuronali staminali. I nostri risultati hanno mostrato che, 9 settimane dopo il trapianto, le cellule trapiantate sono localizzate correttamente nella zona ventrale del CA3.** Inoltre, le cellule trapiantate mostrano un fenotipo caratterizzato principalmente dall'espressione di marcatori di staminalità in entrambe le condizioni valutate (con o senza l'alginato).

Nel complesso, questi risultati forniscono un'evidente prova dell'efficacia dei differenti trattamenti utilizzati (alginato, a5, WNT3a) nel migliorare *in vitro* il differenziamento, la maturazione e la funzionalità neuronale e la specificità regionale in senso ippocampale degli organoidi cerebrali. Queste evidenze mettono in risalto la possibilità di utilizzare gli organoidi cerebrali come una nuova strategia terapeutica nella medicina rigenerativa e apre le strade per lo studio di approcci combinati utili per sviluppare terapie efficaci basate sul trapianto di organoidi cerebrali per le malattie del SNC come l'epilessia.

ABSTRACT

For decades, biochemical and pharmaceutical researchers have worked to develop innovative and effective therapies for the cure of Central Nervous System (CNS) pathologies. Despite enormous progress in medicine and pharmacotherapy, handling CNS disorders is still challenging. To date, most of these diseases lack of effective cure, prescribed drugs are extremely expensive and induce troublesome side effects. Recently, the introduction of the tridimensional (3D) organoids technology is revolutionizing the fields of developmental and stem cell biology and it is emerging as the latest frontier in regenerative medicine for the treatment of neurodegenerative disorders, such as epilepsy, Alzheimer's disease and Parkinson's disease. Specifically, brain organoids are 3D structures which mimics the brain identity (e.g., whole-brain organoids), or specific brain regions (e.g., dorsal and ventral forebrain organoids, midbrain organoids, cortical organoids, thalamic organoids, striatal organoids, cerebellar organoids, hippocampal organoids). Therefore, they become an excellent model to study the brain development and to modeling neurological disorder conditions.

In this scenario, **the overall objective of my PhD thesis was to set the stage to develop functional hippocampal brain organoids that can be used for regenerative medicine to cure the Temporal Lobe epilepsy (TLE).** Specifically, I aimed to **i)** increase neuronal maturation and functionality in mouse brain organoids, **ii)** induce hippocampal brain region specific commitment of mouse brain organoids and to **iii)** apply the organoid technology as new therapeutic strategy for the treatment of TLE.

For ***the first aim*** of my PhD thesis project we generated mouse brain organoids according to our previously in-house established three-phase protocol using mouse NSCs (mNSCs), isolated from E14.5 embryos as primary cell source (Ciarpella et al., 2021) and **we investigated the effects of i) a vegetal-derived extracellular matrix alginate and of ii) a selection of bioenergetic molecules, called α5, on brain organoid differentiation, maturation and functionality.**

i) A key aspect for organoid 3D spatial organization is the presence of an extracellular matrix (ECM) which provides structural and biochemical support to the cells. Among the

commercially available ECMs, alginate is a highly bio-compatible and low immunogenic algal polysaccharide able to support functional maturation of primary neurons and to sustain multi-lineage differentiation of rodent NSCs. Our results showed that alginate scaffold decreased cell death thus giving trophic support to the organoid and promoted neuronal maturation by significantly increasing excitatory synaptic density.

ii) Accordingly with the literature, cell metabolism could be an attractive target to restore neural cell function and eventually heal pathological conditions. Specifically, the branched-chain amino acids and precursors of the tricarboxylic acid (TCA) cycle, referred to as α5, supplemented to the NSCs culture media showed to drive a metabolic shift towards oxidative phosphorylation and thus to enhance the energy metabolism and promote the neuronal differentiation and maturation (Bifari et al., 2020). In line with these data, the administration of α5 to brain organoids allowed us to promote differentiation, maturation and functionality of brain organoids. Specifically, our results showed that α5 supplementation at later stages of maturation significantly increased the amount of immature and mature neurons compared to control organoids. Moreover, the α5 supplementation promoted an increase of the synaptic density and of the calcium flux oscillations in mature brain organoids compared to control organoids.

The *second aim* of my PhD thesis **was to induce hippocampal lineage commitment of mouse brain organoids.** Although the mechanisms of hippocampal patterning and growth remain unclear, it was shown that a key role in these processes was played by the WNT3a signaling pathway which locally regulates the expansion of the caudomedial cortex from which the hippocampus develop. The hippocampus is one of the brain regions mainly affected in the pathological progression of many SNC disorders including epilepsy and Alzheimer's disease; therefore an *in vitro* 3D structure able to replicate the hippocampal tissue can be extremely useful for drug testing and neurodegenerative disease modeling.

The supplementation of WNT3a factor in brain organoid culture media allowed us to generate brain organoids with specific hippocampal region identity, specifically the CA3 field of the hippocampus. Indeed, our results showed that WNT3a supplementation in the brain organoid culture media affected the whole transcriptomic of brain organoid increasing the expression of genes related to the hippocampal patterning.

Notably, the WNT3a supplementation promoted a higher expression of markers specifically related to the Cornu Ammonis (CA) 3 hippocampal region and an increase of the calcium flux oscillations in mature brain organoids compared to control.

The *third aim* of my PhD thesis **was to apply the organoid technology as new therapeutic strategy for the treatment of epilepsy.** Temporal Lobe Epilepsy (TLE) is the most common focal epilepsy characterized by several symptoms which affect mainly the hippocampus. Seizures in TLE are often resistant to anti-epileptic drugs. Surgical resection of the epileptogenic tissue is thus offered as an alternative, but it is costly and at times impracticable. An exploitable strategy to treat TLE is the pursuing self-repair process of dysfunctional brain circuits with the use of bioengineered brain tissue (brain organoids), neuromorphic microelectronics, and artificial intelligence (AI).
As starting point of the application of the organoid technology in the treatment of CNS disorders, we evaluated the effects of the transplantation of rat hippocampal–derived NSCs, with or without being resuspended in an alginate solution, in the ventral (v) CA3 in a TLE rat model. **We were able to set up a standardized protocol for NSCs transplantation. Results showed that after 9 weeks from the transplantation, grafted NSCs were present and correctly localized in the vCA3.** Transplanted NSCs displayed a phenotype characterized by the expression of stemness markers in both the conditions evaluated (with/without alginate).

Overall, these results provide a proof-of concept of the efficacy of the different treatments (alginate, a5, WNT3a) to improve *in vitro* the neuronal differentiation, maturation and functionality, and the hippocampal specification of brain organoids. These findings highlight the possibility to use the brain organoid technology as a novel tool for regenerative medicine and pave the way to explore combinatorial approaches, useful to develop an effective organoid transplantation therapy for CNS disorder, such as epilepsy.

1. INTRODUCTION

1.1 The Central Nervous System

The Central Nervous System (CNS) is a bilateral and symmetric structure part of the Nervous System consisting of two major structures: the *Brain* and the *Spinal Cord*. The brain is encased in the skull and protected by the cranium, the spinal cord is continuous with the brain and lies caudally to it. The CNS is so named due to its role to combine and integrate the information deriving from the entire body, coordinating, and influencing the activity of all parts of the organism.

The brain and the spinal cord are both enclosed by the *Meninges*, a connective tissue that surrounds, protects, and penetrates the CNS (Ghannam & Al Kharazi, 2022). They form a complex microenvironment endowed with soluble trophic factors, extracellular matrix and cells, all playing fundamental roles in both skull and brain development (Bjornsson, Apostolopoulou, Tian, & Temple, 2015; Richtsmeier & Flaherty, 2013). Meninges are formed by three tissue membranes that are primarily known as wrappers of the brain. The *dura mater* or pachymeninx (pachy-thick) is the outer membrane, it is composed of dense connective tissue and forms a sac that envelops the other meningeal layers. It surrounds and supports the dural venous sinuses and it reflects in three infoldings: the first separating the two hemispheres of the cortex (falx cerebri), the second between the cerebellum and the occipital lobe (tentorium cerebelli and falx cerebelli) and the third covering the pituitary gland and the sella turcica. The inner membranes, known as leptomeninges (lepto -, thin), are formed by two layers: the outer, named *arachnoid* (arachn -, spider) and the inner, *pia mater* (pia -, tender). The *arachnoid* is linked to the *pia mater* by arachnoid trabeculae that span the subarachnoid space filled with cerebrospinal fluid (CSF) that is produced by the choroid plexus. This fluid is distributed to the entire CNS thanks to the ciliated ependymal cells of the ventricles, the pressure gradient, and the presence of one-way valves (the arachnoid villi) (Barshes, Demopoulos, & Engelhard, 2005) **(Figure 1)**. These meningeal layers originate from the mesenchymal cells around the neural tube. In the early embryo, both mesenchymal and neural crest-derived cells are involved in the formation of the primary meninx that will differentiate during development by forming two different layers: the *dura mater* and the leptomeninges respectively (O'Rahilly & Muller, 1986). Embryologic differences exist

between the meninges of the brain and the spinal cord. Encephalic meninges originate from both the mesenchymal cells and the encephalic neural crest, while the meninges of the spine and the caudal regions of the head originate from the paraxial mesenchyme (Etchevers, Couly, Vincent, & Le Douarin, 1999; O'Rahilly & Muller, 1986).

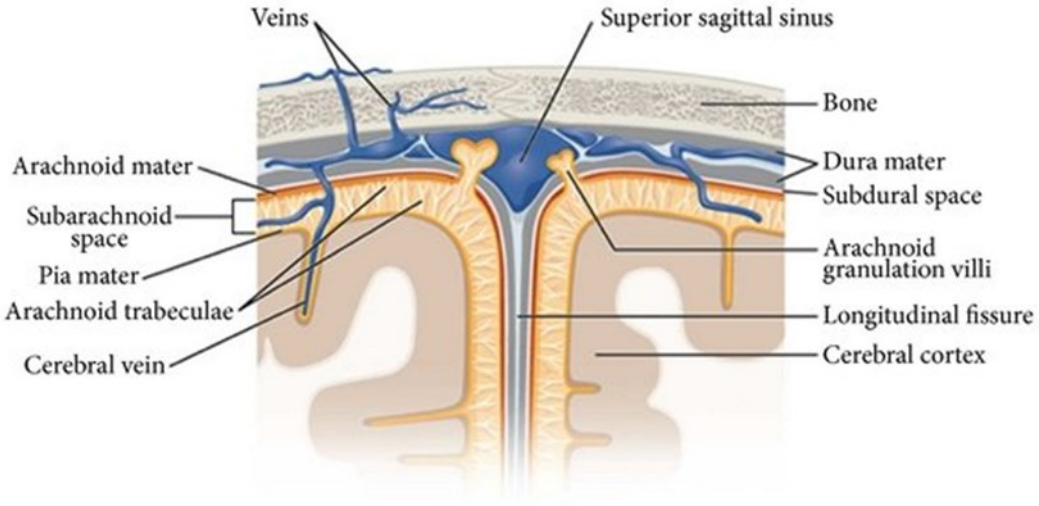

Figure 1: Schematic drawing of the meningeal structure. *The meninges are composed of three layers: the dura mater, the arachnoid mater and the pia mater. The space between the arachnoid and pia mater, known as the subarachnoid space (SAS), is filled with cerebrospinal fluid (CSF). Adapted from (Saboori & Sadegh, 2015).*

1.1.1 Brain Anatomy

The brain is part of the CNS and is responsible for responses, sensations, movement, emotions, communication, thought processing, and memory. Protection for the human brain comes from the skull, meninges, and cerebrospinal fluid. The brain consists of three main structural divisions: **i)** the cerebrum or forebrain, **ii)** the brainstem or middle of brain and **iii)** the cerebellum or hindbrain **(Figure 2)**.

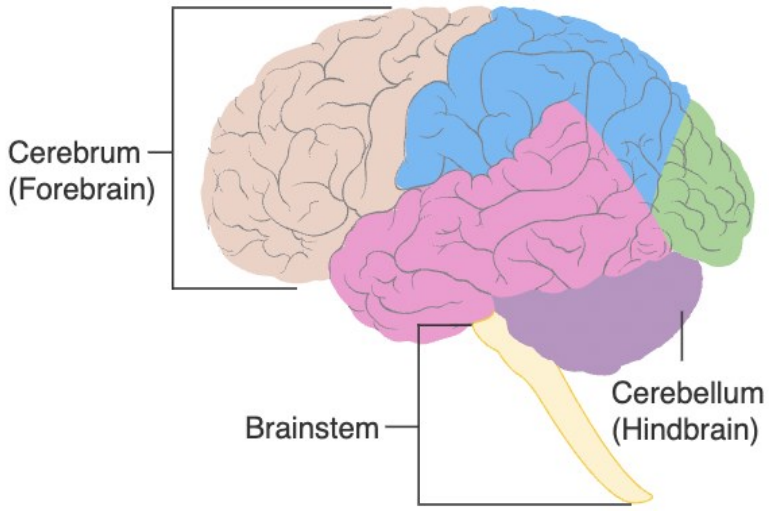

Figure 2: Brain gross anatomy. *The brain is composed of three main structures: the cerebrum, the cerebellum and the brainstem. Copyright © The McGraw-Hill Companies, Inc.*

i) The *cerebrum (forebrain):* is the largest part of the brain derived from the prosencephalon in the developing brain and contains the large outermost layer of the brain, the wrinkly *cerebral cortex*, which is composed of depressions or grooves (sulci) and ridges or raised areas (gyri), that increase the surface area of the cerebrum without an increase in the size of the brain. Gray matter, approximately 2 to 4 mm thick, forms the outer surface of the cerebrum, which processes and integrates information from white matter fiber tracts, that form the inner surface of the cerebrum (Jernigan & Stiles, 2017). The cerebral cortex consists of two cerebral hemispheres, the right and the left, which are connected by a fibrous bridge called the corpus callosum; each hemisphere controls the contralateral side of the body i.e., the left hemisphere of the cerebrum receives information from the right side of the body resulting in motor control of the right side of the body and vice versa. They have different roles: the left hemisphere is involved in language, logic, and math abilities, while the right one is more creative, being dominant in artistic and musical situations, and intuition. Each hemisphere is divided into four lobes: 1) frontal lobe, 2) parietal lobe, 3) temporal lobe and 4) occipital lobe **(Figure 3)**.

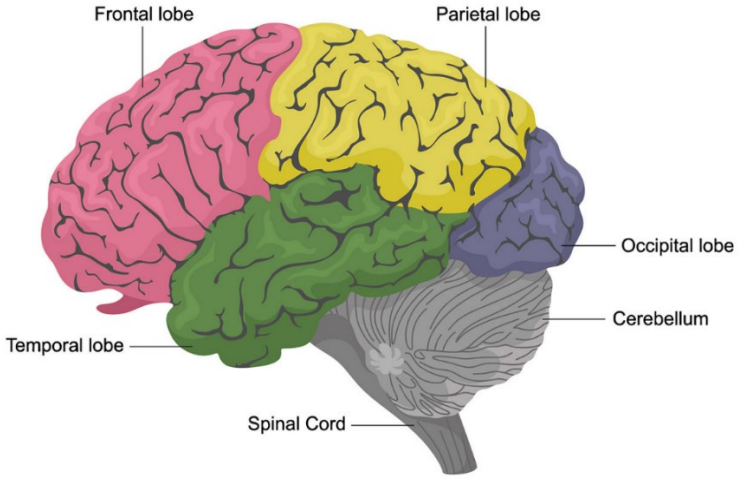

Figure 3: Representation of the four lobes of the brain hemispheres. *Each hemisphere of the cerebral cortex consists of four lobes: frontal lobe, temporal lobe, parietal lobe and occipital lobe. Copyright © The McGraw-Hill Companies, Inc.*

1) The *frontal lobe* is the largest lobe of the brain located in the front of the head and is involved in personality characteristics, emotional regulation, decision-making and movement. Recognition of smell usually involves parts of the frontal lobe. Moreover, the frontal lobe contains Broca's area, which is associated with speech ability.

2) The *parietal lobe* is the middle part of the brain which allows the identification of objects and the understanding of spatial relationships. Areas in the parietal lobe are also responsible for integrating sensory information, including touch, temperature, pressure and pain. This lobe houses Wernicke's area, which helps in understanding spoken language.

3) The *temporal lobe* contains regions dedicated to processing sensory information, particularly important for hearing, recognizing language, and forming memories. Indeed, this lobe contains the primary auditory cortex which receives auditory information from the ears and secondary areas, and processes the information, so we understand what we're hearing. The medial temporal lobe contains the hippocampus, a region important for memory, learning and emotions.

4) The *occipital lob*e is the major visual processing centre in the brain. The primary visual cortex, also known as V1, receives visual information from the eyes. This

information is relayed to several secondary visual processing areas, which interpret depth, distance, location and the identity of seen objects **(Figure 4)**.

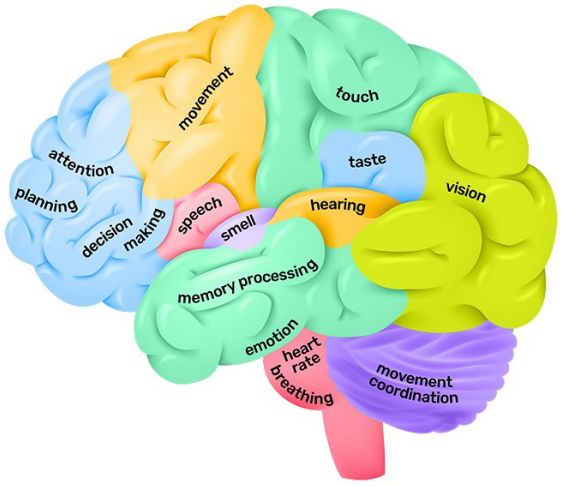

Figure 4: Representation of lobes functions. *Each lobe of the two hemispheres controls specific functions of the brain. Copyright © The McGraw-Hill Companies, Inc.*

ii) The *brainstem (middle of brain):* is the most inferior and primitive part of the brain, derived from the mesencephalon in the developing brain. It is a vital connection point between the forebrain and the hindbrain and includes the midbrain (or mesencephalon), the pons (or metencephalon) and the medulla oblongata (or myelencephalon) (Benghanem et al., 2020; Sciacca, Lynch, Davagnanam, & Barker, 2019) **(Figure 5)**.

- The *midbrain* is the most rostral and shorter part of the brainstem, which connects the brain with the spinal cord. It consists of two major parts: the cerebral peduncles and tectum. The cerebral peduncles consist of the crura cerebri and tegmentum. They are separated from each other by a darkened stripe called the substantia nigra, a large gray matter structure involved in dopamine production, a neurotransmitter crucial for motor and movement control. The dorsal part of the tegmentum is traversed by the cerebral aqueduct, which connects the third and fourth ventricles of the brain. The tectum lies dorsal to the tegmentum and cerebral aqueduct and contains two pairs of bulging, layered bundles of neurons called the superior colliculi, involved in processing of

visual signals, and inferior colliculi, which participate in processing of auditory signals.

- The *pons* connects the brain to the cerebellum and can be divided into a ventral part and a dorsal tegmentum (Hirsch et al., 1989). The ventral part contains longitudinal fibers primarily from the corticospinal, corticobulbar, and corticopontine tracts. The dorsal tegmentum is composed of four cranial nerves: the abducens nerve helps to coordinate eye movement; the facial nerve coordinates movement and sensation in the face; the vestibulocochlear nerve processes sound and helps in maintaining balance; and the trigeminal nerve coordinates chewing and carries sensory information from the face and the head.
- The *medulla oblongata* is at the bottom of the brainstem, where the spinal cord meets the foramen magnum of the skull. It is responsible for autonomic functions, some of which are crucial for survival: it regulates many bodily activities, including heart rhythm, breathing, blood flow, and oxygen and carbon dioxide levels.

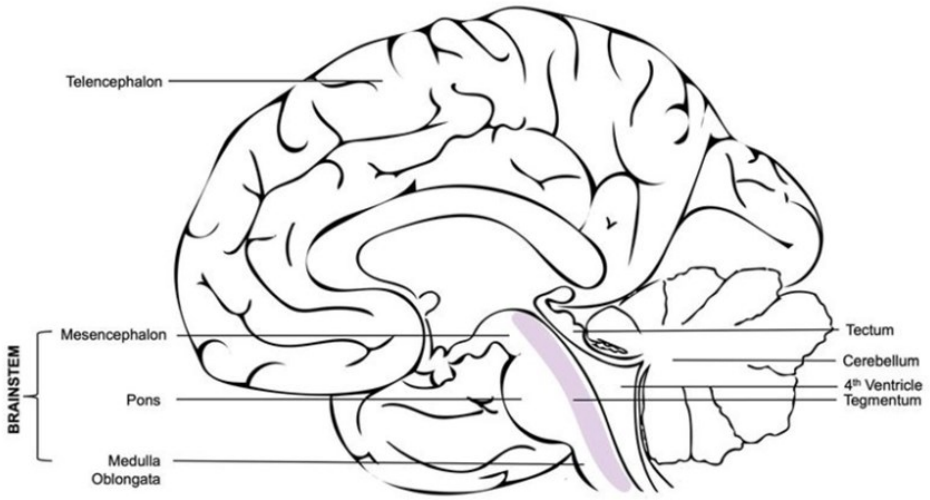

Figure 5: Brainstem anatomy. *The midbrain (or mesencephalon), the pons and the medulla oblongata are the three fundamental structures composing the brainstem. Copyright © The McGraw-Hill Companies, Inc.*

iii) *The cerebellum (hindbrain):* also known as the "little brain", is the portion of the brain located at the back of the head, below the temporal and occipital lobes, deriving from the rhombencephalon in the developing brain. Just like the cortex, it has two hemispheres with a dense layer of the gray matter surrounding an inner region of white

matter. The cerebellum contains Purkinje cells and cerebellar peduncles which play an important role in the communication with the other parts of the brain. Indeed, the superior cerebellar peduncle is composed of white matter that connects the cerebellum to the midbrain, allowing coordination in the arms and legs. The inferior cerebellar peduncle connects the medulla and cerebellum using proprioceptors to maintain balance and posture. Lastly, the middle cerebellar peduncle allows the communication of voluntary motor actions from the pons to the cerebellum. Moreover, the cerebellum is in constant communication with the cerebral cortex, taking higher-level instructions about the brain's intentions, processing them through the cerebellar cortex and then sending messages to the cerebral motor cortex to make voluntary muscle contractions (Beckinghausen & Sillitoe, 2019) **(Figure 6)**.

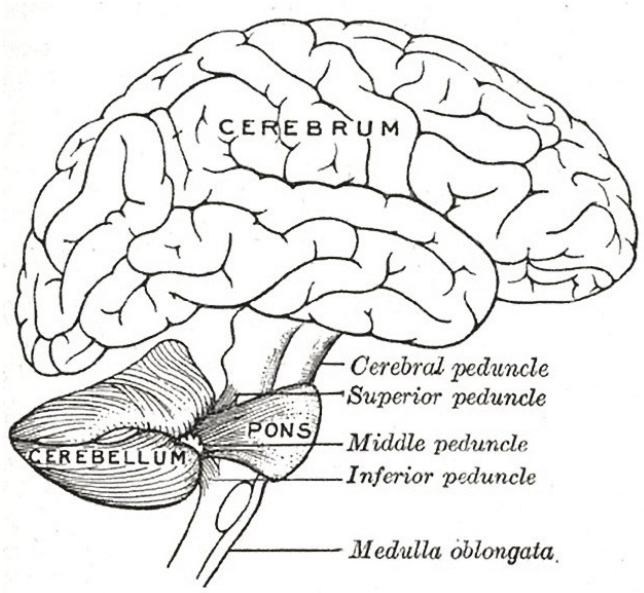

Figure 6: Representation of the cerebellum. *The cerebellum is located at the lower back part of the brain and is responsible for maintaining balance, coordinating movements and motor learning. Adapted from https://radiopaedia.org/articles/superior-cerebellar-artery.*

1.1.1.1 The Hippocampus

The Hippocampus is part of the limbic system and is one of the most studied formations in the brain for many reasons: its role in long-term memory and spatial navigation, its involvement in a wide spectrum of pathological conditions, like epilepsy and Alzheimer's

disease, and because it has the most protracted span of neurogenesis, compared to other brain structures. This structure is located under the cerebral cortex, in the medial temporal lobe; the elongated hippocampal structures lie along the longitudinal axis of the brain and form the medial walls of the inferior horns of the lateral ventricles. The hippocampus as a whole has the shape of a curved tube and has been compared to a seahorse (hence the name), a ram's horn or a banana. Like the cerebral cortex, to which it is closely associated, it's a paired structure, with mirror-image halves in the left and right sides of the brain. In rodents, the hippocampus is a relatively large, cashew-shaped structure lying just beneath the neocortex.

A distinction needs to be made between different terms, when talking about the hippocampus: (i) hippocampal region, (ii) hippocampal formation and (iii) hippocampal complex. In the mammalian brain the *hippocampal region* is the central component of the limbic system, which also includes the amygdala, the septum and some other structures (Hamilton, 1976; Maclean, 1952) and it is divided into two major cortical structures: the hippocampal formation and the parahippocampal formation. The *hippocampal formation* is referred to as the classically known "hippocampus" and consists of three regions: i) the hippocampus proper, also known as Ammon's horn or Cornu Ammonis – CA, ii) the dentate gyrus (DG) and iii) the subiculum. The *parahippocampal formation* instead comprehends areas that surround the ventral and caudal portions of the hippocampal formation, including the presubiculum, the parasubiculum and the entorhinal, perirhinal and postrhinal cortices (EC), all of which possess more than three lamina layers and reciprocally connects with the hippocampus (Blackstad, 1956; Lorente De Nó, 1934). The hippocampal complex includes the hippocampus proper and the dentate gyrus.

As mentioned above, the hippocampal formation is divided into two major U-shaped interlocking regions: the dentate gyrus and the Cornu Ammonis. The DG is composed by an internal and an external blade; the CA was initially divided, based on differences in cell morphology, in regio superior, which merges with the subiculum, and regio inferior, that is close to the DG. The CA has been divided into seven layers, starting from the ventricular surface: (1) *the alveus*, containing the efferent fibers from the axons of the pyramidal cells; (2) the stratum oriens, situated between the alveus and the pyramidal cell bodies, that contains the axon and basal dendrites of the pyramidal cells, some basket cells and few inhibitory basket-cell interneurons; (3) *the stratum pyramidalis* which forms

the principal cellular component of Cornu Ammonis and consists of 10–30 layers of excitatory pyramidal cells; (4) the *stratum radiatum* which comprises apical dendrites of the pyramidal cells and some stellate cell and (5) the *stratum lacunosum/moleculare* that represents the proximal and distal segments of the apical dendrites, respectively and contains also inhibitory interneurons that project into the retrosplenial cortex. In the CA3 is possible to recognize an additional layer, the stratum lucidum, interposed between the pyramidal cell bodies and the stratum radiatum, which receives the mossy fiber input from the dentate granule cells (Itopa, 2020; G. Li & Pleasure, 2014). Based on cell types and laminar organization, in 1934 Lorente de Nó divided the Cornu Ammonis into four fields: CA1, CA2, CA3 and CA4. He called the regio superior CA1 and the regio inferior CA3, with a small transitional field called CA2; CA4 designated the cells scattered inside the space between CA3 and DG, also called the hilus. Except for CA4, the basic pattern in all areas of the hippocampus is the same: an ordered and a tightly packed sheet of large neurons, whose cell bodies are all in one layer and whose dendrites runoff in the same direction. The CA1 field corresponds to the largest part of the regio superior and is delimited laterally by the presubiculum and medially by CA2. Most neurons (90%) of CA1 are medium-sized pyramidal cells (glutamatergic projection neurons), whose main apical dendrite only has small side branches and does not divide for several hundred microns, and the rest (10%) are interneurons. The CA3 layer is directed towards the hilus of the dentate gyrus and is limited medially by the CA2 layer. It contains the giant pyramidal cells whose apical dendrites bifurcate shortly after leaving the soma; the part of the dendrite close to the cell body has thorn-like spines and receives contacts from the mossy fibers of the granular cells of the dentate gyrus. Axons of the CA3 pyramidal cells contribute to the alveus, fimbria, and fornix. The CA2 layer is present towards the dentate gyrus bounded laterally by the CA1 and medially by the CA3 layer and consists of CA3-type pyramids which receive input from the supramammillary region of the hypothalamus but lack input mossy fibers (MF) from the dentate gyrus (Chauhan, Jethwa, Rathawa, Chauhan, & Mehra, 2021). The dentate gyrus is a narrow crenated strip of gray matter and contains architectural fascia dentata that consists of three layers: (i) the *granule layer* containing the densely packed cell bodies of granule cells; (ii) the *molecular layer* formed by the apical dendrites of the granule cells intertwining with each other and with their afferents; (iii) the *polymorphic layer*, which merges with CA4, and contains the basket

cells, some pyramidal cells and the axons of the granule cells, which form the mossy fibers. **(Figure 7)**.

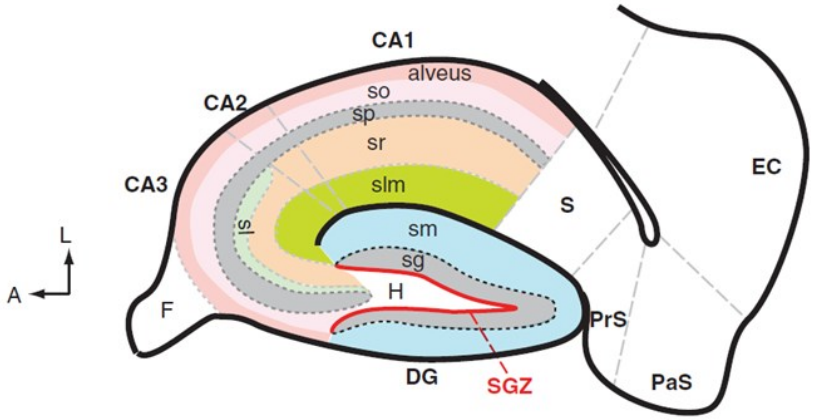

Figure 7: Schematic representation of the layer organization in the hippocampus. *A, anterior; L, lateral; CA, the abbreviation of cornu ammonis; DG, dentate gyrus; EC, entorhinal cortex; F, fimbria; H, hilus; PrS, presubiculum; PaS, parasubiculum; S, subiculum; Alveus is the deepest layer that contains the axons from the pyramidal neurons; SO, stratum oriens, which mostly contains the inhibitory local interneurons; SP, stratum pyramidale, is the principal layer of the hippocampus proper; SR, stratum radiatum of CA3 and CA1, which contains self-associated fibers from the stratum pyramidale of CA3 and Schaffer collateral fibers projected from CA3, respectively; SLM, stratum lacunosum-moleculare, which contains the perforant path fibers projected from the entorhinal cortex; SL, stratum lucidum, which is occupied by mossy fibers projecting from the dentate granule cells; SM, stratum moleculare or molecular layer; SG, stratum granulosum or granular cell layer. Adapted from (G. Li & Pleasure, 2014).*

The hippocampus is characterized by a highly complicated internal unidirectional synaptic circuit able to link all the hippocampal regions, known as "the trisynaptic loop" **(Figure 8)**. The entorhinal cortex provides the major cortical input to the hippocampus, with its strongest excitatory projections via the perforant path to the dentate gyrus region (Synapse 1). Neurons of the DG project to the hilus of the CA3 field via the mossy fiber pathway (Synapse 2). The CA3 pyramidal cells in turn project to the CA1 region via the Schaffer Collateral pathway (Synapse 3). Finally, the CA1 projects to the subiculum, which sends projections back to the entorhinal cortex, completing the loop. An important addition to the classic trisynaptic circuitry is that CA3 axons, in addition to their projections to CA1, send collaterals that make synapses onto other CA3 neurons. This

recurrent collateral pathway inspired several influential theories of CA3 as an auto-associative memory system, displaying attractor dynamics that are critical for supporting a distributed memory (Itopa, 2020; Knierim, 2015)

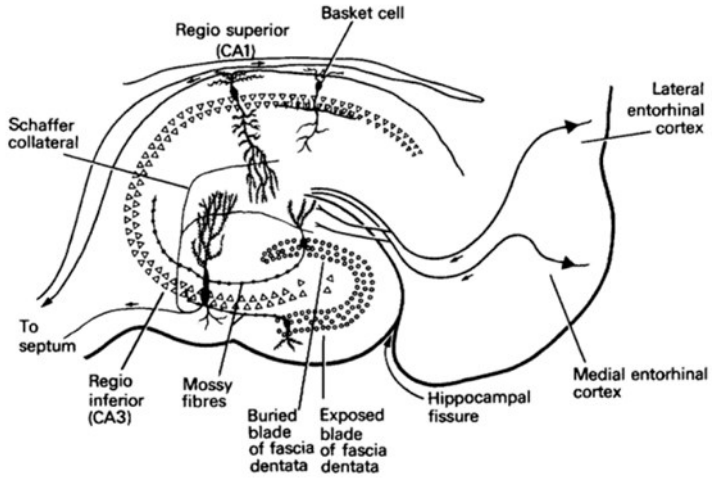

Figure 8: Schematic representation of the mouse hippocampal regions and the unique unidirectional intrinsic circuit of the hippocampus. *The hippocampus is characterized by a complicated system of afferent, efferent and intrinsic connections, known as the trisynaptic circuitry. Adapted from (John O'Keefe & Nadel, 1979).*

1.1.1.1.1 Hippocampal Development

Hippocampal development in mouse starts from embryonic day 8.5 (E8.5), when the dorso-medial region of the telencephalon invaginates to form the telencephalic vesicles. Medio-lateral and rostro-caudal boundaries of the developing medial telencephalon are formed by a cross regulation of factors that result in the precise definition of the *cortical hem* and *choroid plexus*, two important structures in the resulting medial wall (Khalaf-Nazzal & Francis, 2013). Specific non-overlapping molecular marker signatures accompany boundary definitions in the developing medial telencephalon. These markers assign distinct identities, for both the cortical hem and the choroid plexus **(Figure 9**).

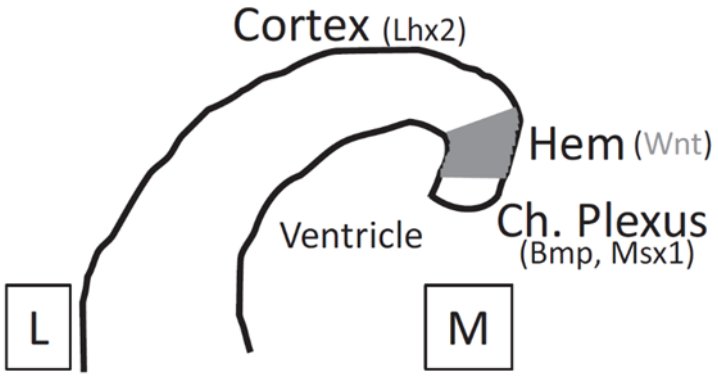

Figure 9: Schematic representation of the cortical hem and the choroid plexus structures. *The image shows the position of the hem (expressing Wnt molecules) with respect to the cortex (expressing Lhx2) and the choroid (Ch) plexus (expressing Bmps and Msx1). Adapted from (Khalaf-Nazzal & Francis, 2013).*

The Cortical hem, residing in the medial edge of the telencephalon, adjacent to the presumptive cortex (where the future hippocampus will arise), plays a fundamental role as signalling centre in the hippocampal development initiation as well as helping the hippocampal establishment in its medial position (Subramanian & Tole, 2009). The cortical hem is characterized by Wnt3a expression at E9.5 before invagination of the dorsal midline region. Later on, Wnt5a and Wnt2b expression defines the cortical hem, and these molecules contribute to the instruction of hippocampal development (Grove, Tole, Limon, Yip, & Ragsdale, 1998). Wnts are secreted glycoproteins that have been identified as key regulators of regional identity in the early developing brain. By E11.5, the homeobox Msx1 is strongly expressed in the choroid plexus; the strong expression of Bmps 4 and 7, further confirms the identity of this structure (Bulchand, Grove, Porter, & Tole, 2001). An instrumental role of the cortical hem was suggested by experiments showing that the hippocampus was largely missing when the hem was deleted, or when the hem-specific expression of Wnts molecules, Wnt3a in particular, was disrupted (Caronia-Brown, Yoshida, Gulden, Assimacopoulos, & Grove, 2014; Lee, Tole, Grove, & McMahon, 2000). Definitive evidence concerning the hem came from chimeras in which the cortical committer LIM homebox 2 (Lhx2) gene was deleted: this gene is responsible for the specification of cortical identity and when it is null cells adopted

cortical hem identity, which could induce and organize ectopic hippocampal fields (Mangale et al., 2008).

The three major fields of the hippocampus, the CA1, CA2, CA3 and the DG, are each defined by distinct morphologies, cell types, physiological properties, and connectivity (Khalaf-Nazzal & Francis, 2013). A panel of specific CA1, CA2 and CA3 pyramidal cell markers has been identified which distinguish between the cell classed and label almost all cells in a category (Datson et al., 2004; Tole, Christian, & Grove, 1997). Specifically, in early molecular studies, two robust field-defining markers, acting from embryonic to adult stages, were identified: KA1, a glutamate receptor subunit, and SCIP, a PUO-domain gene, expressed in the pyramidal neurons of CA3 and CA1 respectively (He et al. 1989). The expression of KA1 is weakly detectable around E14.5, while SCIP is expressed at E15.5 in CA3 of the mouse; these markers have been shown to appear at the poles of the hippocampus (dentate and subicular) until to get contact and fuse, only at birth, in the CA2 region, in a "pole-inward" fashion precisely (Tole et al., 1997) **(Figure 10)**.

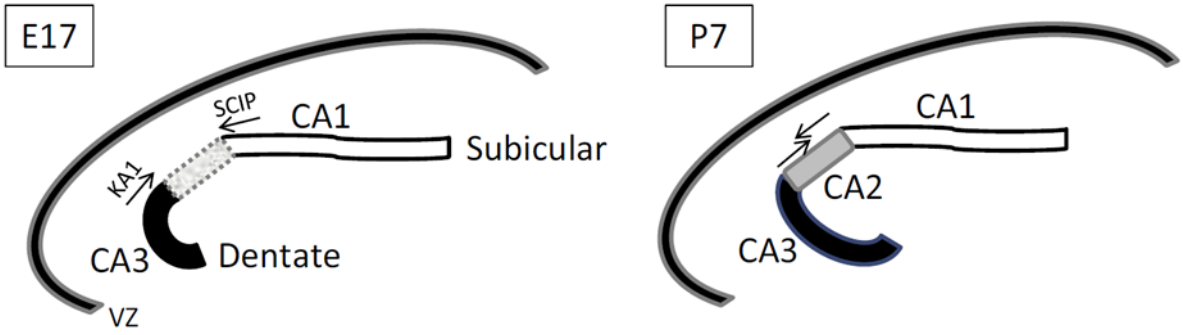

Figure 10: Representation of the KA1 and SCIP expression in CA3 and CA1, respectively. *Embryonic and mature hippocampal pyramidal cells are identified by the expression of field specific markers. The hippocampus is schematized at E17 (left) and at P7 (right). SCIP, expressed at E15.5, marks the CA1 field depicted in white, and persists into adulthood. KA1, a CA3 specific marker, is expressed in the embryonic CA3 region depicted in black at E14.5 and persists in the adult. During embryogenesis, expression of these respective markers starts at the subicular and dentate poles to finally join in the CA2 region (shown in gray in the P7 schema). Adapted from (Khalaf-Nazzal & Francis, 2013).*

The subgranular zone (SGZ) of the hippocampus plays a key role in neurogenesis since, together with the subventricular zone (SVZ), is the only neurogenic brain region after birth. Neurogenesis is a process of generation of new functional neurons in the CNS through division of neural stem cells (NSCs) and neuronal differentiation of newly born cells. This process occurs in four different steps that are: (i) cell proliferation by asymmetric division; (ii) cell fate specification; (iii) cell migration; (iv) cell differentiation, maturation and synaptic integration in the already present circuitry (Pino, Fumagalli, Bifari, & Decimo, 2017). Neurogenesis in the hippocampus occurs over a long period of time starting at E10 in mice both in CA fields and in DG, extending well beyond birth. Cajal-Retzius cells are among the first neurons to be generate in the embryonic telencephalon, invading the early cortical plate (CP) termed pre-plate; they are essential for the start of radial neurons migration and the formation of cortical layers, for the regulation of radial glia morphology and for providing guides for migrating neurons (del Río, Martínez, Fonseca, Auladell, & Soriano, 1995). The duration of the neurogenesis process differs among CA and DG region of the hippocampus: pyramidal neurons of CA and granular neurons of DG arise at the same time; however, cells in the DG continue to be generated even when neurogenesis in CA fields has been completed. The earliest pyramidal cells born before E11 are found to reside in the deep layers of CA1 and CA2, the generation of CA3 cells start approximately 1 day after, and these neurons will also reside in the deepest hippocampal layers. In CA1 and CA3, neurogenesis reaches its peak at E15 and E14 respectively and then continues until E19 (Angevine, 1965; Stanfield & Cowan, 1979). Neurogenesis in DG peaks at E16 with a massive birth of granule cells, and their accumulation becomes visible at E18. The production of granule neurons continues postnatally until the first postnatal week (Bayer, 1980), and persists even in adult animals, under specific conditions.

The migration of the pyramidal neurons follows an “inside-out” sequence: first, neurons in the inner zone (bordering to the stratum oriens) are generated, and in the last turn, neurons in the outermost zone of the pyramidal layer. Contrarily, the granular layer of the DG is characterized by the “outside-in” gradient with neurons in the outmost zone (bordering the stratum moleculare) firstly generated, and then neurons in the deep zone of the granular layer. Hippocampal interneurons, like basket and chandelier cells, come from ventral areas of the telencephalon at E12-13 and E13-14 in CA and DG respectively

(Danglot, Triller, & Marty, 2006). After leaving the ventricular germinal zone (VZ) of the hippocampal primordium around E14, newly born neurons sojourn for about 4 days in the subventricular zone (SVZ) and intermediate zone (IZ) before settling into the hippocampal plate, the presumptive pyramidal stratum. During the postnatal period these ventricular germinal zones become "exhausted" and the dentate gyrus becomes the main source of neurogenesis in the adult hippocampus (Tabata & Nakajima, 2003).

Differentiation in the mouse Ammon's horn and DG occurs mainly during postnatal development. Pyramidal neurons at post-natal day 5 (P5) show insignificant branching of dendrites, whereas an increase in the number of dendrite spines and the appearance of myelinated axons in all areas of Ammon's horn are reported between P10 and P28. The growth of the mouse hippocampus continues until P40, achieving a volume nearly six-to fivefold from the moment of birth (Kretschmann & Wingert, 1968). The late maturation of the DG is also shown in the formation of afferent and efferent connections, that begin to take form in the first days after birth (Stanfield & Cowan, 1979). Overall, the growth of the hippocampus in the mouse continues until P40, and its volume increases five- to six-fold from the moment of birth.

1.1.1.1.2 Hippocampus functions

Over the years, different hypotheses were carried out regarding the functions of the hippocampus; specifically, three main ideas have dominated the scientific literature: inhibition, memory and space function. Historically, the earliest hypothesis was the involvement of the hippocampus in olfaction, since it receives direct input from the olfactory bulb (Soudry, Lemogne, Malinvaud, Consoli, & Bonfils, 2011). In 1960 the idea of the hippocampus involvement in inhibitory pathways caught on, principally based on observations of animals with hippocampal damages, that seemed to be hyperactive and unable to inhibit certain responses (J. O'Keefe, Nadel, Keightley, & Kill, 1975). Nowadays this theory is the least popular (Best & White, 1999). The hypothesis of the implication of the hippocampus in memory derived principally from studies conducted on the patient Henry Gustav Molaison, known as HM, which developed severe anterograde and partial retrograde amnesia following surgical destruction of hippocampus due to refractory epilepsy. Following this surgery, HM was unable to form new episodic memory (Scoville & Milner, 1957). Therefore, neuroscientists and

psychologists concluded that the hippocampus is crucial for the formation of new memory about experienced events (episodic memory) and that severe damage to the area results in profound difficulties in forming new memories (anterograde amnesia) and often affects memories formed before the damage (retrograde amnesia). The third idea was the involvement of the hippocampus in space, that was originally championed by O'Keefe e Nadel, who discovered neurons in the rat hippocampus that appeared to show activity related to the rat's location within the environment (*place cell response*). Specifically, these place cells fired bursts of action potentials when a rat passed through a particular part of the environment, specifying a particular orientation together with a signal, so indicating movement or intention to move in space (J. O'Keefe & Dostrovsky, 1971). The discovery of these cells in the 1970s led to a theory that the hippocampus might act as a "cognitive map", or rather a neural representation of the layout of the environment (John O'Keefe & Nadel, 1979). The "cognitive map hypothesis" has been further advanced by recent discoveries of head direction cells, grid cells, and border cells in several parts of the rodent brain that are strongly connected to the hippocampus and produce a system of coordinates by which animals determine their spatial position and navigate their environment (Solstad, Boccara, Kropff, Moser, & Moser, 2008).

1.1.2 Neural Stem cells niches

Neural stem cells (NSCs) are defined as self-renewing, multipotent cells with the ability to differentiate into different cell types of the adult CNS: neurons, oligodendrocytes and astrocytes. NSCs reside in specific sites called niches and generate new cells throughout life. A niche provides conditions for maintenance of the stem cell pools in a quiescent state as well as signals for activation and differentiation when neurogenesis is required. The stem cells state (quiescence, self-renewal, amplification or differentiation) is determined by a combination of cell specific properties (intrinsic determinants) and of signals residing and/or spreading in the microenvironment hosting the stem cells (extrinsic determinants). Intrinsic determinants are mainly related to the epigenetic status of the stem cells and to their molecular repertoire required to sense the complex net of extrinsic signals operating in the niche. Extrinsic determinants include extracellular signals/factors, such as growth factors, cell-to-cell and cell-to-extracellular matrix (ECM)

contacts. Therefore, NSCs and their niche form a functional as well physical unit endowed of specific, and sometimes unique, molecular properties (Conover & Notti, 2008).

The NSCs niches are found in the mainly neurogenic areas of the fetal and adult brain, including the subventricular zone (SVZ) that lies along the lateral wall of the lateral ventricles in the forebrain (Shen et al., 2008), the sub-granular layer of the dentate gyrus (DG) of the hippocampus (Palmer, Takahashi, & Gage, 1997) and the olfactory bulb (OB). NSCs niches outside of the "classical" neurogenic region have been also identified, such as the retina (Moshiri, Close, & Reh, 2004) and the spinal cord meninges (Decimo et al., 2011). Indeed, recent studies (Bifari et al., 2009) have changed the view of meninges as only a merely protective membrane: a stem cell population, sharing many features with the bona fide neural stem cells and with neural differentiation potential, were found into the meninges. Therefore, the meninges were described as a novel stem cell niche thanks their peculiar morpho functional properties: they have the potential to modulate stem cell homeostasis since they contain laminin-enriched ECM organized in fractones, N-sulfated heparan sulphate molecules, functional gap junctions and secrete several trophic factors (Decimo, Fumagalli, Berton, Krampera, & Bifari, 2012).

1.2 Central Nervous System disorders

1.2.1 Hippocampal Pathologies

A range of adverse conditions can damage the hippocampus, including ischemia, hypoglycemia, epileptic seizures and other neurological conditions. Evidence reported that atrophy of hippocampal region in brain is one of the most consistent features of Alzheimer's Disease; stress and depression are associated with a loss of ability to generate new cells in the dentate gyrus, together with a loss of dendritic spines and reduced dendritic branching throughout the hippocampus; hippocampal volume reduction is one of the most consistent findings found in MRI of schizophrenic patients (V. Dhikav & K. Anand, 2007; V. Dhikav & K. S. Anand, 2007). Moreover, the development of uncontrolled local hippocampal inflammation, the blood-brain barrier damage, and repeated seizures cause hippocampal sclerosis, leading to epilepsy (Chang & Lowenstein, 2003).

1.2.1.1 Epilepsy and Temporal Lobe Epilepsy

Epilepsy is a chronic disease of the CNS characterized by an imbalance in neuronal electrical activity, which leads to various recurrent and unpredictable seizures, to immediate CNS insult (structural, systemic, toxic, or metabolic), and to neurobiological, cognitive, psychological, and social consequences of seizure recurrences. According to the latest Global Burden of Disease study, epilepsy is considered the second most serious neurological disease in the world in terms of disability-adjusted life years and affects people of all ages, races, social classes, and geographical locations. In 2016, it was estimated that there were 45.9 million people with all-active forms of epilepsy worldwide, with an age-standardized mortality rate of 1.74 per 100,000 individuals (Beghi et al., 2019). The epileptic seizures are excessive or hypersynchronous recurrent paroxysmal events characterized by stereotyped behavioral alterations, that reflect the underlying neural mechanisms of the disease. They are the result of bursts of abnormally excessive or synchronous neuronal activity in the brain, that can cause a wide range of symptoms. Seizures can involve a specific brain area or network, thus generating a focal-onset seizures, arising in one hemisphere of the brain or a synchronic bihemispheric discharge, leading to generalized-onset seizures originating in both hemispheres simultaneously. Epilepsy classification is complex and includes different levels, from seizure types to epilepsy syndromes, which encompass several clinical features, such as age of onset, specific etiologies, and comorbidities. According to the latest International League Against Epilepsy (ILAE) classification, epilepsy etiologies can be classified into structural, genetic, infectious, metabolic, immune, or unknown etiologies (Fisher et al., 2017). Moreover, the ILAE classification defines epilepsy according to the following conditions: (1) at least 2 unprovoked (or reflex) seizures occurring > 24 h apart; (2) one unprovoked (or reflex) seizure and a probability of further seizures like the general recurrence risk (at least 60%) after 2 unprovoked seizures, occurring over the next 10 years and (3) diagnosis of an epilepsy syndrome. The ILAE recently defined *status epilepticus (SE)* as: “a condition resulting either from the failure of the mechanisms responsible for seizure termination or from the initiation of mechanisms, which lead to abnormally, prolonged seizures (after timepoint T1). It is a condition, which can have long-term consequences (after timepoint T2), including neuronal death, neuronal injury, and alteration of neuronal networks, depending on the type and duration of seizures”

(Trinka et al., 2015). The T1 is defined as the timepoint of 5 min after seizure onset, characterized by generalized tonic–clinic status epilepticus. T2 instead is a timepoint at 30 min, after which there is an increased risk of irreversible consequences.

At the molecular level, the main cause of neuronal hyperexcitability, that triggers the abnormal electrical activity characteristic of epileptic seizures, is the depolarization of the presynaptic membrane. This neuronal hyperstimulation causes a conformational change in several ion channels and membrane receptors, which leads to a massive flow of Ca^{2+} and/or Na^{+} ions into the neuron and an outflow of K^{+} ions. In turn, this ionic imbalance causes the activation of different signaling cascades that promote neurotoxic effects and neuronal plasticity changes, ultimately leading to cell death (YueMei Zhang & Bhavnani, 2006) **(Figure 11)**.

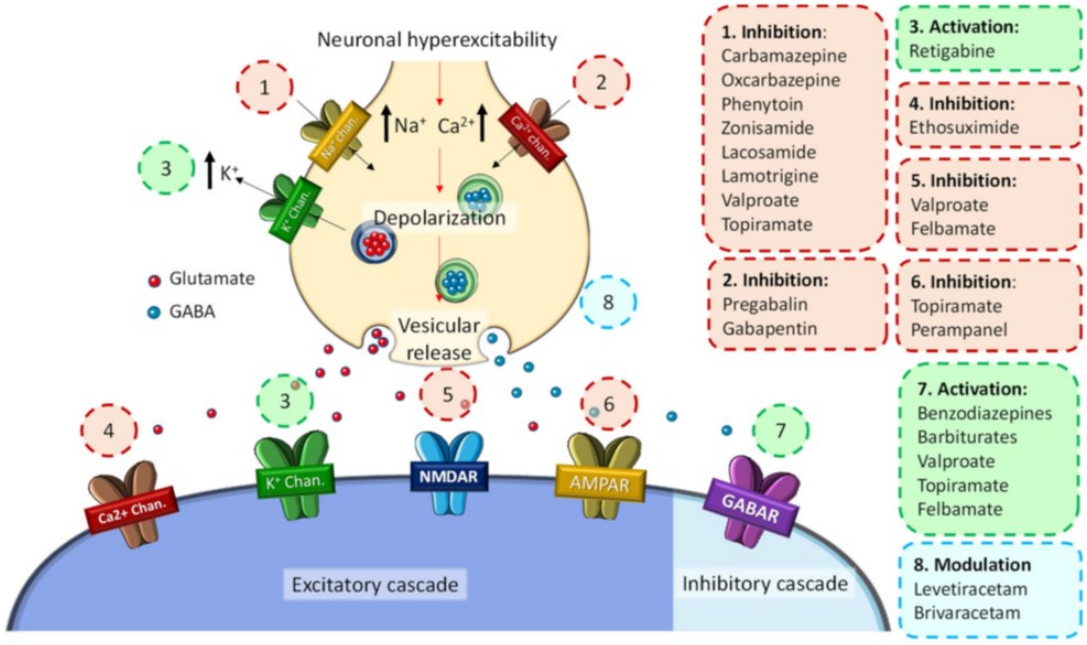

Figure 11: General molecular mechanisms of the development of seizure activity in epilepsy and associated antiseizure drugs (ASDs). *Adapted from (Cano et al., 2021).*

Since the late 19th century, the cerebral cortex has been considered the predominant anatomical source of seizures (Jackson, 1890). In recent years, histopathological, electrophysiological, and quantitative neuroimaging studies have provided ample

evidence that both focal- and generalized-onset seizures involve diverse interactions between neural networks of cortical and subcortical structures (Paz & Huguenard, 2015). Indeed, in focal epilepsy, the most common type of epilepsy in adults, the main area of seizure initiation is the temporal lobe, although foci of origin have also been observed in the frontal, parietal, and occipital lobes. Likewise, the amygdala-hippocampal complex is considered one of the key anatomical circuits involved in the epileptogenic process.

Temporal Lobe Epilepsy (TLE) is the most common focal epilepsy. According to the ILAE classification, TLE can be divided into mesial temporal lobe epilepsy (mTLE) and lateral or neocortical temporal lobe epilepsy (nTLE) (Scheffer et al., 2017). mTLE is the most common subtype and seizures originate from the hippocampus, entorhinal cortex, amygdala, and parahippocampal gyrus (Maillard et al., 2004). The main features of TLE are: i) the localization of seizure foci in the limbic system, particularly in the hippocampus, entorhinal cortex and amygdala (Bartolomei et al., 2005); (ii) the frequent finding of an "initial precipitating injury" that precedes the appearance of TLE (Mathern et al., 2002); (iii) a seizure-free time interval following the precipitating injury known as "latent period"; and (iv) a high incidence of mesial or Cornu Ammonis (CA) sclerosis, i.e., a unilateral hippocampal lesion leading to atrophy, typically caused by neuronal loss and gliosis in the pyramidal cell layer of Sommer's sector (the subiculum-CA1 transition zone) and the endfolium (dentate hilus) (Mathern, Kuhlman, Mendoza, & Pretorius, 1997). In addition to the hippocampal sclerosis, which represents the most common cause of TLE, other causes lead to TLE, including perinatal injury, malformations of cortical development (MCD), arteriovenous malformations (cavernous hemangiomas, meningioangiomatosis), infections of the CNS, glial tumors (i.e., ganglioglioma, dysembryoblastic neuroepithelial tumours, astrocytomas, oligodendrogliomas, meningiomas, or CNS metastasis), hamartomas, head trauma, and limbic encephalitis (Williamson et al., 1993).

1.2.1.1.1 Animal Models of Temporal Lobe Epilepsy

The unpredictable and recurrent nature of seizures associated to TLE is the most disabling feature of this neurological disorder. Seizures in TLE are often resistant to anti-epileptic drugs. Surgical resection of the epileptogenic tissue is thus offered as an alternative, but

it is costly and at times impracticable. To fully understand TLE pathophysiology and to develop new therapeutic approaches, animal models that reproduce the electroencephalographic, behavioural, and neuropathological features of this epileptic disorder have been developed over the last four decades (Levesque, Avoli, & Bernard, 2016). Nowadays, two main animal models of TLE, which involve the systemic administration of chemoconvulsants, are being extensively used in research, due to their high similarity with the human disease. One of these is the *Kainic acid*, a cyclic analog of L-glutamate and an agonist of the ionotropic kainic acid receptors. The use of this drug as a model of TLE was originally proposed by Ben-Ari and Lagowska (Ben-Ari & Lagowska, 1978; Ben-Ari, Lagowska, Tremblay, & Le Gal La Salle, 1979), who reported that intra-amygdaloid injections of kainic acid in rodents induce the status epilepticus (SE) followed by the occurrence of spontaneous seizures and produce neuropathological lesions that are similar to those occurring in some patients with epilepsy, i.e., neuronal degeneration in the CA3 region of the dorsal hippocampus. Specifically, within 48 h after injection of kainic acid, in animals that showed robust convulsions during status epilepticus, there is a loss of pyramidal cells in the CA1, CA3 and CA4 regions of the hippocampus. Indeed, in this model, the hippocampus and the amygdala are often the sites of origin of electrographic seizures, which then rapidly propagate to the thalamus, CA1 region and frontal cortex (Ben-Ari, Tremblay, Riche, Ghilini, & Naquet, 1981). The other animal models of TLE involve the use of *Pilocarpine*, a muscarinic acetylcholine receptor agonist. The pilocarpine model was first described by Turski et al. in 1983 (Turski et al., 1983), who showed that systemic intraperitoneal (i.p) administration of pilocarpine in rodents was followed by a sequence of automatisms and motor limbic seizures evolving into status epilepticus; these animals showed spontaneous seizures approximately 2 weeks after the initial status epilepticus. The pilocarpine model presents important features: (i) the induction of acute SE is more rapid than with intraperitoneal injection of kainic acid; (ii) this model is characterized by the presence of a latent period followed by the appearance of spontaneous recurrent seizures (SRSs, chronic phase); (iii) the pilocarpine models show the occurrence of widespread lesions, some of them localized in the same brain areas affected in TLE patients and associated with neuronal network reorganization in hippocampal and parahippocampal regions. Indeed, pilocarpine in animals induces mossy fibre sprouting, interneuron loss and ectopic dentate

granule cell proliferation like in TLE patients (Curia, Longo, Biagini, Jones, & Avoli, 2008).

1.3 Regenerative approaches for the treatment of Central Nervous System diseases

CNS disorders, such as epilepsy, traumatic brain injury (TBI), Parkinson's disease (PD) and Alzheimer's disease (AD), resulting from the progressive loss of structure and/or function of neurons, contribute to different paralysis degrees and loss of cognition and sensation. Unfortunately, currently available treatment options are insufficient in arresting the neurodegenerative processes and this leads to a considerable burden on society and a high economic impact. Over the past 20 years, regenerative cell therapy, innovative technologies like 3D culture systems known as organoids, and pharmacological therapies have been providing new insight into basic biology and human disorders, and drive innovation toward new treatments for these disorders.

1.3.1 Cell Therapy: from stem cells to organoid transplantation

Cell therapy has revolutionized medicine over the years; indeed, its therapeutic applications have provided invaluable and attractive options for treating numerous disorders, including neurodegenerative diseases. The potential of cell therapy in neurodegenerative diseases was first examined in the 1980s when patients suffering from PD were treated with fetal mesencephalic tissue transplantation (Hedlund & Perlmann, 2009). Nowadays, cell therapy offers promising strategies, including the regeneration of neural tissue, stabilizing the neuronal networks, providing neurotrophic support, and alleviating neurodegeneration at different neuronal circuitry levels for the treatment of these diseases (Sakthiswary & Raymond, 2012). Despite the remarkable advances in stem cell research for neurodegenerative disorders, several critical issues must be addressed. A major hindrance in stem cell therapies' progression is learning how stem cells work in the body and how they integrate with the targeted tissue/organ. Furthermore, there is the problem of reducing the risk of post-implant rejection, which adds the burden of needing

a close compatible donor for the cells' recipient. Identifying the proper conditions to culture these cells, the most suitable route of administration, delivery, and the target site is also crucial to maximizing the benefit of the treatment and improving the outcome.
In recent years, the introduction of tridimensional (3D) cell culture systems – known as organoids, is revolutionizing the fields of developmental and stem cell biology. Conversely to two-dimensional cultures, which fail to replicate biological interactions among cells and between cells and extracellular matrix (ECM), organoids preserve the cellular interactions that capture key structural and functional aspects of real organs at the micrometer to millimeter scale. Therefore, they hold a huge potential in regenerative medicine, including cell replacement therapies (Mansour et al., 2018).

1.3.1.1 Stem Cell therapy

Stem cell are characterized by the capacity to proliferate, self-renew, and differentiate into various mature cell lineages. Stem cells are classified as embryonic stem cells (ESCs), induced pluripotent stem cells (iPSCs), mesenchymal stem cells (MSCs), neural stem cells (NSCs) and adult stem cells (ASCs), based on the range of possible cell type production and derivation methods. Over the years, different types of stem cells were used for the potential treatment of several CNS diseases, such as Alzheimer's disease (AD) and epilepsy; indeed, stem cell therapy has emerged an alternative approach to treat these disorders. Studies on AD reported the beneficial effects of NSCs transplantation in rescuing the cognitive phenotype in transgenic mice that exhibit advanced AD-related pathology (Blurton-Jones et al., 2009). Moreover, the transplantation of NSCs overexpressing choline acetyltransferase (Ach) has been seen to reverse spatial memory and learning deficits in aging mice, not only by producing ACh directly but also by restoring cholinergic neuronal integrity (D. Park et al., 2013).
Cell-based therapy has emerged also as an alternative option in pre-clinical and clinical studies for Temporal Lobe Epilepsy, as this approach has great promise for restraining epileptogenesis by suppressing spontaneous seizures in patients with drug-resistant epilepsy (Rao, Hattiangady, Rai, & Shetty, 2007; Turner & Shetty, 2003). Recent progress in cell transplantation in a TLE model is well described by Shetty et al. (Shetty, 2011). The TLE model resembles many of the patients' pathological conditions, including

cell loss of excitatory neurons in discreet hippocampal regions, decrease of inhibitory gamma-aminobutyric acid positive (GABAergic) interneurons, aberrant synaptic reorganization, hippocampal hyperexcitability and changes in expression level of several receptors and ion channels. To replace the damaged hippocampal neurons, fresh hippocampal precursor cells obtained from the fetal brain, GABAergic progenitors and NSCs/neuronal progenitors expanded from diverse sources, including the human ES cells and the human iPS cells, have been tested as efficacious transplantable cells in hippocampal injury and TLE animal models. Studies reported that grafting of specific post-mitotic hippocampal precursor cells shortly after hippocampal injury or *status epilepticus* allows the replacement of the lost neurons, as well as facilitates the reconstruction of the disrupted hippocampal circuitry (Hattiangady, Rao, Zaman, & Shetty, 2006; Shetty, Zaman, & Turner, 2000). Studies on cognitive performance after cell transplantation in TLE animal models are controversary. Transplantation of medial ganglionic eminence-derived neural stem cells (MGE-NSCs) into hippocampi of adult rats exhibiting chronic TLE has been seen to suppress the spontaneous recurrent motor seizures (SRMS) by promoting considerable reductions in seizure frequency, duration and severity, and the amount of time spent in seizures at 1–3 months after grafting. However, MGE-NSC grafting did not improve the hippocampal-dependent learning and memory function (Morris water maze test) in chronically epileptic rats (Waldau, Hattiangady, Kuruba, & Shetty, 2010). Moreover, Lee et al. demonstrated that, despite the human fetal telencephalon-derived NSPC (huNSPCs) transplantation into the adult epileptic rat brain exerted a therapeutic effect in suppressing kindling-induced evoked seizures and spontaneous recurrent seizures in the pilocarpine-induced TLE model, such cell grafting did not reverse spatial learning and memory function (Morris water maze test) (H. Lee et al., 2014). On the contrary, in 2013 Hunt et al. demonstrated that the transplantation of medial ganglionic eminence (MGE) progenitor cells into the adult epileptic brain reduced the occurrence of electrographic seizures and restored behavioral deficits in spatial learning (Morris water maze test), hyperactivity, and the aggressive response to handling; however, not significant differences were found in motor coordination (rotarod assay) and general anxiety (elevated plus maze) between the control and transplanted group (Hunt, Girskis, Rubenstein, Alvarez-Buylla, & Baraban, 2013). Recently, Upadhya et al. (Upadhya et al., 2022) investigated whether graft-derived

gamma-aminobutyric acid positive (GABAergic) interneurons directly regulate spontaneous recurrent seizures (SRS) and cognitive function in a rat model of chronic TLE. In this study, human pluripotent stem cell-derived medial ganglionic eminence-like GABAergic progenitors were grafted into hippocampi of chronically epileptic rats. The authors demonstrated that such grafting substantially reduced SRS and improved hippocampus-dependent cognitive function (Upadhya et al., 2022).

In the last years, the integration of cells with appropriate biomaterials has been reported to potentially shift the cell therapy paradigm to a regenerative medicine therapeutic option for the brain. Indeed, studies reported that intracerebral transplantation of neural stem cells in combination with biomaterials provides an important structural support to NSCs, enhances NSC engraftment, survival, neuronal differentiation and therapeutic function (Bible et al., 2012; Jin et al., 2010).

1.3.1.2 Organoid technology

Animal models and two-dimensional (2D) cell cultures have continuously been exploited in the biomedical research field, helping generations of scientists to uncover the molecular mechanisms that underlie pathological states and to design innovative therapeutic approaches. Although these standardized models were useful to bring to light many basic concepts behind diseases and development, human-specific features and related defects cannot be directly studied in animal models, due to the important gap in terms of species-specific complexity and animal-human biology. This issue can be overcome with the advent of 3D cell culture systems - known as ***organoids*** - in which cells, usually ESCs or pluripotent stem cells (PSCs), are coaxed to aggregate, and grow in all dimensions, resembling the tissue or the organ of interest. 3D culture methods allow *in vivo* and *in vitro* studies and are one of the latest innovations in the search for describing and synthesizing the pathophysiologic processes that usually occur in humans.

The “organoid” definition refers to an *in vitro* 3D multicellular structure containing different cell types with self-organization as seen in human tissues, typically derived from PSCs or adult stem cells (AdSCs, also known as tissue stem cells). The ability of stem cells to produce highly organized structures that reproduce features similar to the embryo and adult tissues is based on the “self-organization” cell capacity, which involves three

different categories: first, the control of relative cell position, named “self-assembly”; second, the spatiotemporal control of the cell stage, defined as “self-patterning”; and lastly, the capacity to promote growth and remodeling, which is termed “self-morphogenesis” (T. P. Silva et al., 2019) **(Figure 12)**.

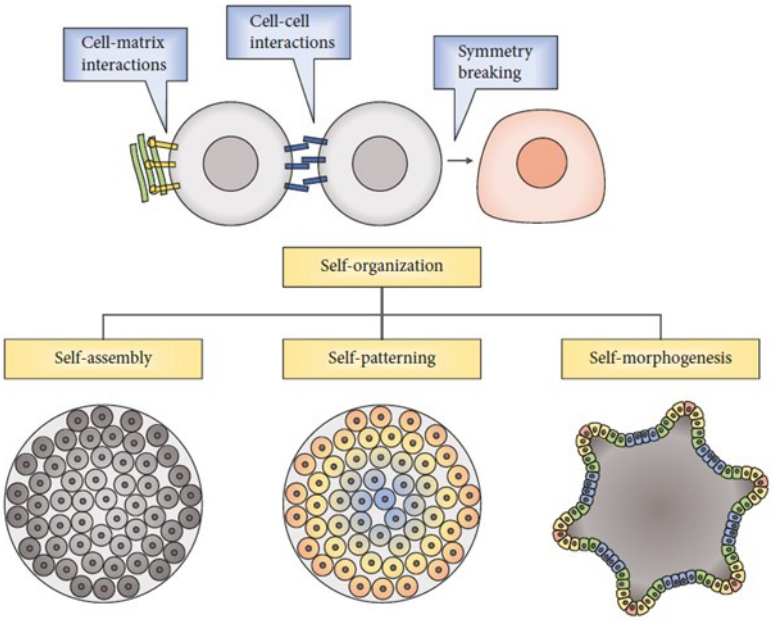

Figure 12: Principle of “cell-organization”. *The ability of stem cells to produce 3D systems is based on the combination of self-assembly, self-patterning, and self-morphogenesis capacities. Adapted from (T. P. Silva et al., 2019).*

In recent years, generation of organoids from AdSCs have gained much attention for their intrinsic abilities to self-renew and differentiate into the cell types present in adult tissues while retaining genomic stability. Human ASC-based organoids have been used to model several diseases, including cancer, infectious diseases, and inheritable genetic disorders. The first long-term feeder-free adult stem cell-derived organoid culture system to be developed was that of mouse small intestinal organoids (Korinek et al., 1998). Recently, the combination of ECM and 3D culture systems with a deeper knowledge of the signaling pathways important for AdSC maintenance and tissue repair have been instrumental for the development of primary AdSC cultures. Thus, stomach (Bartfeld et al., 2015), mammary gland (Dontu et al., 2003), pancreas (Boj et al., 2015), liver (Huch

et al., 2015), lung (J. H. Lee et al., 2014) and prostate (Gao et al., 2014) organoids have been all derived *in vitro* from AdSCs. These organoids can be generated from biopsies isolated directly from the organ of interest or from diseased patient tissue. However, the establishment of human AdSC-derived organoids is limited by accessibility to the tissue and prior knowledge of the culture conditions for that tissue (J. Kim, Koo, & Knoblich, 2020). Moreover, the main limitation of AdSC-derived organoids is the absence of tissue-resident stem cells in some organs. Therefore, over the years, major advances and discoveries in stem cell research have been made in PSCs, especially in iPSCs technology. Indeed, given their human origin in which drugs are tested and transplantations are received, iPSCs are widely used thanks to their accessibility, abundant reproducibility, potency to differentiate into all cell types, application in personalized medicine and avoidance of the ethical concerns associated with human ESCs. Unlike AdSC-derived organoids, PSC-derived organoids recapitulate the differentiation of the developing embryo into specific organ types and contain various cell populations that closely mimic the tissue.

Nowadays, there are many established protocols to produce different types of organoids from PSCs; the common elements being the inhibition and/or activation of specific signaling pathways that direct cells toward a specific germ layer and then, with further differentiation, into the desired cell types. Recent studies reported the generation of a lot of organoid types resembling different tissues, such as intestinal, kidney, brain, retinal, pancreatic, liver and skeletal muscles organoids (Ho, Pek, & Soh, 2018; Lancaster & Knoblich, 2014b; M. Li & Izpisua Belmonte, 2019; Shin et al., 2022) **(Figure 13)**.

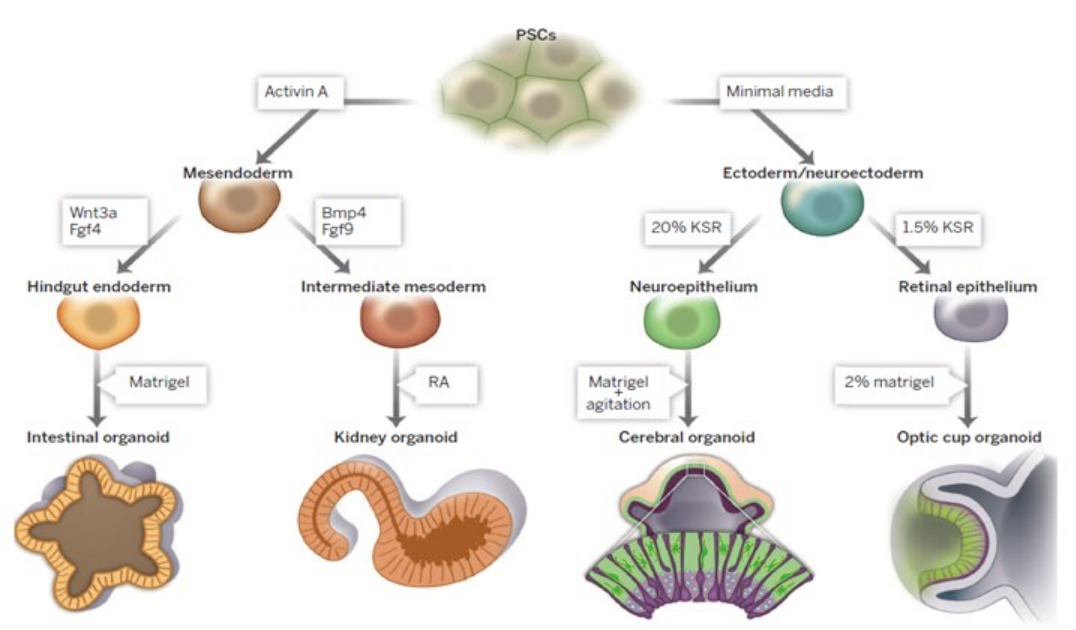

Figure 13: Current organoids methodologies. *Different types of organoids modeling tissues are generated through specific signaling pathways. Adapted from (Lancaster & Knoblich, 2014b).*

Organoids represent a revolutionary technology to study human development. For example, human brain organoids have been used to investigate how neural stem cells behave during the embryonic stages (Lancaster et al., 2013), retinal organoids helped to understand the timing of tissue morphogenesis, both in human and rodents (Eiraku & Sasai, 2011), kidney organoids were generated to facilitate applications for tissue engineering, disease modeling and chemical screening (Morizane & Bonventre, 2017). Moreover, organoids may help in understanding and modeling adult homeostasis (Idowu, Bertrand, & Walduck, 2022). These 3D structures are also a potential system useful for high throughput drug screening, thanks to their easy manipulability and scalability. Unlike current toxicology analysis in animal models and cell-lines, 3D systems could improve the predictability of drug efficacy or side effects and may offer a better alternative because they are genetically more stable than cell lines and in terms of high-throughput screenings they are better than animals. For example, anti-Zika virus drugs were tested in human brain organoids (Zhou et al., 2017); moreover liver organoids can provide an unlimited source of hepatocytes, that are considered the gold standard for *in vitro* toxicology tests (Nantasanti, de Bruin, Rothuizen, Penning, & Schotanus, 2016).

Tumor organoids were used in hyperthermia therapy (Ubink et al., 2019) and immunotherapy (Gronholm et al., 2021). The main application of organoids is disease modeling: several organoids models have been established to investigate different genetic disorders, for example cystic fibrosis with intestine and pancreatic organoids (Dekkers et al., 2016), retinitis pigmentosa using retinal organoids (T. P. Sharma et al., 2017), lissencephaly, Rett syndrome and Autism Spectrum Disorders (ASD) by cerebral organoids (Bershteyn et al., 2017; Gomes et al., 2020; Mariani et al., 2015).

Brain organoids, that can mimic many features of the early brain on many levels, such as architecture, cell-type diversity, omics expression profile and neuronal function, have recently emerged as models to investigate human brain development, to reproduce different neuronal disorders and as a preclinical model in drug screenings. The first step towards the development of brain organoids was a study conducted by Eiraku et al., in 2011, with the generation of self-organizing optic cups from human PSCs; this study provided the first indication that neural tissue maintained in a 3D floating culture could self-organize (Eiraku et al., 2011). Starting from this pioneering study, nowadays a broad range of cerebral organoids can be produced, either resembling macro brain identities (forebrain and midbrain organoids) or specific brain regions (brain-region specific organoids, like thalamic organoids), useful for modeling different aspects of human brain complexity, development, and functionality.

Brain organoids are extensively studied as *in vitro* models of brain development, due to their ability to mimic the cellular architecture as well as the spatiotemporal formation of heterogeneous neural and glial cell types found in the *in vivo* counterpart. In particular, in brain organoids were observed several ventricular-like zone structures containing stem cells which generate neurons, astrocytes, oligodendrocytes and interneurons precursors (Quadrato et al., 2017). Brain organoids allow the modeling of several neurological disorders. Indeed, the generation of patient iPSC-derived cerebral organoids, permits the accurate reproduction of neurodevelopmental and neuropsychiatric disorders *in vitro.* For example, microcephaly patient-derived cerebral organoids, characterized by smaller size, reduced progenitor zones, decreased neurogenesis, and an abnormal neuronal activity compared to the control (Lancaster et al., 2013), were generated. Mutations and molecular mechanisms of schizophrenia were investigated using DISC1-mutated patient-derived

cerebral organoids (Ye et al., 2017). Moreover, cerebral organoids derived from iPSCs with heterozygous knockout of CHD8, a major risk factor for ASD, were used to get many insights about this disease (P. Wang et al., 2017). Brain organoids represent also novel cell sources for neuro-regenerative purposes, like transplants. Indeed, different studies reported that cerebral organoids grafted in animal hosts, like mouse, rat, and monkey, showed progressive neuronal differentiation and maturation, gliogenesis, axonal growth towards multiple regions of the host brain, instauration of functional neuronal networks and also blood vessels formation in the grafted tissue. For example, Mansour et al. in 2018 generated GFP hESC-derived brain organoids and implanted them into a cavity in the retrosplenial cortex of nonobese diabetic-severe combined immunodeficient (NOD-SCID) mice. Eight months after transplantation, cell differentiation and progressive maturation were observed, as well as synaptic connectivity between human axons and the host brain, and axonal outgrowth in cerebral organoids. These organoids also showed a successful vascularization once grafted into the host brain (Mansour et al., 2018). Another study reported that cerebral organoids transplanted in the rat middle cerebral artery occlusion were able to differentiate and migrate into different brain regions and promote the reduction of brain damage volume, synaptic reconstruction, and neurological motor function recovery (S. N. Wang et al., 2020). Recently, Revah et al. (Revah et al., 2022) demonstrated that human stem cell-derived cortical organoids transplanted into the somatosensory cortex of newborn athymic rats developed mature cell types that integrate into sensory and motivation-related circuits. The integration of these organoids into rodent neural circuits allowed the establishment of links between the activity of human cells and learned animal behavior, thus showing that the activation of transplanted cortical organoids could drive reward-seeking behavior responses (Revah et al., 2022).

Brain organoids have been also increasingly used as high-throughput screening platforms for novel candidate drugs: patients' iPSCs-derived organoids were generated and mathematical modeling, considering a network of molecular pathways and relevant genetic factors, was employed to identify several FDA-approved drugs as candidates for drug repositioning and to build high-content screening (HCS) systems (J. C. Park et al., 2021) **(Figure 14)**.

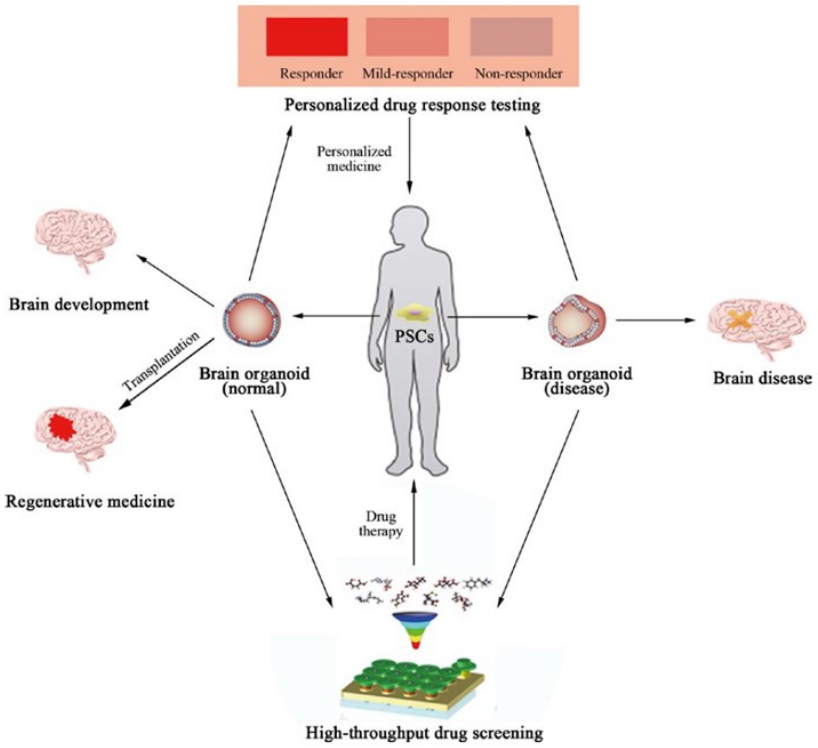

Figure 14: Brain Organoids applications. *Brain organoids emerge as models to study brain development, different neurological diseases, and high-throughput drug screening. Adapted from (P. Wang et al., 2017).*

1.3.2 Rewiring of cell metabolism: a promising pharmacological therapy

Pharmacological research in CNS disorders is oriented to develop new effective therapeutic strategies in order to treat diseases and, at same time, to improve the life quality of patients. Many studies aim to discover new drugs, taking in consideration that their effectiveness is strictly dependent on the administration route and also on their intrinsic ability to access the organs and tissues in suitable amounts and times. Nowadays, few drugs have been successfully used to treat the CNS diseases and, in many cases, the drugs that have demonstrable effects are palliative treatments that have modest effects on disease symptoms and no demonstrable effect on disease progression. One of the major therapeutic limits of these drugs is the impossibility to be transported across the blood–brain barrier (BBB). The transport efficiency of drugs through the BBB largely depends on the properties of size, hydrophilicity, and dissociation of the molecule (Sweeney, Zhao, Montagne, Nelson, & Zlokovic, 2019). Following neurodegenerative disorders, the damaged tissue suffers from a severe metabolic impairment, which contributes to the loss

of crucial cellular functions such as ion/anion pumping (i.e., Na/K or H2CO3), and the mitochondrial membrane potential (LoPachin et al., 1999). These events lead to the impairment of the tricarboxylic acid (TCA) cycle and oxidative phosphorylation (OXPHOS) (Cao et al., 2013; Patel, Sullivan, Lyttle, & Rabchevsky, 2010) that worsen the disease progression and promote glutamate excitotoxicity-driven-neuronal cell death. Therefore, rewiring the cellular metabolism became an attractive and innovative pharmacological strategy for restoring neuronal cell functions. Adult brain has high energy requirements (3.5 ml O2/100 g/min corresponding to approximately 4 × 1021 molecules of ATP/min) contributing to 25% of the body glucose utilization (Attwell & Laughlin, 2001), and accounting for more than 20% of the body oxygen consumption. Neurons need high ATP content to support membrane remodeling, synaptic spine formation, and generation of transmembrane resting and action potential (Hallermann, de Kock, Stuart, & Kole, 2012; Laughlin, de Ruyter van Steveninck, & Anderson, 1998). Such high metabolic costs impose on neurons to use the oxidative metabolism, which produces higher ATP yields than glycolysis. Previous studies reported that long-term dietary supplementation with a specific Branched-chain amino acids (BCAAs) – enriched mixture increases mitochondrial biogenesis, energy metabolism and reduces the oxidative damage both in cardiac and skeletal muscles of middle-aged mice, promoting their longevity (D'Antona et al., 2010). The increased longevity effect of BCAAs has also confirmed in the unicellular organisms *Saccharomyces cerevisiae* (Alvers et al., 2009). Furthermore, BCAAs administration in traumatic brain-injured animals has been seen to lead the reinstatement of the cognitive performance thanks to the restoration of the hippocampal functions (Cole et al., 2010). Moreover, Bifari et al. in 2020 demonstrated that the administration of essential amino acids (EAAs) enriched in branched-chain amino acids (BCAAs) and metabolic substrates increased TCA cycle, OXPHOS, and the mammalian/mechanistic Target of Rapamycin Complex 1 (mTORC1)-driven energy metabolism in neuronal cells *in vitro*. Such energetic availability enhances neuronal axonal branching, synaptic maturation, and NRF2-mediated antioxidant defense (Bifari et al., 2020). The effects of the oral intake of BCAAs have been investigated in many disease models such as metabolic disorders and obesity, cancer, impaired immunity, muscle atrophy, spinal cord injury and in different types of injury (trauma, postoperative, sepsis, burn) (De Bandt & Cynober, 2006; Dolci et al., 2022; B. Sharma, Lawrence, &

Hutchison, 2018). In these diseases, the administration of BCAAs promotes beneficial effects on the organism and thus they have been proposed for the prevention and/or treatment of different human disorders (Dolci et al., 2022; Marchesini et al., 2003; Tamanna & Mahmood, 2014).

2. AIMS

Central Nervous System (CNS) disorders, such as epilepsy, traumatic brain injury (TBI), Parkinson's disease (PD) and Alzheimer's disease (AD), resulting from progressive functional and structural degeneration of the neuronal tissue, are characterized by gradual loss of cognition and sensation and motor functions. Unfortunately, current available treatments are insufficient in arresting the neurodegenerative processes, leading to a considerable burden on society and a high economic impact on public health system. Different innovative approaches have been investigated with the aim to promote regeneration of damaged neuronal tissue underlying incurable neurodegenerative diseases, such as intracerebral transplantation of neural stem cells (NSCs) in combination with biomaterials (Bible et al., 2012; Jin et al., 2010). Although promising results were reported in literature (Hattiangady et al., 2006; Shetty & Turner, 2000), transplanted stem cells (SCs) exhibited low survival rate, host-tissue reaction, poor neuronal differentiation and integration, preventing the full recovery of brain damage and resulting in a low therapeutic efficacy (Henriques, Moreira, Schwamborn, Pereira de Almeida, & Mendonça, 2019; Zhao, Wang, Liang, & Li, 2021). 3D organoid systems are recently emerging as the latest frontier in regenerative medicine to treat brain disorders as they own the potential of being used as functional brain tissue grafts able to regenerate the damaged brain (Bible et al., 2012; Bifari et al., 2020; Gonzalez et al., 2018; Jin et al., 2010; Z. Wang et al., 2017). Considering the complexity of the CNS and in particular of the brain, the transplantation of a 3D structure with a high level of neuron maturation, could boost both its capacity to integrate into an altered circuitry and to restore the damaged functionality.

The work presented in this PhD thesis was part of the European Project HERMES – "Hybrid Enhanced Regenerative Medicine" which has the ultimate goal to overcome Temporal Lobe Epilepsy (TLE) by pursuing self-repair process of dysfunctional brain circuits with the use of bioengineered brain tissue, neuromorphic microelectronics, and artificial intelligence (AI). As part of HERMES project, we have developed a standardized protocol to generate mouse brain organoids (Ciarpella et al., 2021). By using this protocol, we obtained mouse brain organoids able to growth and develop neuronal

differentiated cells, however they displayed low level of functionality and heterogenous brain region identity.

The overall objective of my PhD thesis was to set the stage to develop functional hippocampal brain organoid that can be used for regenerative medicine to cure the TLE. Specifically, I aimed to **i)** increase neuronal maturation and functionality in mouse brain organoid, **ii)** induce hippocampal lineage commitment of mouse brain organoids and to **iii)** apply the organoid technology as new therapeutic strategy for the treatment of TLE.

AIM1: Increase brain organoid neuronal maturation and functionality

The transplantation of 3D brain organoids has recently emerged as the latest frontier in regenerative medicine. In our lab, we have set up a highly standardized mouse brain organoid generation protocol which allowed the generation of brain organoids characterized by a progressive neuronal maturation during the different organoid developmental stages (Ciarpella et al., 2021). Although we found the presence of synaptic components and spontaneous cellular calcium activity, the low number of neuronal cells and their incomplete neuronal maturation did not allow the formation of a robust neuronal network able to mimic a potential information processing.

With these premises, I aimed to improve the brain organoid neuronal differentiation, maturation and functionality by using **a)** the alginate extracellular matrix (ECM) and **b)** a selection of bioenergetic molecules, called α5.

a) Brain organoid embedding with the alginate scaffold

I evaluated the effect of the ***Alginate*** scaffold, a highly bio-compatible, low immunogenic algal polysaccharide extracellular matrix (ECM), on the differentiation and maturation of brain organoids. The use of ECM, a network of extracellular macromolecules such as collagens and glycoproteins, is fundamental for 3D spatial organization since it provides structural and biochemical support to the cells (Johnson, Craig, & Mercer, 1997; Palazzolo, Broguiere, Cenciarelli, Dermutz, & Zenobi-Wong, 2015). Moreover, alginate sustains growth and multi-lineage differentiation of murine neural stem cells (X. Li et al., 2006). The previously in-house established protocol for the generation of brain organoids (Ciarpella et al., 2021) was revised and optimized with the introduction of the alginate ECM to evaluate its effect on organoid development, differentiation and maturation.

Therefore, I evaluated the organoid size and morphology, cellular phenotype, differentiation and maturation by optic and immunofluorescence analysis.

b) α5 supplementation in the brain organoid culture medium

I boosted the brain organoid differentiation, maturation and functionality by adding a selection of bioenergetic molecules, including the tricarboxylic acid (TCA) cycle intermediates, essential amino acids (EAAs), branched-chain amino acids (BCAAs), and the cofactors thiamine and pyridoxine, altogether referred to as ***α5*** (Bifari et al., 2020), in the organoid differentiation medium. I evaluated the organoid size and morphology, cellular phenotype, differentiation and maturation by optic, immunofluorescent and calcium imaging analysis.

AIM2: Induce hippocampal brain region specific commitment

The hippocampus is one of the brain regions mainly affected in the pathological progression of many neurodegenerative disorders, including TLE. This pathology is a disorder condition which affects specifically the hippocampus; therefore an *in vitro* 3D structure able to replicate the hippocampal tissue can be extremely useful for drug testing and CNS disease modeling. In addition, early studies demonstrated the feasibility and great promise of hippocampal tissue transplantation to heal the epileptic brain both functionally and anatomically (Shetty & Turner, 2000).

With the aim to induce the hippocampal CA3 commitment in brain organoids, the in-house established brain organoids generation protocol was optimized by adding, during the expansion and induction phase, the morphogen ***WNT3a***, which play a key role in hippocampal patterning and growth. Specifically, the in-house protocol for the generation of brain organoids (Ciarpella et al., 2021) was matched and revised with the one described by Sarkar and colleagues (Sarkar et al., 2018) which was related to the differentiation of human pluripotent stem cells in CA3 neurons. The addition of WNT3a in the organoid expansion and induction cell media was assumed as crucial for the reliable generation of hippocampal CA3 organoids. Therefore, I evaluated organoid size and morphology, cellular composition, differentiation and maturation by optic, immunofluorescent and calcium imaging analysis.

AIM3: Apply the organoid technology as new therapeutic strategy for the treatment of TLE

TLE is an adulthood focal epilepsy frequently refractory to anti-epileptic medications (Blair, 2012). Current medical treatments for TLE are extremely expensive and have a widespread impact on patients' health-related quality of life. SC therapy has emerged as an alternative option for pre-clinical studies in TLE exhibiting the capability to promote tissue regeneration and repair. Unfortunately, studies reported that the transplantation of SCs in a hostile microenvironment resulted in low survival rate, host-tissue reaction, poor neuronal differentiation and integration, and thus in a low therapeutic efficacy (Henriques et al., 2019; Zhao et al., 2021). As organoids recently emerged as a promising source of transplantable tissues and functional cell types, the direct transplantation of murine-derived bioengineered brain organoids into rodents may represent a valuable tool to deeply investigate how neuron integrate into the brain circuitry and their effect on the damaged brain tissue in TLE rat model.

With the aim to develop an innovative therapeutic strategy for TLE based on the transplantation of brain organoids, the starting point of this study was the set up of a standardized protocol for the transplantation of rat hippocampal-derived NSCs combined with the ECM alginate in the ventral CA3 (vCA3) of hippocampus in a TLE rat model and the evaluation of their potential to integrate, differentiate and maturate in the damaged hippocampal circuitry. First, I characterized the rat hippocampal-derived NSCs phenotype *in vitro* in order to investigate their own neuronal differentiation potential. Second, I set up an *in vivo* standardized protocol to successfully transplant rat hippocampal-derived NSCs with or without alginate solution (in collaboration with Prof. Giulia Curia, UNiMORE). Then, I evaluated grafted cell survival, differentiation, and maturation in the hostile environment by immunohistochemical and immunofluorescence analysis.

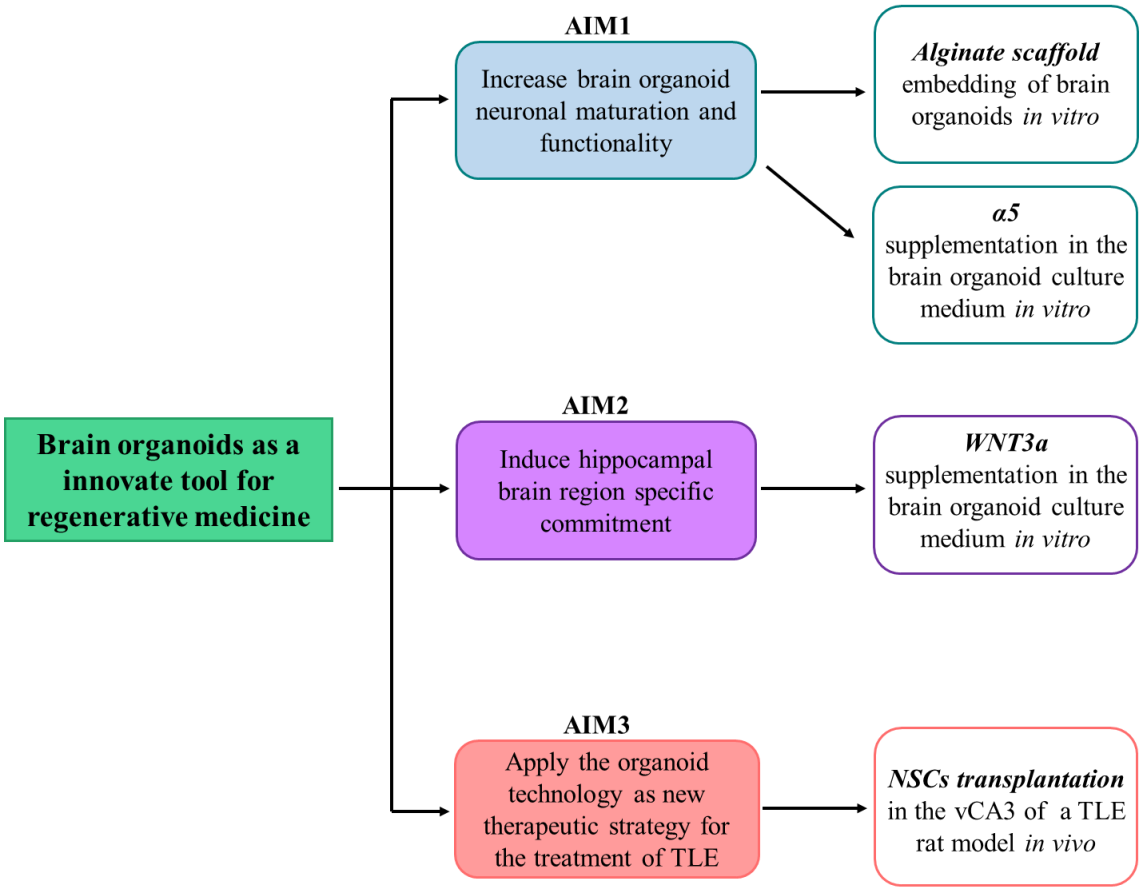

Experimental Plan: *Schematic representation of the three aims of the PhD thesis. First, I aimed to increase the brain organoid neuronal maturation and functionality by using i) the alginate ECM and ii) the α5 mixture in the brain organoid culture media in vitro. Second, I aimed to induce the hippocampal brain region specific commitment by the supplementation of the morphogen WNT3a in the brain organoid culture media in vitro. Finally, I aimed to apply the organoid technology as new therapeutic strategy for the treatment of TLE. The starting point of this last aim is the set up of NSCs transplantation in the vCA3 of a TLE rat model in vivo.*

3. MATERIALS AND METHODS

3.1 *In vitro* cultures

3.1.1 Isolation and culture of murine neural stem cells (NSCs)

Pregnant wild-type (WT) C57Bl/6J female mice and Sprague Dawley female rats were obtained from Charles River Laboratories (Wilmington, MA). Animal housing and all experimental procedures were approved by the Istituto Superiore di Sanita` (I.S.S., National Institute of Health; protocol n. C46F4.N.N4E, Italy) and the Animal Ethics Committee (C.I.R.S.A.L., Centro Interdipartimentale di Servizio alla Ricerca Sperimentale) of the University of Verona (Italy). E14.5 mice subgranular zone (SGZ) was isolated to obtain NSCs and to generate organoids; E18.5 rat hippocampus was isolated to obtain NSCs for intracerebral transplantation in TLE animal model (see *Section 3.3.2*). Briefly, pregnant C57Bl/6J female mice and Sprague Dawley female rats were sacrificed by cervical dislocation; NSCs were extracted from the SGZ of E14.5 embryos' brains and from the hippocampus of E18.5 using fine tweezers under stereo microscope and collected into ice-cold HBSS solution: sterile water, HBSS 10X (GIBCO, Cat#14180-046), HEPES 0.3 M (Sigma, Cat# H3375-250G), 1% Penicillin/Streptomycin (GIBCO, Cat#15140-122). After centrifugation at 300g per 1 min, HBSS was substituted with PBS 1X and then the sample was centrifuged again at 300g for 1 min. The pellet was suspended in a solution containing DNase (Sigma Aldrich) and Trypsin 1X (GIBCO, Cat#25200-056) diluted 1:5; the first round of dissociation was performed using the gentleMACS @Dissociator (Miltenyi Biotec). After incubation for 10 min at 37 °C, other two rounds of dissociation were done. PBS was added to inactivate the enzymes and then the sample was filtered with a cell strainer (40 mm diameter). After 10 min final centrifugation at 300g, samples were suspended in DMEM-F12 (GIBCO, Cat#31331-028) with 2% B27 (GIBCO, Cat#17504-044), 1% N2 (GIBCO, Cat#17502-048), 1% Pen/Strep (GIBCO, Cat#15140-122) enriched with 20ng/ml basic fibroblast growth factor - bFGF (Prepotech, Cat#100-18B) and Epidermal growth factor - EGF (Prepotech, Cat#AF-100-15). Cells were stained with Trypan blue 0.4% (Lonza BioWhittaker, Cat#17942E), counted and cultured as neurospheres in suspension in T75 flasks (Falcon) up to the second passage at 37 °C in a humidified atmosphere of 5% CO2 in air. After 7

– 10 days of culture, neurospheres were collected, centrifuged, mechanically dissociated to a single-cell suspension (Dolci et al., 2017). The mouse SGZ single-cell suspension were used for organoid generation. The rat hippocampus single cells were transduced with a lentivirus carrying the Green Fluorescent Protein (GFP) reporter (LV-CMV-GFP, creative biogene, 1.5 MOI) in order to allow their identification after transplantation in the ventral hippocampal CA3 of LTE rat models (see *Section 3.3.3*).

3.1.2 Brain organoid generation protocol

Brain organoids were obtained starting from E14.5 murine-derived SGZ NSCs (see *Section 3.1.1*). A three-phase organoid generation protocol was developed, each stage relying on a different media composition (see *Section 3.1.3* for media composition of organoid generation protocol). Specifically, the protocol consisted of the i) expansion phase, ii) induction phase and (iii) differentiation phase. The expansion phase starts after the seeding of the single cells (day 0) and lasts 5 days. Briefly, 20000 cells/well were seeded into each well of 24-well plates (Thermofisher) in 500 ml of medium enriched with 20 ng/ml EGF and 20 ng/ml bFGF (*Expansion medium*). During the induction phase, that continues for up to day 14, the concentration of bFGF and EGF was gradually scaled down: first, at day 5, both EGF and bFGF were decreased to a concentration of 10 ng/ml (*Induction medium I*); second, at day 7, bFGF concentration was reduced to 5 ng/ml, while EGF was eliminated altogether (*Induction medium II*). During the last step (differentiation phase), starting at day 15, the organoids were cultured in the *differentiation medium* enriched with 50 ng/ml BDNF (Prepotech, Cat#450-02). Cells plates were kept in continuously agitation (65 rpm) using the ORBi-SHAKER CO2 (Benchmark Scientific) at 37 °C in a humidified atmosphere of 5% CO2 in air for all the culture time. Three different batches of SGZ - NSCs belonging to seven different embryos extraction were used to generate organoids. The organoids used in this work were generated starting from single cells obtained after no more than 3/4 subsequent phases of expansion following tissue isolation.

3.1.3 Media composition of brain organoid generation protocol

- ***Expansion medium*** (day 0-4): DMEM/F-12 GlutaMAX, (GIBCO), 2% B27 supplement (GIBCO), 1% N2 supplement (GIBCO), 1% Pen/Strep (GIBCO), 20 ng/ml EGF, 20 ng/ml bFGF.
- ***Induction medium I*** (days 5-6): DMEM/F-12 GlutaMAX, (GIBCO), 2% B27 supplement (GIBCO), 1% N2 supplement (GIBCO), 1% Pen/Strep (GIBCO), 10 ng/ml EGF, 10 ng/ml bFGF.
- ***Induction medium II*** (days 7-14): DMEM/F-12 GlutaMAX, (GIBCO), 2% B27 supplement (GIBCO), 1% N2 supplement (GIBCO), 1% Pen/Strep (GIBCO), 5 ng/ml bFGF.
- ***Differentiation medium*** (days 15-42): Neurobasal medium (GIBCO, Cat#21103-049), 2% B27 supplement (GIBCO), 1% Pen/ Strep (GIBCO), 0.25% L-glutamine (GIBCO, Cat# 25030081), 50 ng/ml BDNF.

3.1.4 Brain organoid embedding in the vegetal-derived extracellular matrix (v-ECM) Alginate

Embedding in alginate matrix of organoids was performed at day 15 of the generation protocol. For the encapsulation in alginate matrix, the organoids were first plunged in 0.3% (w/v) alginate in HEPES (Sigma, H3375-250G) solution, then transferred to 0.3 mM $CaCl^2$. After 30 minutes in the incubator at 37°C the matrix polymerized, CaCl2 was aspirated, and excess was washed two times with culture medium. The embedded organoids were then cultured with differentiation medium (see *Section 3.1.3*). Cells plates were kept in continuously agitation (65 rpm) using the ORBi-SHAKER CO2 (Benchmark Scientific) at 37 °C in a humidified atmosphere of 5% CO2 in air for all the culture time.

3.1.5 *In vitro* α5 supplementation in brain organoid culture medium

During the differentiation phase (see *Section 3.1.2*) of the organoid generation protocol (*see Section 3.1.2*), 0.5% of α5 and 10mM of Glutamate were added to the culture medium (differentiation medium) for 7 days, from days 15 to 21. Starting from 22 days, brain

organoids were cultured in the differentiation medium (see *Section 3.1.3*) until 28 days. Control organoids were cultured in the standard differentiation medium for all the differentiation phases. Cells plates were kept in continuously agitation (65rpm) using the ORBi-SHAKER CO2 (Benchmark Scientific) at 37 °C in a humidified atmosphere of 5% CO2 in air for all the culture time.

3.1.6 *In vitro* WNT3a supplementation in brain organoid culture medium

During the expansion (days 0-4) and the induction phase (days 5-14) of the brain organoid generation protocol (see *Section 3.1.3*), 5 ng/ml of WNT3a factor (Genetex, Cat#GTX109037-Pro) was added to the culture medium in order to allow the hippocampal commitment of brain organoids. The neuronal differentiation was then reached by providing 50 ng/ml BDNF to the culture media from day 15, as for the standard protocol (see *Section 3.1.2*). Cells plates were kept in continuously agitation (65rpm) using the ORBi-SHAKER CO2 (Benchmark Scientific) at 37 °C in a humidified atmosphere of 5% CO2 in air for all the culture time.

3.2 Cell cultures analyses

3.2.1 Brain organoid analyses

3.2.1.1 Organoid maximum diameter measurements

To determine the organoids' maximum diameter, bright field images were acquired, during the various stages of the protocol (5, 7, 9, 11, 14, 18, 21, 28, 32, 35 and 40d; n>50) using the Axiovert 200M (Carl Zeiss, Munch, Germany) microscope. The maximum diameter was measured using the ''straight line'' tool of ImageJ software (U.S. National Institutes of Health). The pixel obtained value was converted in mm.

3.2.1.2 Viability assay

Organoid viability was assessed using a fluorescence staining solution containing propidium iodide (50%), fluorescein diacetate (50%) and Hoechst (1:1200), freshly prepared the day of the experiment and protected from light. The propidium iodide is an intercalating red fluorescent dye labeling dead cells, fluorescein diacetate is hydrolized to fluorescent fluoresceine in live cells, whereas Hoechst is used for total nuclei staining. Whole mount organoids (n=3 sample/time point) were washed in PBS 1X and incubated for 5 min in the staining solution. Three PBS 1X washes were performed. Then, the samples were fixed in a 4% PFA and 4% sucrose solution for 10 min, before being acquired at Zeiss LSM710 confocal microscope (Carl Zeiss, Munich, Germany). Quantification of the propidium iodide positive cells was done by counting positive cells on total nuclei. Then, the number of viable cells was obtained. The quantification was performed using a specific plugin of ImageJ software (U.S. National Institutes of Health) and a semi-automated cell count.

3.2.1.3 Organoid Immunofluorescence

Murine NSCs-derived organoids were selected at 7, 21, 28, 32 and 36 days after seeding and fixed for 15 min in 4% PFA/4% sucrose, then rinsed and stored in PBS 1X at 4 °C. For cryosectioning, each organoid was embedded in Cryobloc (Diapath, Italy) and cut at 30 µm. After 1 hour of incubation in blocking solution (PBS 1X with 0.25% Triton X-100, 2% bovine serum albumin for cytosolic antigens and PBS 1X with 0.5% Triton X-100, 2% bovine serum albumin (BSA) for nuclear antigens) (Formaggio et al., 2010), sections were incubated with primary antibodies in blocking solution at room temperature for 2 hours. After rinsing 3 times for 10 min in blocking solution, appropriate secondary antibodies were applied for 1.5 hours at room temperature. After final washing steps in blocking solution and then in PBS 1X, nuclear staining with TO-PRO^{TM-3} (1:3000, Molecular Probes-Thermo Fisher Scientific, Cat#T3605) was performed, and slides were mounted using 1,4-Diazabicyclo [2.2.2] octane (DABCO) (Sigma-Aldrich). For whole-mount immunofluorescence staining, whole organoids were incubated in blocking solution (PBS 1X with 0.5% Triton X-100, 2% bovine serum albumin) for 1 hour; then, they were incubated with primary antibodies in blocking solution and kept on a shaker

overnight at 4 °C. After rinsing 3 times for 10 min in PBS 1X, secondary antibodies were applied for 6 hours at room temperature. After final washing steps in PBS 1X, nuclear staining with TOPRO^{TM}-3 or DAPI (InvitrogenThermo Fisher Scientific) was performed; in order to preserve the 3D structure of the organoid, an in-house method was set up, using a parafilm chamber fixed on a glass slide; the whole organoids were inserted in the chamber and mounted using DABCO.

The following primary antibodies were used: anti-SOX2 (goat, 1:200, R&D System, Cat#AF2018), anti-Vimentin (chicken 1:400, Millipore, Cat#AB5733), anti-Ki67 (rabbit, 1:200, Abcam, Cat#ab16667), anti-DCX (rabbit, 1:400, Cell Signaling Technology, Cat#4604), anti-b3Tubulin (mouse, 1:400, Promega, Cat#G7121), anti-MAP2 (mouse, 1:200, Sigma-Aldrich, Cat#M1406), anti-ZBTB20 (rabbit, 1:200, Genetex, Cat#GTX121616), anti-KA1 (rabbit, 1:200, Abcam, Cat#ab67404), anti-GFAP (goat, 1:200, Abcam, Cat#ab53554), anti-synaptophysin (guinea pig, 1:200, Synaptic System, Cat#101004), anti-PSD95 (mouse, 1:200, Millipore, Cat#MAB1596), anti-gephyrin (mouse, 1:200, Synaptic Systems, Cat#147011) and anti-VGAT (guinea pig, 1:400, Synaptic Systems, Cat#131004). Appropriate secondary antibodies were used: donkey anti-mouse Alexa Fluor 488 (donkey, 1:1000, Thermo Fisher Scientific, Cat#A21202), donkey anti-rabbit Alexa Fluor 488 (donkey, 1:1000, Thermo Fisher Scientific, Cat#A21206), donkey anti-guinea pig CY3 (donkey, 1:1000, Jackson Immuno Resarch, Cat#AB2340460), goat anti-mouse CY3 (goat, 1:1000, Amersham, Cat#PA43002), donkey anti-goat Alexa Fluor 546 (donkey, 1:1000, Invitrogen by Thermo Fisher Scientific, Cat#A-11056), goat anti-rabbit CY3 (goat, 1:1000, Amersham, Cat#PA43004), goat anti-chicken Alexa Fluor 546 (goat, 1:1000, Thermo Fisher Scientific, Cat#A11040).

3.2.1.4 Tissue Immunofluorescence

Intact adult mice brain tissues were extracted after animal perfusion in 4% PFA then rinsed in PBS and stored in sucrose 30% at 4°C. Medio-lateral sagittal or coronal sections were cryosectioned at 35 µm throughout the entire samples. Slides were stored at -20 °C. Immunostaining on cryosections was performed after 30 min incubation in blocking

solution (PBS 1X with 0.25% Triton X-100, 2% bovine serum albumin). Sections were then incubated with primary antibodies in blocking solution overnight at 4°C. After rinsing 6 times for 5 min in blocking solution, appropriate secondary antibodies were applied for 4 hours at room temperature. After final washing steps in blocking solution and then in PBS 1X, nuclear staining with TOPRO^{TM}-3 (Invitrogen Thermo Fisher Scientific) was performed and slides were mounted using DABCO (Sigma-Aldrich).

The following primary antibodies were used: anti-GSX2 (rabbit, 1:200, Genetex, Cat#GTX129390), anti-FOXG1 (rabbit, 1:200, Abcam, Cat#18259), anti-NKX2.1 (mouse, 1:200, Genetex, Cat#GTX34907), anti-Frizzled9 (rabbit, 1:200, Genetex, Cat#GTX71581), anti-PreAlbumin (chicken, 1:200, Genetex, Cat#GTX85112)anti-OCT6 (rabbit, 1:200, Abcam, Cat#ab272925), anti-PROX1 (rabbit, 1:200, Abcam, Cat#ab101851). Appropriate secondary antibodies were used: donkey anti-rabbit Alexa Fluor 488 (donkey, 1:1000, Thermo Fisher Scientific, Cat#A21206), goat anti-mouse CY3 (goat, 1:1000, Amersham, Cat#PA43002), goat anti-rabbit CY3 (goat, 1:1000, Amersham, Cat#PA43004), goat anti-chicken Alexa Fluor 546 (goat, 1:1000, Thermo Fisher Scientific, Cat#A11040).

3.2.1.5 Immunofluorescence image acquisition, analysis and quantification

Immunofluorescence imaging of sliced and whole-mount organoids was performed using a 40x and 63x oil objective of confocal microscope (Carl Zeiss LSM710 confocal microscope, Munich, Germany). Both reconstruction of 3D images and quantification were performed using a specific plugin of ImageJ software (U.S. National Institutes of Health) and a semiautomated cell count. Organoid quantification was done in blind. For Alginate-embedded and WNT3a organoids, the quantification of positive-immunoreactive cells for Ki67, Vimentin, SOX2, DCX, TUBB3, ZBTB20, KA1, GFAP and MAP2 was done by counting positive cells over the total number of nuclei (TOPRO^{TM}-3) per field. Instead, quantification of organoid supplemented with α5 was done by measuring the area of SOX2, TUBB3 and MAP2 positive cells over the total fluorescence organoid sliced area. Synaptic density was expressed as synaptophysin (Syn) -positive area against the MAP2^{+} neuronal cells area. For the quantification of organoid marker expression, at least 3 slices for each organoid sample were analyzed,

from n ≥ 3 different organoids. For whole-mount staining, at least 10 plane sections were acquired and analyzed for each organoid Statistical differences between marker expression at different time points were calculated by unpaired t-test for two datasets. $P < 0.05$ was considered statistically significant.

3.2.1.6 Intracellular calcium imaging in organoids

To test spontaneous calcium activity, WNT3a-treated organoids at different time points (7d: n=2; 14d: n=3; 21d: n=3; 32d: n=3) were assessed with Fluo-4 Direct Calcium Assay Kit (Invitrogen). CTRL (n=7) and α5-treated organoids (n=7) at 28d of maturation were likewise assessed. For calcium dye loading, the organoids were first incubated 10 min with HEPES pH 7.3 (Sigma, H3375-250G), rinsed and then with equal parts of physiological salt solution (PSS) pH 7.4 (140mMNaCl, 5mMKCl, 1.2mMNa2PO4, 1.4mMMgCl2, 1.8mM CaCl2, 11.5 mM glucose, 10 mM HEPES) and Fluo-4 acetoxymethyl ester solutions for 3 hours at 37 °C. Excess dye was removed by washing with culture medium, and a 30-min incubation was done at 37 °C in order to allow the complete de-esterification of the dye and avoid artifacts such as continuous increase in fluorescence intensity during the experiment. Imaging was carried out at 37 °C and 5% CO2 using epifluorescence microscopy optics (Eclipse Ti Nikon Microscope), while the organoids were placed in glass bottom 96-well cell imaging plate (Eppendorf #0030741030), maintained in the appropriate culture medium (see *media composition of organoid generation protocol, 3.1.3 Section*). Time-lapse imaging was performed at 1 frame/100 ms for 3 min using 10x and 20x objective (Nikon Ti Eclipse fluorescent microscope) and then processed using ImageJ software. For calcium imaging analysis the intensity signal of the calcium indicator of different cells of interest (n=10/organoid) within the organoids over the entire time of acquisition was measured using the ‘‘Plot Z-axis profile’’ plugin of ImageJ. The fluorescence change over time was defined as DF/F=(F-Fbasal)/Fbasal, where F is the fluorescence of a ROI at a specific time point and Fbasal is the corresponding fluorescence of a background area. Cells were considered active when at least a change in the fluorescence intensity (peak) was detected. For each ROI corresponding to a selected cell within an organoid, the number of intensity fluorescence peaks were counted and expressed as mean of peaks per minute.

3.2.1.7 RNAseq Analysis

Total RNA was extracted from 14 samples (7d organoids: n=3 pools of 3 organoids each, 14d organoids: n=3 pools of 3 organoids each, 30d organoids: n=3 pools of 3 organoids each, adult – 3 months – cerebral tissue: n=3, P0 cerebral tissue: n=2) using the RNeasy Plus Micro Kit (Qiagen, Cat No. 74034) according to the manufacturer's protocol and RNA integrity was evaluated using the Fragment Analyzer (Agilent Technologies). RNAseq library preparation was performed starting from 100 ng high-quality total RNA using the ''TruSeq Stranded mRNA library prep kit'' (Illumina, San Diego, USA). Briefly, the mRNA fraction was purified from total RNA by polyA capture, fragmented and subjected to cDNA synthesis. Barcoded DNA adapters were ligated to both ends of the double-stranded cDNA and subjected to PCR amplification. The library products were evaluated using Fragment Analyzer (Agilent Technologies), then sequenced on an Illumina NextSeq500 sequencer using 75bp single-end reads, generating about17 million reads per sample. Quality control was conducted using the software Scythe (v0.991) and Sickle (v1.33). Transcript expression levels were then quantified in each sample by running the computer software Salmon v.1.0.0 against the reference sequence of the mouse transcriptome (Gencode M23-GRCm38).

Differential expression analysis on sequence count data was performed using negative binomial distribution models as implemented in the library DESeq2 of R software (https://www.r-project.org/), using the Benjamini-Hochberg method to adjust the p-values for multiple comparisons. Transcript expression fold-changes were estimated for each expressed transcript in every comparison. The most relevant upregulated genes were then summarized into biological processes and molecular functions by an enrichment analysis based on gene ontologies as implemented in the library dnet of R. Gene Set Variation Analysis was performed using the package GSVA (ver 1.38.2) of R to identify functionally enriched gene sets.

Selected gene lists were adapted from literature: (i) neural stem cell dataset, neuronal progenitors (Bifari et al., 2020); (ii) mature neurons (Bifari et al., 2020; Cahoy et al., 2008; Y. Zhang et al., 2014); (iii) astrocytes (Boisvert, Erikson, Shokhirev, & Allen, 2018; Y. Zhang et al., 2014); (iv) inhibitory synapses and excitatory synapses (Hayamizu,

Mangan, Corradi, Kadin, & Ringwald, 2005); (v) hippocampal development (Lein, Zhao, & Gage, 2004; Wheeler et al., 2015). The possible contribution from hippocampal (H) cells in the organoid tissue based on gene expression was estimated by investigating different proportions of H cells into the organoid tissue according to gene expression profiles of selected genes (hippocampal signature: Zbtb20, Sipa1l3, Gpr161, Crlf1, Glis3, Dcx, Nrp2, Tgf2b, Gria1, Tnip2, Slc39a6, Prox1, Slc26a10, Trpc6, Neurod1, C1ql2, Gqrik4, Elavl2, Elavl4, Dkk3, Nectin3, Scip, Spock1) defining hippocampal phenotype. For each gene lists and different amounts of H cells, it was calculated the sum of the difference of gene expression levels (log-TMP transformed values) with the organoid sample (7d organoids: n=3 pools of 3 organoids each, 14d organoids: n=3 pools of 3 organoids each, 30d organoids: n=3 pools of 3 organoids each) under investigation. The difference between samples was estimated as the normalized values of the squared differences between samples (H and organoid tissues). Lower overall values of differences suggested a higher confidence of the suggested proportion H cells in the organoid tissue. In order to validate the selected gene list, we performed the above analysis by including adult murine hippocampal tissue (adult – 3 months – hippocampal tissue: n=3). A low value of differences was obtained by hippocampal samples, thus suggesting reliability of the analysis performed.

3.2.1.8 Quantitative RT-PCR analysis for SGZ-NSCs characterization and hippocampal phenotype

Total RNA was extracted from 4 different SGZ-NSCs samples (500000 cells/sample) and from 6 different mature (32d) organoids sample (3 CTRL organoids: n=3 pools of 6–8 organoids each, 3 WNT3a-treated organoids: n=3 pools of 6–8 organoids each) using the RNeasy Plus Micro Kit (Qiagen, Cat No. 74034) according to the manufacturer's protocol and RNA abundance was evaluated using the NanoDropOne/OneC Microvolume UV-Vis Spectrophotometer (ThermoFisher Scientific). Reverse transcription was carried out using Superscript VILO Master Mix (Invitrogen, Thermo-Fisher Scientific, #11755050, Waltham, USA). Expression level of specific hippocampal or embryonic and neural stem cells genes (see Table S7) was quantified by Sybr Green-based real-time quantitative RT-

PCR (7900HT Real-time PCR System, Applied Biosystems) according to the DDCt method and by using Tbp and Gapdh as reference genes for data normalization.

3.2.2 Rat hippocampal-derived NSCs analyses

3.2.2.1 Rat hippocampal-derived NSCs immunofluorescence

Cells were plated onto poly-D-lysine coated glass slides and fixed with 4% paraformaldehyde (PFA, Mondial, Cat#FM0622). Non-specific binding sites were blocked by incubation in a blocking solution (0.25% Triton X-100, 2% BSA). Cells were incubated with primary antibodies in blocking solution for 2 hours at room temperature, washed three times with blocking solution and appropriate secondary antibodies in blocking solution were applied for 1.5 hours at room temperature. After three washes in PBS 1X, slides were incubated for 10 min with the nuclear dye 4'.6-Diamidino-2-Phenylindole (DAPI, 1:2000, Thermo Fisher Scientific, Cat#D-1306) and coated glass slices were mounted using 1.4-Diazabicyclo (2.2.2) octane (DABCO, Sigma Aldrich, Cat#D-2522).

The following primary and secondary antibodies were used: anti-Ki67 (rabbit, 1:200, Abcam, Cat#ab16667), Cleaved Caspase-3 (Asp175) Antibody (rabbit, 1:200, Cell Signalling, Cat#9661), anti-SOX2 (goat, 1:200, R&D System, Cat#AF2018), anti-Vimentin (chicken 1:400, Millipore, Cat#AB5733), anti-DCX (rabbit, 1:400, Cell Signaling Technology, Cat#4604), anti-β3Tubulin (mouse, 1:400, Promega, Cat#G7121), anti-MAP2 (mouse, 1:200, Sigma-Aldrich, Cat#M1406), NeuN (mouse, Millipore, Cat#MAB377, 1:200). Appropriate secondary antibodies were used: donkey anti-rabbit Alexa Fluor 546 (donkey, 1:1000, Thermo Fisher Scientific, Cat#A10040), donkey anti-goat Alexa Fluor 546 (donkey, 1:1000, Invitrogen by Thermo Fisher Scientific, Cat#A-11056), goat anti-chicken Alexa Fluor 546 (goat, 1:1000, Thermo Fisher Scientific, Cat#A11040), donkey anti-rabbit Alexa Fluor 488 (donkey, 1:1000, Thermo Fisher Scientific, Cat#A21206), donkey anti-mouse Alexa Fluor 488 (donkey, 1:1000, Thermo Fisher Scientific, Cat#A21202), DAPI (1:2000, Invitrogen Thermo Fisher Scientific, Cat#D-1306).

3.2.2.2 Immunofluorescence image acquisition, analysis and quantification

Immunofluorescence imaging of rat hippocampal NSCs were acquired using a 20x objective of Nikon Ti Eclipse fluorescent microscope. For each glass slides, 5 fields were acquired and for each field 2x2 large images were taken. Quantification was done using a specific plugin of ImageJ software (U.S. National Institutes of Health) and a semiautomated cell count. Quantification of positive-immunoreactive cells for Ki67, Caspase-3, Vimentin, SOX2, DCX and TUBB3 was performed by counting positive cells over the total number of nuclei (DAPI) per field.

3.3 Animal model

3.3.1 Temporal Lobe Epilepsy (TLE) rat model

All experimental procedures were approved by Istituto Superiore di Sanità (I.S.S., National Institute of Health; protocol N.154/2014-B, Italy) and the Animal Ethics Committee (Centro Servizi Stabulario Interdipartimentale) of the University of Modena - Reggio Emilia (Italy). The Temporal Lobe Epilepsy (TLE) was performed as described (Curia et al., 2008; Turski et al., 1983). Briefly, 380 mg/kg of pilocarpine were intraperitoneally injected in seven-week-old Sprague Dawley male rats of about 200 g (n=22) to induce *status epilepticus* (SE). The pilocarpine injection was preceded by scopolamine methyl nitrate (1 mg/kg, i.p.) administration to prevent the peripheral effects of cholinergic stimulation (Curia et al., 2008). Rats were monitored for up to 4 hours after pilocarpine injection, and behavioral manifestations were scored according to a modified Racine's scale (Racine, 1972) (see *Section 3.3.3*). In all rats experiencing SE, a cocktail of ketamine/diazepam (20/4 mg/kg, i.p.) was injected 30 min after the SE onset to stop convulsive SE and reduce mortality. Spontaneous recurrent seizures usually appear between 2 and 4 weeks after SE resulting in the epileptic condition (chronic phase). Rats not experiencing SE were excluded from the experimental group. This work is in collaboration with Dr. Giulia Curia, University of Modena – Reggio Emilia, Italy.

3.3.2 Status epilepticus (SE) evaluation

The evaluation of the SE in TLE rats was carried out according to Racine Score System (Racine, 1972) **(Table 1)**. Briefly, animals were motionless for 5–10 min after pilocarpine administration and subsequently were monitored in order to observer oro-facial movements, salivation, eye-blinking, twitching of vibrissae, and yawning. This activity persisted up to 45 min. Then, discontinuous seizures were observed 30 min after injection and lasted up to 90–150 min, before giving way to limbic motor seizures with intense salivation, rearing, upper extremity clonus, and falling. Such seizures were observed every 5–15 min, presenting maximal frequency after 1–2 hours. After pilocarpine injection, around 60% of the rats successfully developed SE (Cavalheiro et al., 1991).

Table 1: *Racine Score System: status epilepticus evaluation*

RATE	BEHAVIOUR
0	No reaction/subclinical
1	Stereotype mouthing automatisms Facial automatisms Eye blinking Mild facial clonus Freezing/stearing
2	Head nodding Severe facial clonus Head tremors
3	Myoclonic jerks in the forelimbs Limb clonus Body clonus Jumps Body tremors
4	Rearing Clonic convulsions Tonic-clonic convulsions maintaining posture
5	Rearing and falling Straub tail Tonic – clonic convulsions with loss of posture
6	**Status Epilepticus (SE)**

3.3.3 *In vivo* rat hippocampal-derived NSCs transplantation in TLE rat model

In order to inject the NSCs avoiding increase in the intracranial pressure, the ventral hippocampal area was first ablated using the cytotoxic agent ibotenic acid (IBO). Since implant of NSCs were performed 4 days after IBO treatment (Hampson, Jarrard, & Deadwyler, 1999), in order to reduce the number of major surgeries, a coaxial canula was implanted in each hemisphere (coordinates: AP -0.55 mm; ML ± 0.45 mm; DV -0.15 mm), of which the inner channel was used as guide for IBO and NSCs injection. Briefly, four weeks after SE, rats were bilaterally injected, through a stereotaxic apparatus, with the cytotoxic agent ibotenic acid (1 mg/ml in PBS 1X, 0.3 µl, 1 µl/min) in the ventral hippocampal CA3 area in order to induce localized brain lesion. IBO was injected at specific coordinates accordingly with the "The Rat Brain in Stereotaxic Coordinates" (George Paxinos and Charles Watson, Academic Press, 2004): right hemisphere above Dental Gyrus (DG): Antero-Posterior (AP): -0.55 mm; Medio-Lateral (ML): ± 0.45 mm; Dorso-Ventral (DV): -0.35 mm; left hemisphere above Hippocampus (HPC): AP: -0.55 mm; ML: ± 0.45 mm; DV: -0.15 mm. Four days after IBO injection, TLE rats received infusion in the right and left hemispheres of GFP rat hippocampal-derived NSCs alone ($1.5*10^6$ cells in NaCl/HEPES 135/20 mM for a total of 5 µl) or in combination with the vegetal matrix Mg^{2+}-alginate ($1.5*10^6$ cells + 50% Mg^{2+}-alginate labeled with the fluorophore Alexa fluo 568, fluorescent RED; 25 % NaCl/HEPES 135/20 mM; 25% Ca^{2+} 8 mM – for a total of 5 µl) at specific coordinates (right hemisphere above DG: AP -0.55 mm; ML ± 0.45 mm; DV -0.35 mm; left hemisphere above HPC: AP -0.55 mm; ML ± 0.45 mm; DV -0.15 mm), through a stereotaxic apparatus. The solution was injected at a rate of 1 µl/min for a total of 5 µl by using a 27G needle and a 10 µl Hamilton syringe attached to a microinjector apparatus. Pre-operatory operations included a subcutaneous injection of Baytril (5 mg/kg) and Rimadyl (5 mg/kg). 500 µl of Saline solution were subcutaneously administered at the end of the surgical procedure. During all the surgical procedure rats were anesthetized with 2% isoflurane and maintained under anesthesia. This work is in collaboration with Dr. Giulia Curia, University of Modena – Reggio Emilia, Italy.

3.4 Brain tissue analyses

3.4.1 Brain fixation and processing

Animals were intracardially perfused with 4% paraformaldehyde (PFA) and 4% sucrose. Brains were extracted, incubated overnight in 4% PFA, 4% sucrose, and stored in 30% sucrose at 4°C. For histochemical analysis, brains were embedded with Optimal Cutting Temperature compound (OCT) and cryo-sectioned (35 µm-thick coronal sections) and stored at -20 °C before analysis.

3.4.2 Hematoxylin and Eosin staining

Coronal sections of brain tissue were immunostained for Hematoxylin and Eosin. Briefly, frozen slides were thawed for 1 min in PBS 1X, incubated for 4 min with Hematoxylin solution (DiaPath, cat#CP813) diluted 1:20 in water and then rinsed in tap water until the water was colorless. The brain slides were stained for 1 sec with alcoholic Eosin-solution (DiaPath, Cat#CO353) and washed again in tap water. Then, the sections were hydrated with an increased EtOH concentrations: 50% EtOH for 30 sec, 70% EtOH for 30 sec and 95% ETOH for 30 sec. The slides were cleared with Xilene (Carlo Erba) and finally were mounted with Entellan (Merck-Millipore) for light microscopy analysis (Zeiss Axioscop 2).

3.4.3 Brain tissue immunofluorescence

Cryosections were blocked for 1 hour in 0.5% Triton X-100, 2% BSA, and incubated with primary antibodies in blocking solution overnight at 4 °C. After rinsing 6 times for 5 min in blocking solution, appropriate secondary antibodies were applied for 4 hours at room temperature. After final washing steps in blocking solution and then in PBS 1X, nuclear staining with TO-PRO^{TM-3} (1:3000, Invitrogen Thermo Fisher Scientific, Cat#T3605) or 4'.6-Diamidino-2-Phenylindole (DAPI, 1:2000, Thermo Fisher Scientific, Cat#D-1306) was performed and slides were mounted using 1.4-Diazabicyclo (2.2.2) octane (DABCO, Sigma Aldrich, Cat#D-2522). Images were acquired using a 40x oil objective (Carl Zeiss

LSM710 confocal microscope, Munich, Germany), and 10x and 20x objective (Nikon Ti Eclipse fluorescent microscope).

The following primary antibodies were used: Cleaved Caspase-3 (Asp175) Antibody (rabbit, 1:200, Cell Signalling, Cat#9661), anti-SOX2 (goat, 1:200, R&D System, Cat#AF2018), anti-Vimentin (chicken 1:400, Millipore, Cat#AB5733), anti-β3Tubulin (mouse, 1:400, Promega, Cat#G7121), anti-MAP2 (mouse, 1:200, Sigma-Aldrich, Cat#M1406), anti-NeuN (mouse, Millipore, Cat#MAB377, 1:200) and anti-GFP (rabbit, 1:400, Invitrogen, Cat#A11122). Appropriate secondary antibodies were used: donkey anti-rabbit Alexa Fluor 546 (donkey, 1:1000, Thermo Fisher Scientific, Cat#A10040), donkey anti-goat Alexa Fluor 546 (donkey, 1:1000, Invitrogen by Thermo Fisher Scientific, Cat#A-11056), goat anti-chicken Alexa Fluor 546 (goat, 1:1000, Thermo Fisher Scientific, Cat#A11040), goat anti-mouse CY3 (goat, 1:1000, Amersham, Cat#PA43002), donkey anti-rabbit Alexa Fluor 488 (donkey, 1:1000, Thermo Fisher Scientific, Cat#A21206), TO-PRO^{TM-3} (1:3000, Molecular Probes-Thermo Fisher Scientific, Cat#T3605) or DAPI (1:2000, Invitrogen Thermo Fisher Scientific, Cat#D-1306).

3.5 Statistical analyses

Statistical differences were calculated by two-tailed unpaired t-test for two datasets and ordinary one-way or two-way analysis of variance (ANOVA) test for multiple datasets using GraphPad Prism software (GraphPad Inc., La Jolla, CA, version 7.0). Data are shown as mean ± SEM and statistical significance was set at $p < 0.05$. ****$p < 0.0001$; ***$p < 0.001$; **$p < 0.01$; *$p < 0.05$; ns=no statistical differences.

4. RESULTS

4.1 Alginate matrix improves neuronal differentiation and maturation of mouse brain organoids and preserves the organoid structure

The possibility to obtain *in vitro* 3D brain organoids from neural stem cells represents a potentially exploitable procedure for cell-based treatment of neurodegenerative diseases (Mansour et al., 2018). We set up a protocol for 3D culture starting from neural stem cells (NSCs) from the subgranular zone (SGZ), coupled to a biocompatible, low-immunogenic ECM of vegetal origin (Alginate). We isolated and cultured *in vitro* NSCs from the SGZ, a well-known stem cell niche (Pino et al., 2017), of mouse brain embryos (E14.5) following a three-step culture (Ciarpella et al., 2021). During the first phase of the protocol, referred to as "*expansion phase*" (days 0–4), the SGZ-derived NSCs were seeded at a specific cell density (20,000 cells/well) (Lancaster & Knoblich, 2014a) in each well of a 24-well plate (day 0) and kept in dynamic culture in growth media (DMEM/F12-Glutamax, 2% B27, 1% N2 and 1% Penicillin/Streptomycin) supplemented with 20 ng/mL of epidermal growth factor (EGF) and 20 ng/mL of basic fibroblast growth factor (bFGF). At this phase, cells started to self-assemble into neurospheres. To reduce cell proliferation and trigger cell differentiation, we subsequently lowered the growth factors concentration to 10 ng/mL EGF and bFGF (day 5) and then 5 ng/mL bFGF (day 7) (induction phase, days 5–13). To support the organoid structural organization and to provide a favorable microenvironment for *in vitro* development of brain organoids, we introduced the use of ECM-like matrix. In particular, among the commercially available ECMs (Nicolas et al., 2020), we took advantages by the use of alginate hydrogel, a marine polysaccharide that is highly biocompatible, low-immunogenic and extremely tunable in elasticity to resemble brain tissue mechanical properties (Johnson, Craig, & Mercer, 1997; Palazzolo, Broguiere, Cenciarelli, Dermutz, & Zenobi-Wong, 2015). The alginate embedding occurred at day 14, in correspondence of the *Differentiation Phase* of the protocol. To specifically induce neuronal differentiation and maturation, in this late stage of culture we also supplemented the culture medium with 50 ng/mL of brain-derived neurotrophic factor (BDNF) (*Differentiation phase*, days 14–40), a key molecule which is involved in neural development and function, and is required to increase neurite

number, length and complexity, as well as dendritic spine density in primary 2D NSC-derived neuronal cultures (A. Silva, Pereira, Oliveira, Relvas, & Rego, 2009) **(Figure 15)**.

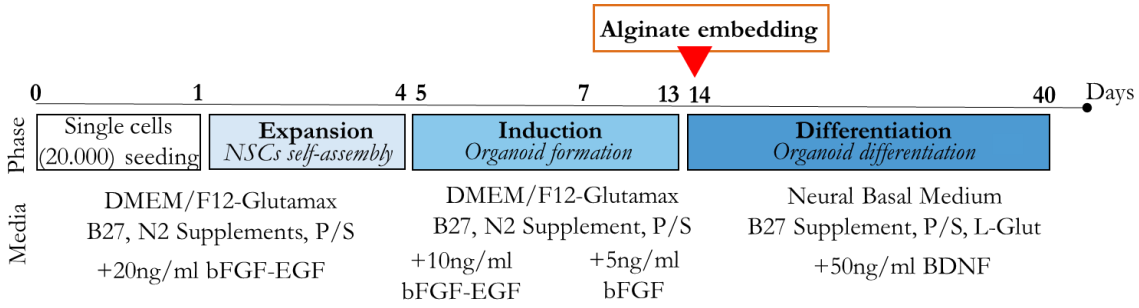

Figure 15: Time course representation of the three-phase alginate-embedded organoid generation protocol. *The three-phase organoid generation protocol is characterized by three phases: the Expansion phase, the Induction phase and the Differentiation phase. After single cell seeding (20,000 cells/well) on a 24-well plate (day 0), the protocol starts with the Expansion Phase (days 0-4) in which NSCs proliferate and neurospheres form in a culture medium enriched with 20ng/ml of bFGF and EGF. The Induction phase (days 5-13) is characterized by early organoid formation in a culture medium supplemented with gradual decrease of bFGF and EGF concentrations (day 5 to day 6: bFGF and EGF both 10ng/ml; day 7 to day 13: bFGF 5ng/ml). The alginate embedding (orange box) was performed at day 14, in correspondence of the Differentiation phase. The Differentiation phase (day 14-40) is characterized by organoids maturation in differentiation medium (medium supplemented with BDNF 50ng/ml). In all the three phases, organoids were maintained on an orbital shaker (dynamic culture). Adapted from (Ciarpella et al., 2021).*

To evaluate the impact of alginate on organoid growth, we firstly characterized and compared the morphology, viability, and cell proliferation.

Firstly, to investigate the effect of alginate embedding on the cell proliferation rate, immunofluorescence analysis using the specific marker of the G1/S cell cycle phase Ki67 was performed during the Induction (day 7) and the Differentiation phase (day 32) **(Figure 16A and B)**. Results showed that at 7 days in culture, the percentage of Ki67-expressing cells was 41.38%±12.42% of the total nuclei cells (n=4, **Figure 16B**) in control organoids and it was significantly (****p<0.0001) reduced by the end of the differentiation phase (day 32) (8.02%±0.57%, n=24, **Figure 16B**). Interestingly, at day 32, alginate-embedded organoids showed a lower number of proliferative cells (CTRL organoids: 8.02%±0.57%, n=24 vs alginate-embedded organoids: 2.34%±0.37%, n=18, *p<0.05, **Figure 16B**) compared to control organoids.

Then, in order to assess the organoids' cell viability, we evaluated the percentage of dead cells at day 20 and day 40 of the organoid maturation by quantifying the number of cells incorporating the propidium iodine (Jiajia et al., 2017). At day 20, control and alginate-embedded organoids showed a similar percentage of dead cells (CTRL and alginate – embedded organoids_day 20: 5.730%±0.48% of the total cells, n=3/condition, **Figure 16C**). A difference was observed at day 40. At this time point, the percentage of dead cells significantly increased in control organoids compared to alginate-embedded organoids (CTRL organoids_day 40: 18.69%±1.72% vs alginate-embedded organoids_day 40: 6.58%±1.87%, n=3/condition, **p<0.01, **Figure 16C**).

Lastly, we investigated the organoid size and morphology by analyzing the maximum diameter in organoids cultured for up to 40 days (n=250) and we found that the maximum diameter of organoids increased during the Induction phase reaching a peak of 1.164mm±0.25mm (day 11) while it decreased at a later stage of differentiation (CTRL organoids: 0.754±0.09 mm at day 21; 0.598±0.07 mm at day 28; 0.578±0.09 mm at day 32; 0.503±0.00 mm at day 40, **Figure 16D and E**). The presence of alginate matrix did not impact the organoid growth and morphology (alginate-embedded organoids: 0.705±0.11 mm at day 21; 0.472±0.05 mm at day 28; 0.460±0.05 mm at day 32; 0.496±0.00 mm at day 40, **Figure 16D and E).** Overall, these data indicated that the use of alginate as ECM provides structural and trophic support to the brain organoids and suggested that it could impact the cellular maturation.

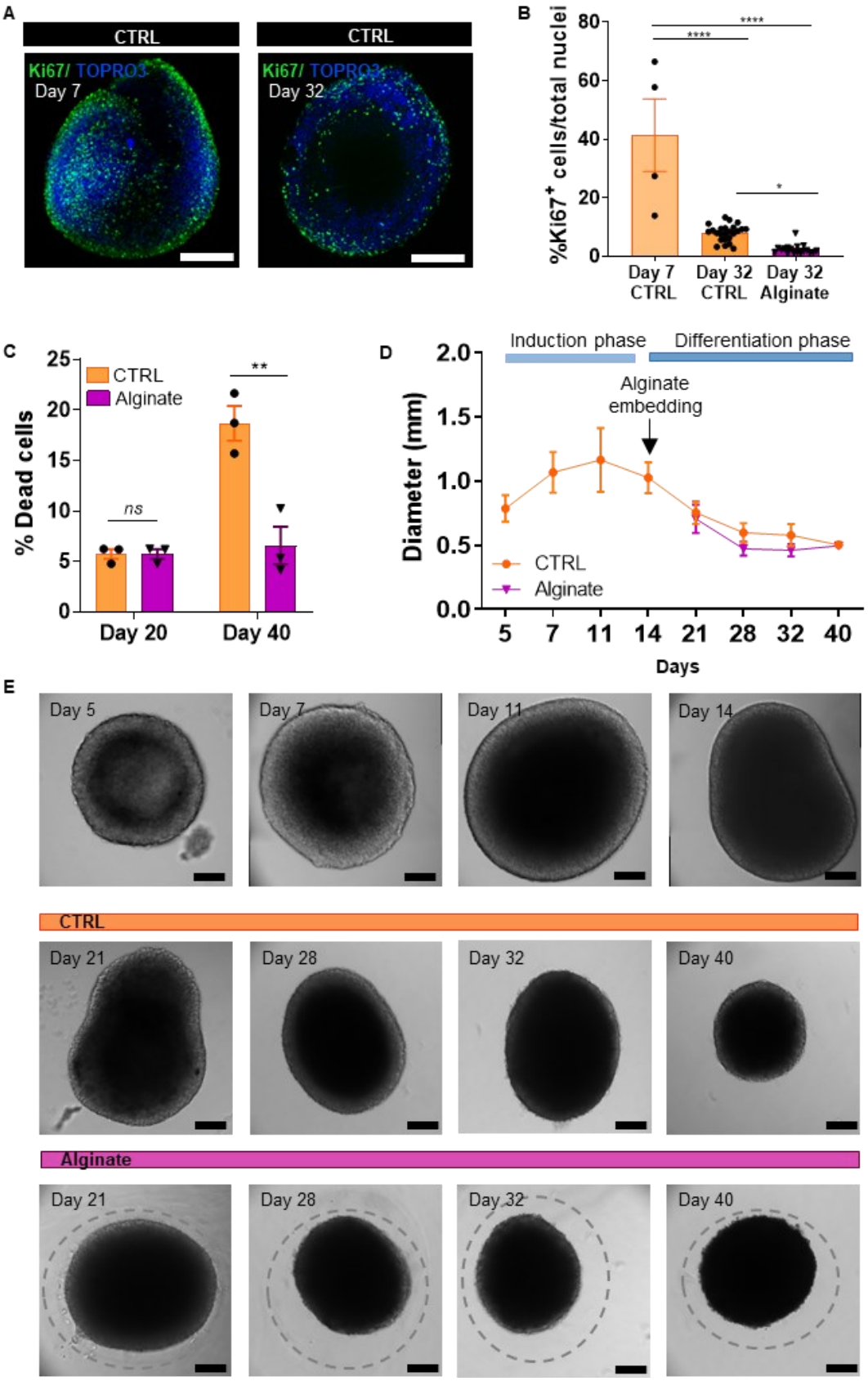
A
CTRL
CTRL
Ki67/ TOPRO3
Day 7
Ki67/ TOPRO3
Day 32
B
%Ki67+ cells/total nuclei
80
60
40
20
0
****
****
*
Day 7 CTRL
Day 32 CTRL
Day 32 Alginate
C
% Dead cells
25
20
15
10
5
0
CTRL
Alginate
**
ns
Day 20
Day 40
D
Induction phase
Differentiation phase
Alginate embedding
Diameter (mm)
2.0
1.5
1.0
0.5
0.0
CTRL
Alginate
5
7
11
14
21
28
32
40
Days
E
Day 5
Day 7
Day 11
Day 14
CTRL
Day 21
Day 28
Day 32
Day 40
Alginate
Day 21
Day 28
Day 32
Day 40

Figure 16: Assessment of alginate-embedded organoid growth, cell survival and proliferation. (A) *Representative confocal whole-mount immunofluorescence images of a control organoid (CTRL) at day 7 (Induction phase) and at day 32 (Differentiation phase) showing $Ki67^+$ (green) cells. TOPRO3: total nuclei.* ***(B)*** *Graph showing the percentage of $Ki67^+$ cells normalized for the total nuclei in CTRL and alginate-embedded organoids at day 7 and 32. Analysis performed on n=3/time point organoids and at least 10 entire Z-stack sections for each organoid.* ***(C)*** *Graph representing the percentage of dead cells among the total cells at day 20 and day 40 in CTRL and alginate-embedded organoids. Analysis performed on n=3/time point organoids.* ***(D)*** *Graph representing the growth curve (maximum diameter, mm) of CTRL and alginate-embedded organoids at different time points (day 5, 7, 11, 14, 21, 28, 32 and 40). Data are expressed as mean ± SEM of the maximum diameter (n=250).* ***(E)*** *Representative brightfield images of the time-course of CTRL and alginate-embedded organoids development (day 5, 7, 11, 14, 21, 28, 32 and 40). Grey dotted circles delimit the alginate scaffold. Scale bars: 200 µm. Data in all graphs are expressed as mean ± SEM. Differences between experimental conditions were analyzed using one-way and two-way ANOVA followed by Tukey post-test. *p<0.05, **p<0.01, **** p < 0.0001, ns: no statistical differences.*

4.1.1 Alginate increases brain organoid neuronal maturation

In order to assess the influence of alginate on the brain organoid differentiation and maturation, we assessed the expression of the specific immature neuronal marker Beta3 Tubulin (TUBB3), of the mature neuronal marker Microtubule-Associated Protein 2 (MAP2) and of the presynaptic vesicle protein synaptophysin (Syn) marker in control and alginate-embedded organoids at day 21 and day 36 by immunofluorescence analysis **(Figure 17A, C, D and E)**.

At day 36, alginate-embedded organoids showed a significantly lower number of $TUBB3^+$ cells compared to control organoids (CTRL organoids_day 36: 32.22%±1.76%, n=6 vs alginate-embedded organoids_day 36: 17.11%±3.39%, n=4, **p<0.01, **Figure 17B**), although the neuronal cells appeared to be differentiated to a greater extent than in control organoids. As shown in **Figure 17C**, in control organoids mature $MAP2^+$ neuronal cells (day 36) were characterized by elongating processes forming a neuronal net covering the whole 3D structure. Moreover, $MAP2^+$ cells were found to co-localize with Syn expression in both control and alginate-embedded organoids **(Figure 17D and E)**. As expected, during the differentiation and maturation processes (day 21 and day 36), both control and alginate-embedded organoids showed a significant progressive increase of $MAP2^+$ cells (CTRL organoids_day 21: 22.52%±1.14%, n=10 vs CTRL

organoids_day 36: 30.95%±1.76%, n=16, ***p<0.001; alginate-embedded organoids_day 21: 8.165%±1.00%, vs alginate-embedded organoids_day 36: 17.11%±3.39%, n=6/time point, *p<0.05, **Figure 17F**). Interestingly, at each of the analysed time points, alginate-embedded organoids showed a significantly lower content of $MAP2^+$ cells compared to control organoids (CTRL organoids_day 21: 22.52%±1.14%, n=10 vs alginate-embedded organoids_day 21: 8.16% ±1.00%, n=6, ****p<0.0001; CTRL organoids_day 36: 30.95%±1.76%, n=16 vs alginate-embedded organoids_day 36: 17.11%±3.39%, n=6, *** p<0.001, **Figure 17F**). In line with the overall increase of $MAP2^+$ cells across organoid differentiation and maturation stages, we observed an increased expression of the Syn marker both in control (CTRL organoids_day 21: 0.25%±0.03%, n=11 vs CTRL organoids_day 36: 1.42%±0.18%, n=14, ****p<0.0001, **Figure 17G**) and alginate-embedded organoids (alginate-embedded organoids_day 21: 0.34%±0.04%, n=17 vs alginate-embedded organoids_day 36: 1.76%±0.84%, n=12, *p<0.05, **Figure 17G**). Notably, while at day 21 the Syn expression was similar between the two groups, at day 36 alginate-embedded organoids expressed a higher number of Syn^+ punctae compared to control organoids (CTRL organoids_day 36: 1.42%±0.18%/100 μm^2, n=14 vs alginate-embedded orgnaoids_day 36: 1.76±0.84%/100 μm^2 vs, n=12, **Figure 17G**). Accordingly with these results, at day 36 the synaptic density, expressed as Syn^+ area against the area covered by the $MAP2^+$ neuronal cells, was significantly increased in alginate-embedded organoids as compared to control organoids (CTRL organoids_day 36: 7.31%±2.01%, n=5 vs alginate-embedded organoids_day 36: 16.77±1.76%, n=4, *p<0.05, **Figure 17H**). Overall, these results suggested that the alginate scaffold promotes neuronal maturation by increasing the Syn expression.

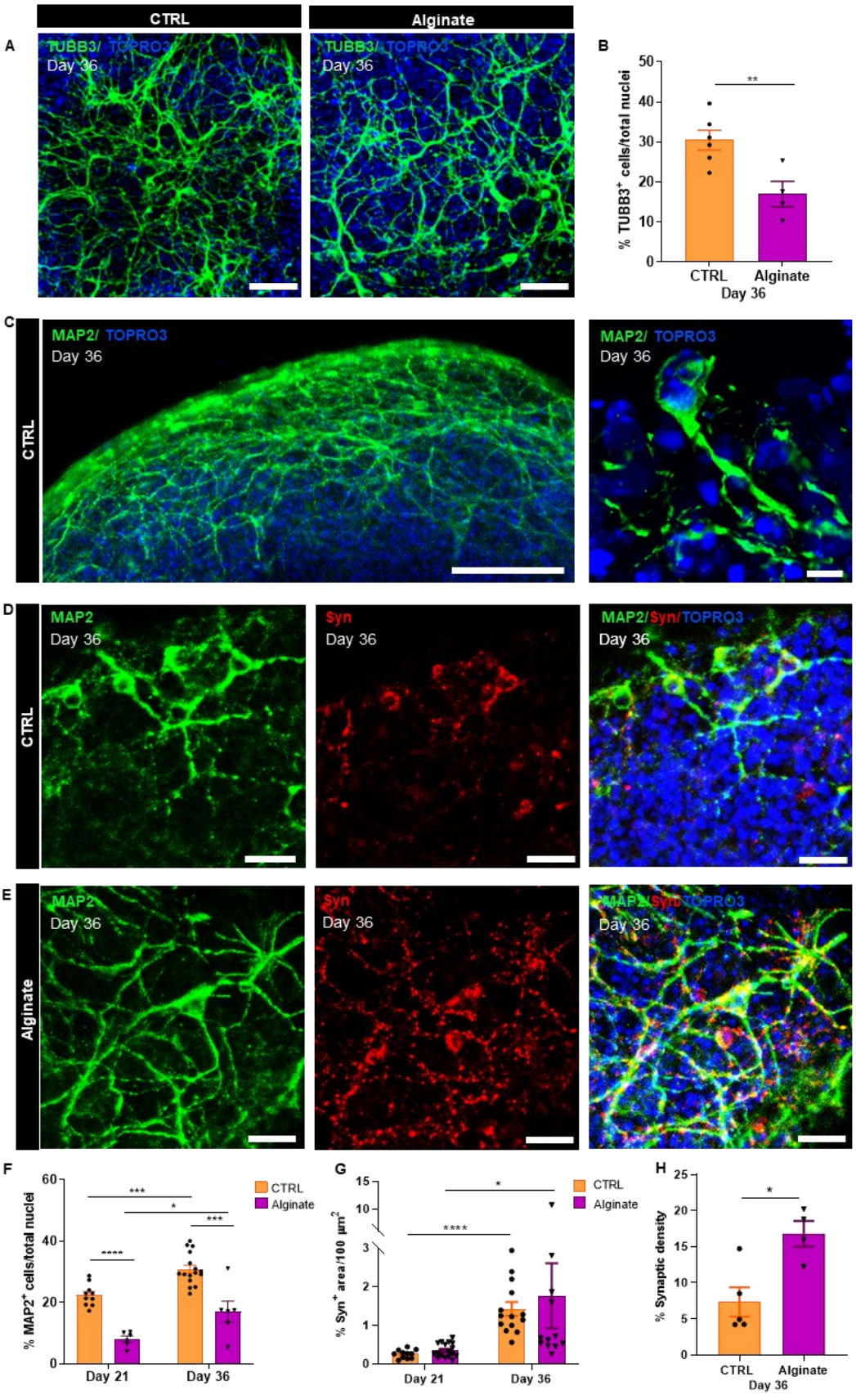
CTRL
Alginate
A
TUBB3/ TOPRO3
Day 36
B
% TUBB3+ cells/total nuclei
CTRL
Alginate
Day 36
C
MAP2/ TOPRO3
Day 36
D
MAP2
Syn
MAP2/Syn/TOPRO3
E
F
% MAP2+ cells/total nuclei
Day 21
Day 36
G
% Syn+ area/100 µm2
H
% Synaptic density

***Figure 17: Alginate promotes neuronal maturation**. **(A)** Representative confocal immunofluorescence images of sliced CTRL (left panel) and alginate-embedded (right panel) organoids at day 36 immunostained for the specific immature neuronal (TUBB3, green) and nuclei (TOPRO3) markers. Scale bar: 50 µm. **(B)** Graph showing the percentage of TUBB3$^+$ cells normalized for the total cell nuclei in CTRL and alginate – embedded organoids at day 36. **(C)** Left: representative maximum Z-projection of confocal images of whole mount of a control (CTRL) organoid at day 36 immunostained for the specific mature neuronal (MAP2, green) and nuclei (TOPRO3) markers, showing the neuronal net covering the whole organoid. Scale bar: 200 µm. Right: Magnification of an immunofluorescent image of a CTRL organoid stained for MAP2 (green) and nuclei (TOPRO3) markers, showing a mature neuronal cell with elongated processes integrated inside the organoid 3D structure. Scale bar: 20 µm. **(D, E)** Representative confocal immunofluorescence images of sliced CTRL **(D)** and alginate-embedded **(E)** organoids immunostained for MAP2 (green) and for the specific presynaptic vesicle protein Synaptophysin (Syn, red) at day 36. TOPRO3: total nuclei. Scale bars: 50µm. **(F)** Graph showing the percentage of MAP2$^+$ cells normalized for the total cell nuclei in CTRL and alginate-embedded organoids at day 21 and day 36. **(G)** Graph representing the percentage of Syn$^+$ area in 100µm^2 in CTRL and alginate-embedded organoids at day 21 and day 36. The analysis was performed across 10-12 confocal images, collected in three independent experiments/time point. **(H)** Graph showing the synaptic density (expressing as Syn$^+$ area against the area covered by the MAP2$^+$ neuronal cells) in CTRL and alginate-embedded at day 36. All the images in **A, B, C** and **D** are maximum intensity projections of z stack confocal acquisitions. Analysis performed on n≥3 different organoids and at least 3 entire sections for each organoid. Data in all graphs are expressed as mean ± SEM. Differences between experimental conditions were analyzed using Two-way ANOVA followed by Tukey post-test. p-value < 0.05 was considered statistically significant. ∗p< 0.05; ∗∗p< 0.01; ∗∗∗p< 0.001; ∗∗∗∗p< 0.0001.*

4.1.2 Alginate enhances synapses formation in brain organoids

Considering the increased synaptic density observed in alginate-embedded organoids at a later stage (day 36) **(Figure 17)**, we further assessed the capability of cells within the organoids to develop neuronal networks. First, we evaluated the presence of synapses by looking at the co-localization of inhibitory and excitatory presynaptic and postsynaptic punctae in control and alginate-embedded organoids at intermediate (day 21) and mature (day 36) stages. Specifically, excitatory synaptic components were identified by the presynaptic marker Syn and the post-synaptic marker PSD95 **(Figure 18A-C)**, while GABAergic inhibitory synapsis were identified by analyzing the presence of the presynaptic marker Vgat and the postsynaptic marker gephyrin **(Figure 18D-F)**. We found that excitatory synapses were formed in both control and alginate-embedded

organoids and that their number increased with maturation. While in control organoids the increase in number of synapses was not statistically significant (CTRL organoids_day 21: 11.59%±2.62%/100 μm^2, n=14 vs CTRL organoids_day 36: 20.18%±7.35%/100 μm^2, n=21, **Figure 18C**), alginate-embedded organoids showed a significant increase of the synaptic puncta number (alginate – embedded organoids_day 21: 70.28%±11.8%/100 μm^2 vs alginate-embedded organoids_day 36: 204.1%±45.52%/100 μm^2, n=17/time point, **p<0.01, **Figure 18C**). Interestingly, we observed that at day 36 the number of synaptic punctae was significantly higher in alginate-embedded organoids compared to control organoids (CTRL organoids_day 36: 20.18%±7.35%/100 μm^2, n=21 vs alginate-embedded organoids_day 36: 204.1%±45.52%/100 μm^2, n=17, ****p<0.0001, **Figure 18C**), suggesting that alginate scaffold may enhance the maturation of neuronal cells and thus the formation of a potentially functional neuronal networks. Looking at the inhibitory GABAergic synapses **(Figure 18D-F)**, we found their presence in both control and alginate-embedded organoids with an increment along the maturation process, especially in alginate embedded-organoids, although not significantly (CTRL organoids_day 21: 6.54%±2.92%/100 μm^2, n=12 vs alginate-embedded organoids_day 21: 15.56%±3.63%/100 μm^2 , n=13; day 36: CTRL organoids_day 36: 28.82%±5.74%/100 μm^2, n=11 vs alginate-embedded organoids_day 36: 41.67%±12.57%/100 μm^2, n=19, **Figure 18F**). Overall, these results indicated that alginate increases the formation of synapses, thus increasing the neuronal network within brain organoids.

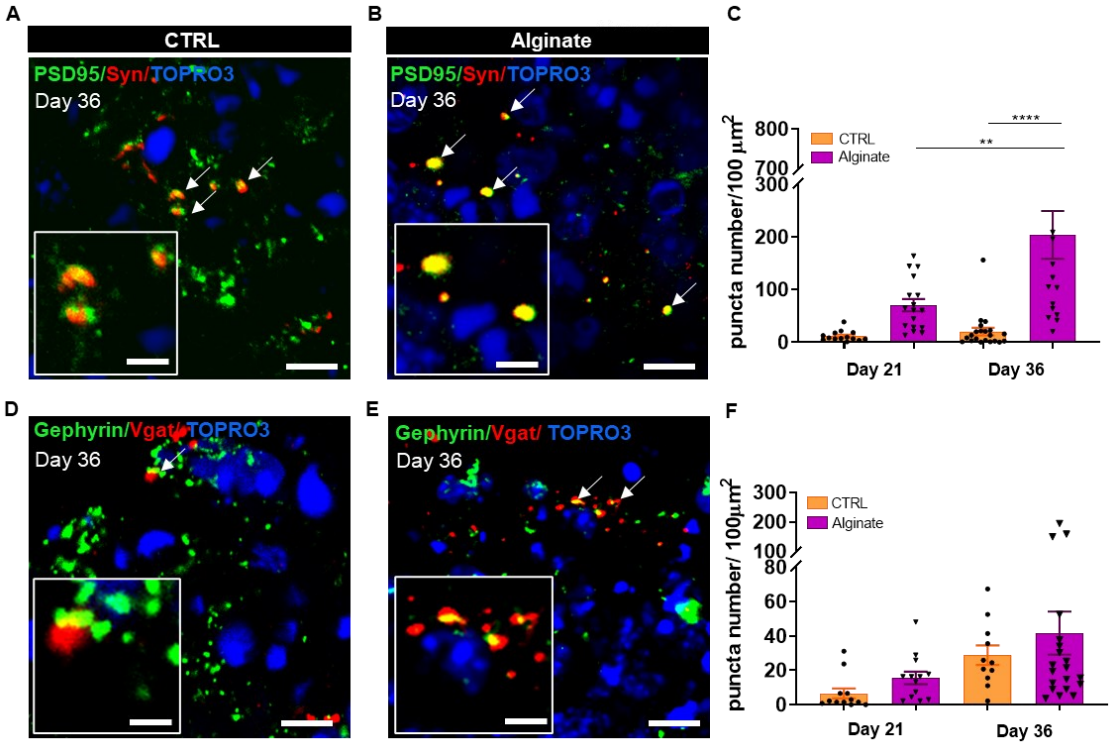

Figure 18: Alginate increases neuronal network formation. ***(A, B)*** *Representative confocal images of the pre-synaptic (Syn$^+$, red) and post-synaptic (PSD95$^+$, green) excitatory punctae in sliced CTRL* ***(A)*** *and alginate-embedded organoids* ***(B)*** *at day 36. TOPRO3: total nuclei. Scale bars: 5 µm. Inserts are higher magnification images of representative punctae co-localization indicated by white arrows. Scale bars: 1 µm.* ***(C)*** *Graph showing the quantification of Syn$^+$ and PSD95$^+$ co-localization expressed as mean number of synaptic puntae in 100µm^2 in CTRL and alginate-embedded organoids at 21 and 36 days.* ***(D, E)*** *Representative confocal images of the pre-synaptic (Gephyrin$^+$, green) and post-synaptic (Vgat$^+$, red) GABAergic punctae in sliced CTRL* ***(D)*** *and alginate-embedded organoids* ***(E)*** *at day 36. TOPRO3: total nuclei. Scale bars: 5 µm. Inserts are higher magnification images of representative punctae co-localization indicated by white arrows. Scale bars: 1 µm.* ***(F)*** *Graph representing the quantification of Gephyrin$^+$ and Vgat$^+$ co-localization expressed as mean number of synaptic puntae in 100µm^2 in CTRL and alginate-embedded organoids at 21 and 36 days. All the images in* ***A, B, D*** *and* ***E*** *are maximum intensity projections of z stack confocal acquisitions. Analysis performed in 5-10 fields (63X objective) from each organoid (n=3 CTRL organoids; n=3 alginate – embedded organoids). Data in all graphs are expressed as mem ± SEM. Differences between experimental conditions were analyzed using Two-way ANOVA followed by Tukey post-test. p-value < 0.05 was considered statistically significant. **p < 0.01; ****p < 0.0001.*

4.1.3 Alginate reduces the number of astrocytes in brain organoids

In order to provide a complete cellular phenotype characterization of control and alginate-embedded organoids, we evaluated at day 36 the expression of several markers specific for astrocytes (Glial Fibrillary Acid Protein, GFAP), oligodendrocytes (Olig2) and microglial cells (Iba1) **(Figure 19A)**. Control and alginate-embedded showed the presence of GFAP positive astrocytes. At day 36 the $GFAP^+$ cell content in alginate-embedded organoid was significantly lower compared to control organoid (CTRL organoids_day 36: 8.49%±1.00%, n=5 vs alginate-embedded organoids_day 36: 2.14%±0.24%, n=10, *$p<0.05$, **Figure 19B**), suggesting that alginate did not influence the astrocytic differentiation and that it may favor neuronal rather than astrocyte differentiation. This result was also confirmed by using selective plane illumination microscopy (SPIM) imaging of control and alginate-embedded organoids at 36 days stained for MAP2 and GFAP markers **(Figure 19C)**. Interestingly, the analysis of Olig2 and Iba1 expression in control and alginate-embedded organoids showed no oligodendrocytes nor microglia cells detectable at day 36.

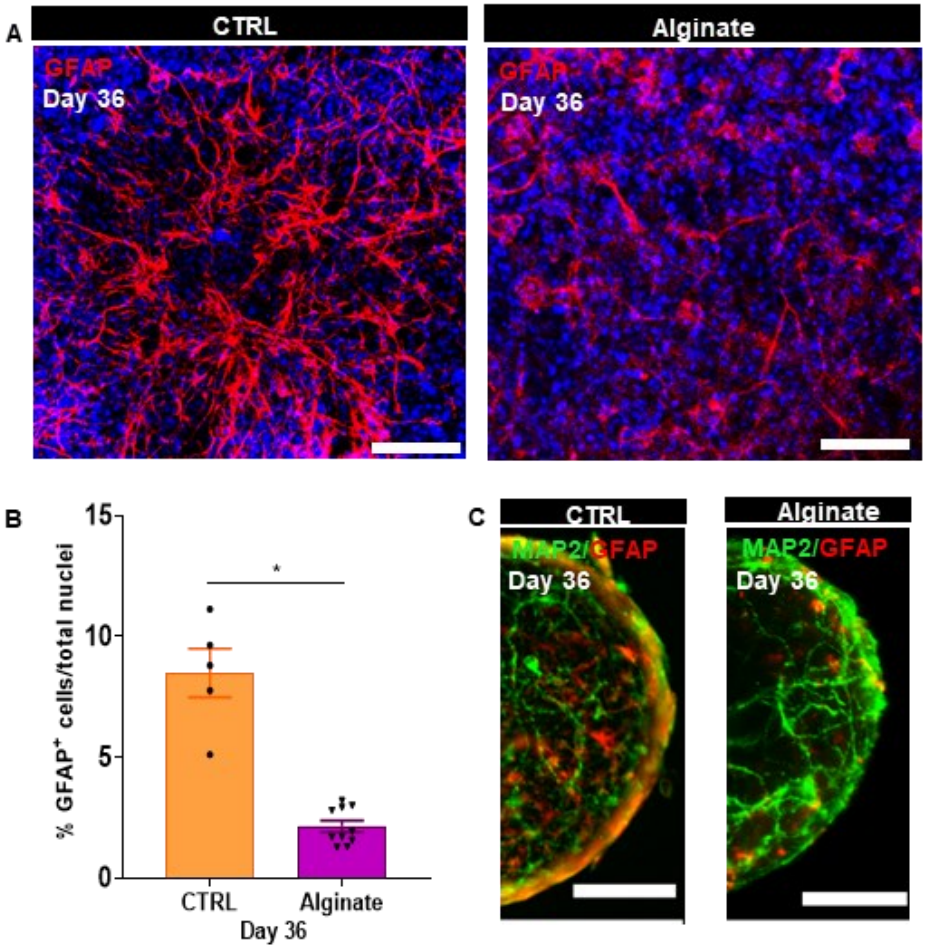

Figure 19: Alginate decreases astrocytic differentiation at mature developmental stages. ***(A)*** *Representative confocal high magnification images showing the GFAP⁺ glial cells (red) in sliced CTRL (left panel) and alginate-embedded (right panel) organoids at day 36. TOPRO3: total nuclei. Scale bars: 100 µm.* ***(B)*** *Graph representing the percentage of GFAP⁺ cells normalized for the total cell nuclei in CTRL and alginate – embedded organoids at day 36.* ***(C)*** *SPIM microscopy images of organoids immunolabeled with MAP2 (green) and GFAP (red) markers at day 36. All the images in* ***A*** *are maximum intensity projections of z stack confocal acquisitions. Analysis performed on n≥3 different organoids and at least 3 entire sections for each organoid. Data in all graphs are expressed as mean ± SEM. Differences between experimental conditions were analyzed using two-tailed unpaired t-test for two datasets (CTRL vs alginate). p-value < 0.05 was considered statistically significant. ⁎p< 0.05.*

4.2 α5 supplementation improves the differentiation and maturation of mouse brain organoids

The modulation of cellular metabolism has been proposed to drive the NSC neuronal differentiation through a metabolic shift towards oxidative phosphorylation. Bifari et al. in 2020 showed that metabolic precursor administration (known as α5) enhanced NSC neuronal maturation improving the OXPHOS metabolism in neuronal cells *in vitro*, increasing the total dendritic length, the mean number of branches and the number and maturation of the dendritic spines (Bifari et al., 2020). In addition, pharmacological modulation of neuronal phenotype and maturation has been proposed as an attractive therapeutic opportunity for the treatment of neurological diseases (Dolci et al., 2022). Considering the effects of metabolic precursors administration on neuronal maturation, we assessed the effects of α5 supplementation on brain organoid differentiation and maturation. We modulated the previously established protocol (Ciarpella et al., 2021) by adding, during the Differentiation phase, for 7 days (from day 14 to 21), to the culture media 0.5% of α5 and 10mM of Glutamate, that is known to support functional recovery and long-term neurons survival and neuronal differentiation (Mattson, 2008) **(Figure 20)**.

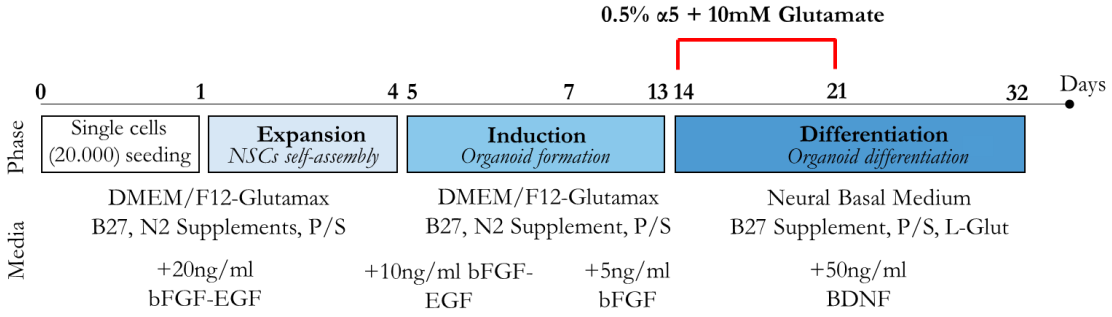

Figure 20: Schematic representation of the three-phase α5-organoid generation protocol. *The three-phase organoid generation protocol is characterized by three phases: the Expansion phase, the Induction phase and the Differentiation phase. After single cell seeding (20,000 cells/well) on a 24-well plate (day 0), the protocol starts with the Expansion Phase (days 0-4) in which NSCs proliferate and neurospheres form in a culture medium enriched with 20ng/ml of bFGF and EGF. The Induction phase (days 5-13) is characterized by early organoid formation in a culture medium supplemented with gradual decrease of bFGF and EGF concentrations (day 5 to day 6: bFGF and EGF both 10ng/ml; day 7 to day 13: bFGF 5ng/ml). The Differentiation phase (day 14-32) is characterized by organoids maturation in differentiation*

medium (medium supplemented with BDNF 50ng/ml). Supplementation of 0.5% of α5 and 10mM of Glutamate occurred during the differentiation phase, from day 14 to 21 (red line). In all the three phases, organoids were maintained on an orbital shaker (dynamic culture). Adapted from (Ciarpella et al., 2021).

Firstly, we assessed the effect of α5 supplementation on growth and morphology of NSCs-derived brain organoids by analysing the maximum diameter of organoids cultured for up to 32 days ($n \geq 50$ for time point). Results showed that that the maximum diameter of organoids increased during the Induction phase reaching a peak of 0.730±0.054 mm at day 9 *in vitro*, while it decreased at a later stage of differentiation (CTRL organoids: 0.638±0.052 mm at day 14; 0.580±0.028 mm at day 18; 0.610±0.019 mm at day 21; 0.581±0.022 mm at day 32, **Figure 21A and B**). Of note, α5 supplementation did not significantly impact the morphology of the brain organoids (α5-organoids: 0.609±0.038 mm at day 14; 0.543±0.037 mm at day 18; 0.588±0.024 mm at day 21; 0.564±0.017 mm at day 32, **Figure 21A and B**). These data indicated that α5-organoids developed with consistent size throughout the different phases of the protocol, showing no significant differences from the control counterpart.

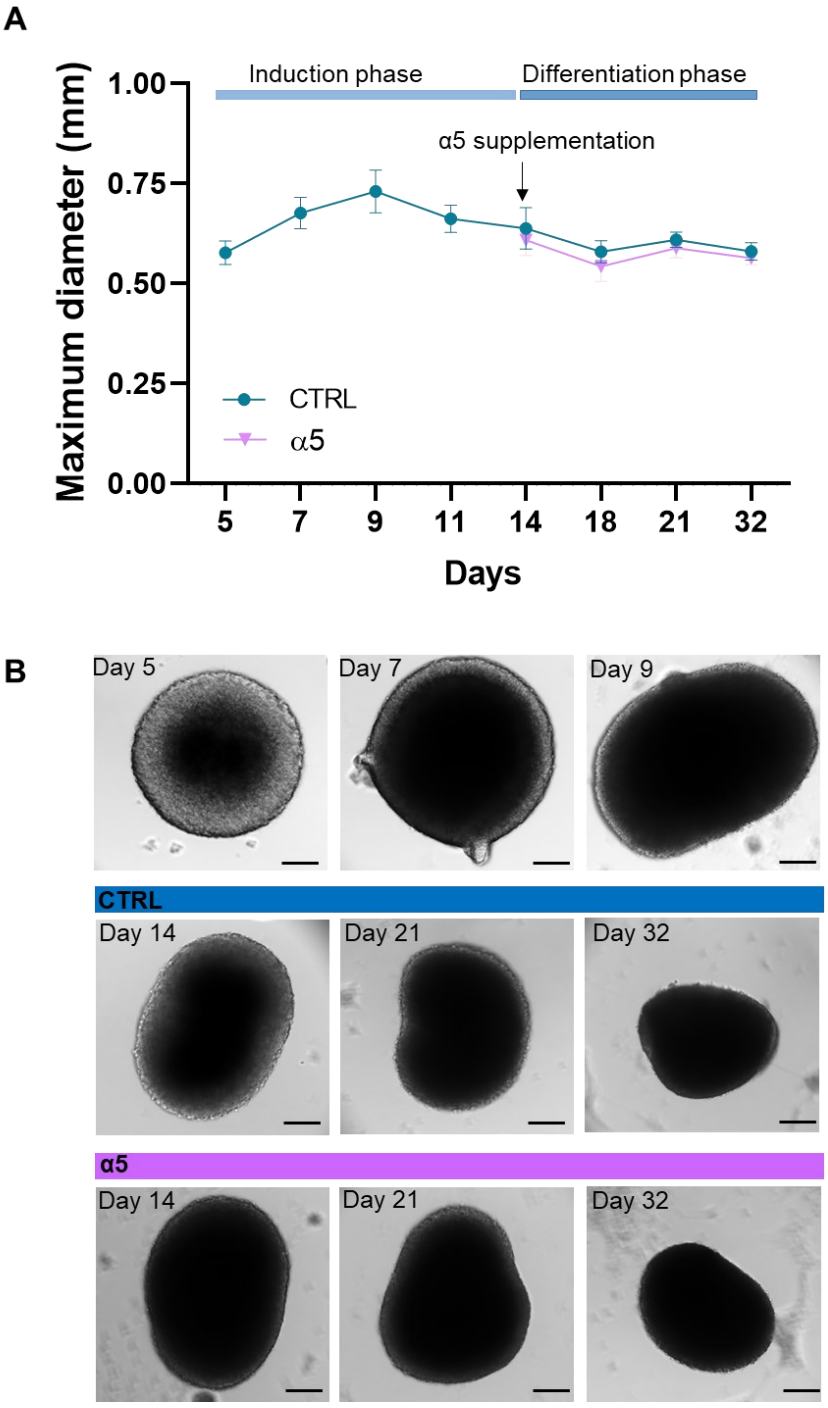

Figure 21: α5-organoid growth and morphology during different stages of the protocol. ***(A)*** *Graph representing the growth curve (maximum diameter, mm) of control (blue line) and α5-(pink line) organoids at different time points (day 5, 7, 9, 11, 14, 18, 21, 32). Data are expressed as mean ± SEM of the maximum diameter (n ≥ 50/time point).* ***(B)*** *Representative brightfield images of the time-course of control and α5-organoids development (day 5, 7, 9, 14, 21, 32). Scale bars: 200µm.*

To evaluated whether α5 supplementation influenced organoid differentiation and maturation, we analysed the expression of markers related to stemness (sex determining region Y-box 2, SOX2), immature neurons (TUBB3) and mature neurons (MAP2) by immunofluorescence analysis at intermediate (day 21) and mature (day 32) phases of organoid development **(Figure 22A-E)**. Moreover, to assess the maturation of MAP2-expressing neurons, we analysed at the same time points the expression of the presynaptic marker synaptophysin (Syn) **(Figure 22D and F)**. The analysis of SOX2 expression, revealed no significant differences between control and α5-organoids (CTRL organoids_day 21: 10.63%±0.82% vs α5-organoids_day 21: 9.26%±0.98%, n=3/condition; CTRL organoids_day 32: 7.11%±2.00% vs α5-organoids_day 32: 9.72%±1.95%, n=4/condition, **Figure 22A and B**). Interestingly, we observed, at each time point considered, a significant increase of the $TUBB3^+$ area in α5-organoids compared to control organoids (CTRL organoids_day 21: 9.75%±0.77% vs α5-organoids_day 21: 16.02%±1.70% vs, n=4/condition, *p<0.05; CTRL organoids_day 32: 7.43%±0.64% vs α5-organoids_day 32: 13.15%±1.78%, n=6/condition, *p<0.05, **Figure 22A and C).** In line with these data, results showed that α5 supplementation significantly increased $MAP2^+$ area and thus the amount of mature neurons compared to control organoids at both day 21 (CTRL organoids_day 21: 12.12%±0.72% vs α5-organoids_day 21: 18.15%±1.98%, n=4/condition, *p<0.05, **Figure 22D and E**) and day 32 (CTRL organoids_day 32: 10.17%±1.01% vs α5-organoids_day 32: 16.03%±1.11%, n=3/condition, *p<0.05, **Figure 22D and E**). Moreover, as shown in **Figure 22D**, at day 32, mature neurons ($MAP2^+$) formed a dense and structured layer in correspondence to the organoid surface, characterized by processes converging toward the formation of a potentially functional neuronal net. Indeed, at day 32, the analysis of the Syn^+ expression revealed an increasing trend of its expression in α5-organoids compared to control organoids (CTRL organoids_day 32: 5.06%±1.45% vs α5-organoid_day 32: 6.56%±0.58%, n=3/condition, **Figure 22D and F**).

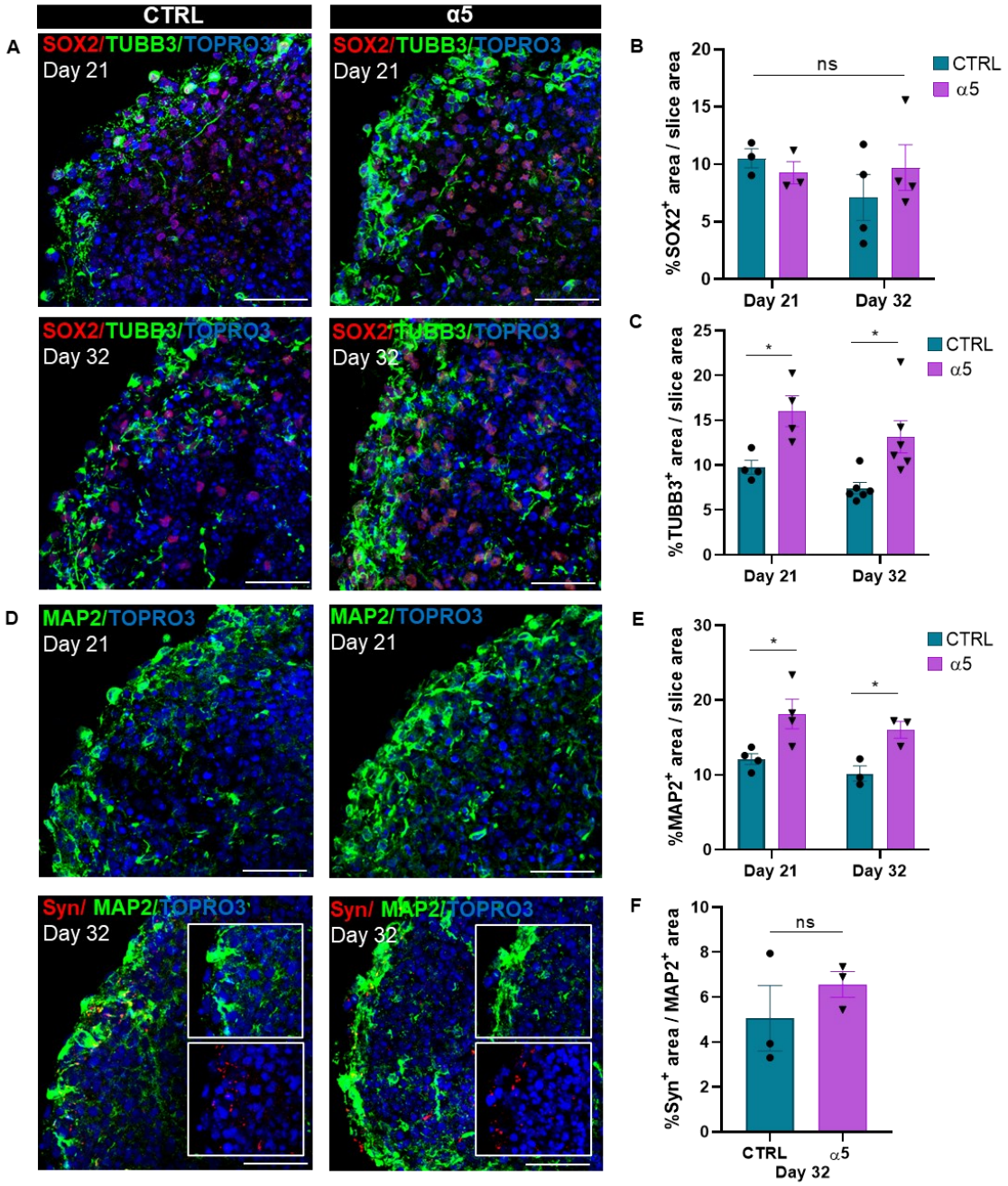

Figure 22: Brain organoids show an increment of neuronal differentiation and maturation after α5 supplementation. ***(A)*** *Representative confocal images of sliced control (left panels) and α5-organoids (right panels) at day 21 and day 32 immunostained for the stemness (SOX2, red) and immature neurons (TUBB3, green) markers. TOPRO3: total nuclei. Scale bar: 50 μm.* ***(B, C)*** *Graphs representing the quantification of the percentage of SOX2⁺ area* ***(B)*** *and TUBB3⁺* ***(C)*** *normalized for the total slice area at day 21 and day 32.* ***(D)*** *Representative confocal images of control (left panels) and α5-organoids (right panels) at day 21 and day 32 showing the mature neuron marker (MAP2, green) and the colocalization of the mature neuron (MAP2, green) and the pre-synaptic (Syn, red) markers. TOPRO3: total nuclei. White*

*boxes in the lower panels in **D** are higher magnification of the dense and structured layer of mature neurons (MAP2$^+$) near the surface of the organoid, expressing the Syn marker at day 32. Scale bar: 50 µm. **(E, F)** Graphs representing the quantification of the percentage of MAP2$^+$ area normalized for the total slice area at day 21 and day 32 **(E)** and Syn$^+$ area relative to MAP2$^+$ area at day 32 **(F)**. All the images in **A** and **D** are maximum intensity projections of z stack confocal acquisitions. Analysis performed on n≥3 different organoids and at least 3 entire section for each organoid. Data in all graphs are expressed as mean ± SEM. Differences between experimental conditions were analyzed using two-way ANOVA followed by Tukey post-test and two-tailed unpaired t-test for two datasets (CTRL vs α5). p-value < 0.05 was considered statistically significant. ⁎p< 0.05. ns=no statistical differences.*

Considering the increasing trend in Syn expression in α5-organoids, we then assessed the cellular activity of selected cells within control and α5-organoids. Therefore, we performed live calcium imaging analysis using Fluo4-AM. Specifically, we evaluated the fluorescence intensity signal of a chemical calcium indicator commonly used to monitor Ca^{2+} activity (Fluo4-AM) (Gee et al., 2000) **(Figure 23A-C)**. Results showed that at day 32, after 3 minutes of live-imaging recording, the mean peaks number for each organoid, was significantly higher in α5-organoids compared to control organoids (CTRL organoids_day 32: 3.07±0.86 peaks/min vs α5-organoids 5.914±0.50, *p <0.05, n=7, **Figure 23C**).

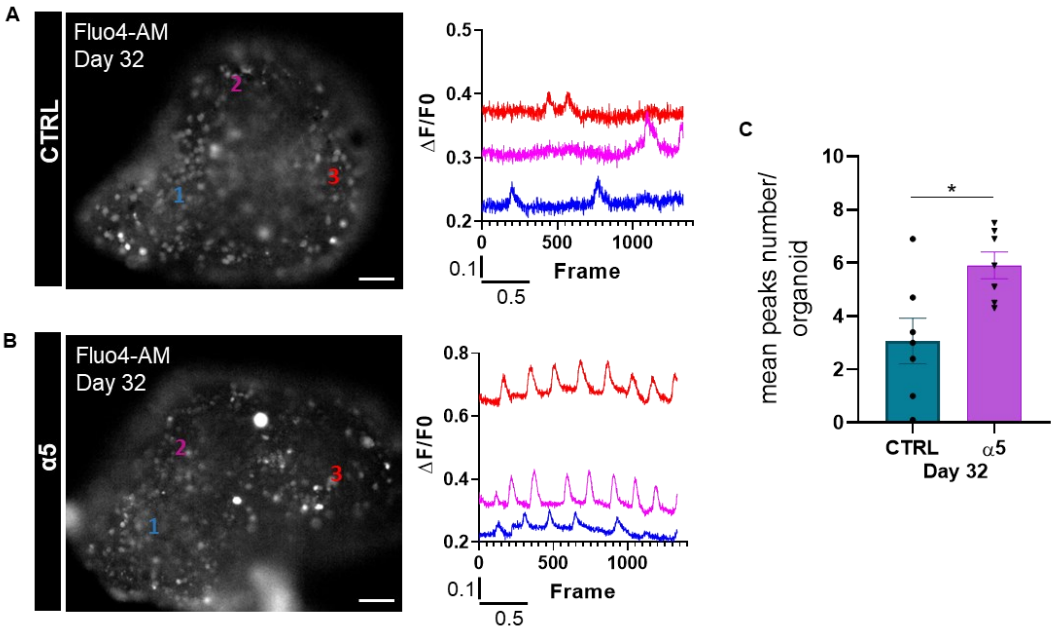

Figure 23: α5 supplementation enhances the spontaneous calcium activity in mature organoids. (A, B) *Time-lapse Fluo4-AM calcium imaging on whole mount control* ***(A)*** *and α5-* ***(B)*** *organoids at day 32, paired to representative graphs of calcium flux. Scale bars: 200μm.* ***(C)*** *Graph representing the average number of the peaks counted for each organoid at day 32 (n=7 organoids/group; n=10 cells selected in each organoid). Data are expressed as mean ± SEM. Differences between experimental conditions were analyzed using two-tailed unpaired t-test for two datasets (CTRL vs α5). p-value < 0.05 was considered statistically significant. *p<0.05.*

Overall, these data suggested that at later stages of the organoid development, α5 supplementation promotes cell differentiation toward the neuronal lineage, neuronal maturation and potentially functional neuronal activity.

4.3 WNT3a supplementation improves hippocampal commitment in mouse brain organoids

The hippocampus is one of the brain regions mainly affected in the pathology progression of many neurodegenerative disorders including epilepsy and Alzheimer's disease. Therefore, an *in vitro* 3D structure able to replicate the hippocampal tissue, can be extremely useful for regenerative medicine, drug testing and neurodegenerative disease modeling.

4.3.1 Modulating the brain organoids development by supplementing the morphogen WNT3a

To improve the hippocampal lineage commitment and to develop a differentiation paradigm that could enriched for hippocampal Cornu Ammonis 3 (CA3) neurons in the cultured organoids, the protocol previously set up from our lab (Ciarpella et al., 2021) was so matched and revised with the one described by Sarkar and colleagues (Sarkar et al., 2018). Accordingly with their protocol, we supplied and modulated the concentration of the morphogen WNT3a, known as a key factor for the hippocampal development, in the organoid culture media in order to mimic the *in vivo* gradient of the molecule exerted by the cortical hem during hippocampal development (Grove et al., 1998), thus specifically promoting the enrichment in CA3 neurons in brain organoids. WNT3a factor

was added in the culture medium starting from the begin of the organoid generation protocol (Expansion phase, days 0-4) till the end of the Induction phase (days 5-13) at a concentration of 5 ng/ml (see *"Materials and methods" section*). By using a low concentration of WNT3a during the first two phases, we attempted to drive specifically the CA3 hippocampal neurons phenotype. The neuronal differentiation was then reached by the supplementation with BDNF (50 ng/ml) of the culture medium during the Differentiation phase (14-32), **(Figure 24)**.

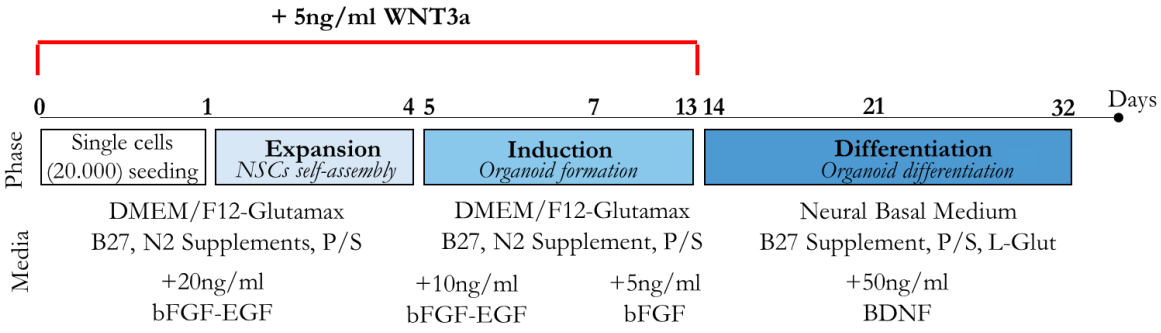

Figure 24: Schematic representation of the three-phase WNT3a organoid generation protocol*. The three-phase organoid generation protocol is characterized by three phases: the Expansion phase, the Induction phase and the Differentiation phase. After single cell seeding (20,000 cells/well) on a 24-well plate (day 0), the protocol starts with the Expansion Phase (days 0-4) in which NSCs proliferate and neurospheres form in a culture medium enriched with bFGF and EGF 20ng/ml). The Induction phase (days 5-13) is characterized by early organoid formation in a culture medium supplemented with gradual decrease of bFGF and EGF concentrations (day 5 to day 6: bFGF and EGF both 10ng/ml; day 7 to day 13: bFGF 5ng/ml). WNT3a supplementation (5ng/ml) in organoid cell media occurred in the Expansion and Induction phases (red line). The Differentiation phase (day 14-32) is characterized by organoids maturation in differentiation medium (medium supplemented with BDNF 50ng/ml). In all the three phases, organoids were maintained on an orbital shaker (dynamic culture). Adapted from (Ciarpella et al., 2021).*

4.3.2 Brain organoids show defined hippocampal signature after WNT3a supplementation

Firstly, we performed whole RNA-seq analysis in order to compare the gene expression profile of control organoids at different stage of development (day 7, day 14 and day 32) with the one characterizing the neonatal (P0) and adult (3 months) hippocampal tissue.

Specifically, this analysis revealed that brain organoids showed a gene signature similar to the hippocampal tissue, for the upregulation of genes related to hippocampal cell growth and division (e.g., Ywhae, Bcan, Ptprs, Usp9x), regulators of proliferation and axon sprouting (e.g., Nr2e1, Uba6, Gli3, DCX, Plxna3, Btg2, Kdm6b, Hdac1). Interestingly, we noted that mouse brain organoid had a lower expression of the genes related to hippocampal neural differentiation and migration, such as Lef1, Drd1, Dlx2, Neurod6, Alk, Dlx1, Fgf13, Wnt3a, Cdk5r2, hippocampal neurogenesis and cell fate determination (e.g., Cdk5r1, Srf, Nr4a3, Prox1), compared to hippocampal tissue **(Figure 25**, **Table 2)**.

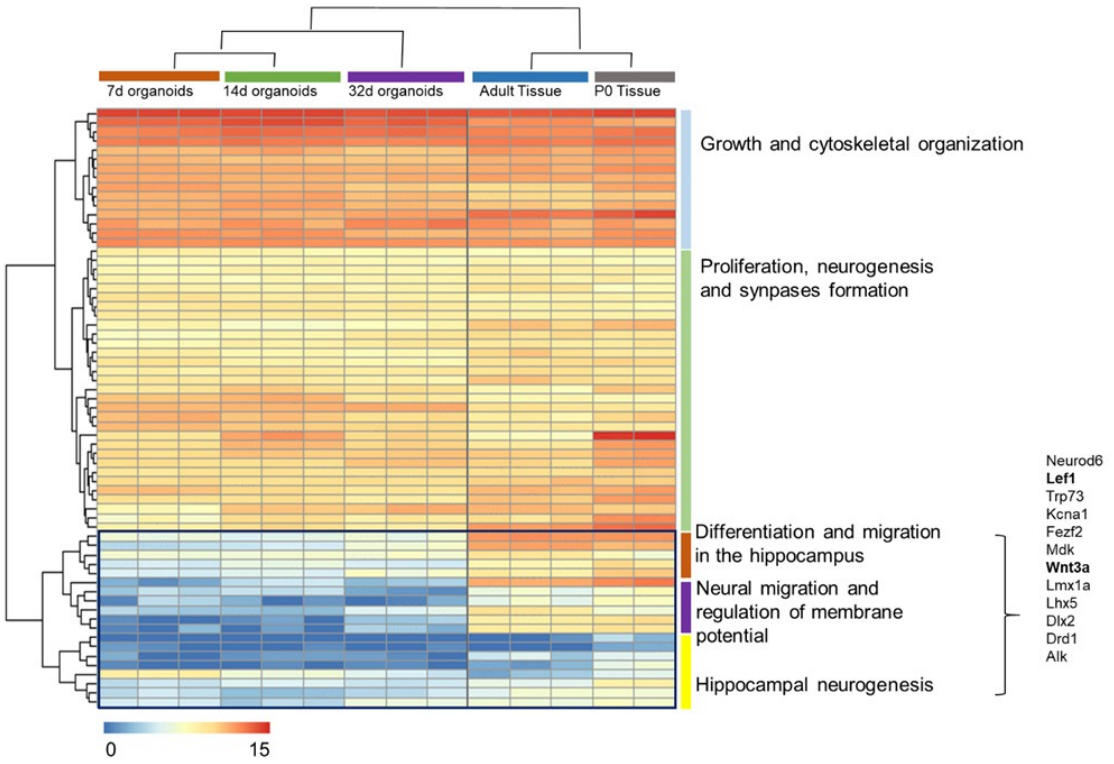

Figure 25: Comparison of gene expression profile of brain organoids with P0 and adult cerebral tissues. *Heatmap of RNA-seq data generated on selected hippocampal gene dataset. By evaluating the genes expression profile on murine P0 and adult cerebral tissues and on organoids at different developmental stages, the analysis reveals no expression of some crucial genes required for the hippocampal genesis (Lef1, WNT3a) into the 3D structures at all the evaluated time points. Blue box highlights the most down regulated hippocampal related genes (Neurod6, Lef1, Trp73, Kcna1, Fezf2, Mdk, Wnt3a, Lmx1a, Lhx5, Dlx2, Drd1, Alk) in organoids respect to the tissue. Adapted from (Ciarpella et al., 2021).*

GENE	padj	Log2FoldChange
Ywhae	0.005424201	3.069025528
Bcan	5.10E-25	10.57776201
Ptprs	1.88E-08	5.897610719
Usp9x	0.424854451	1.001908583
Nr2e1	0.094932196	1.935368493
Uba6	0.252404414	1.381840478
Gli3	0.062419944	2.135685348
Dcx	3.96E-39	13.31853782
Plxna3	4.07E-12	7.200959936
Btg2	1.86E-08	5.898859373
Kdm6b	0.004022945	3.64903452
Hdac1	6.86E-12	7.126560033
Cdk5r1	5.01E-109	-22.38809832
Srf	1.13E-12	-7.379351954
Nr4a3	7,98E-18	-8.857228097
Prox1	6.31E-16	-8.342593401
Lef1	0.022549229	-2.565965341
Drd1	0.051259239	-2.225130449
Dlx2	0.009572507	-2.878319862
Neurod6	2.64E-145	-25.86811259
Alk	0.718873648	-0.485848463
Dlx1	3.81E-08	-5.774644064
Fgf13	1.18E-145	-25.90031399
WNT3a	0.113906933	-1.84109367
Cdk5r2	2.14E-120	-23.5363099
Trp73	1.42E-07	-5.540736952
Kcna1	5.76E-36	-12.75493809
Mdk	1.49E-50	-15.17601342
Lmx1a	0.001758385	-3.417015204
Lhx5	0.501319578	-0.857810381
Fezf2	3.18E-45	-14.34023151

Table 2: Summary of genes related to hippocampal specification and differentiation. *The table reports the down-regulated and up-regulated genes related to hippocampal specification and differentiation obtained by RNA-seq analysis. Padj: adjusted p-values for multiple comparisons using Benjamini-Hochberg method; log2FoldChange: transcript expression fold-changes estimated for each expressed transcript comparing mature organoids and adult cerebral tissue. Adapted from (Ciarpella et al., 2021).*

Considering the lower expression of genes related to hippocampal signature observed in control brain organoids **(Figure 25)**, we then assessed the organoid hippocampal signature following WNT3a supplementation and compared it to the standard control organoid. We performed Real Time (RT)-PCR analysis (Wheeler et al., 2015) for specific hippocampal genes on control and WNT3a organoids at day 32. Interestingly, in WNT3a

organoids we found higher expression of hippocampal-related genes (e.g., Grik4, Alk, Sct, Dkk3, Nectin3, Fzd9, Tgfb2, Neurod1) compared to control organoids **(Figure 26)**, suggesting that the supplementation of the culture medium with WNT3a factor boost the commitment of the NSCs into the hippocampal lineage.

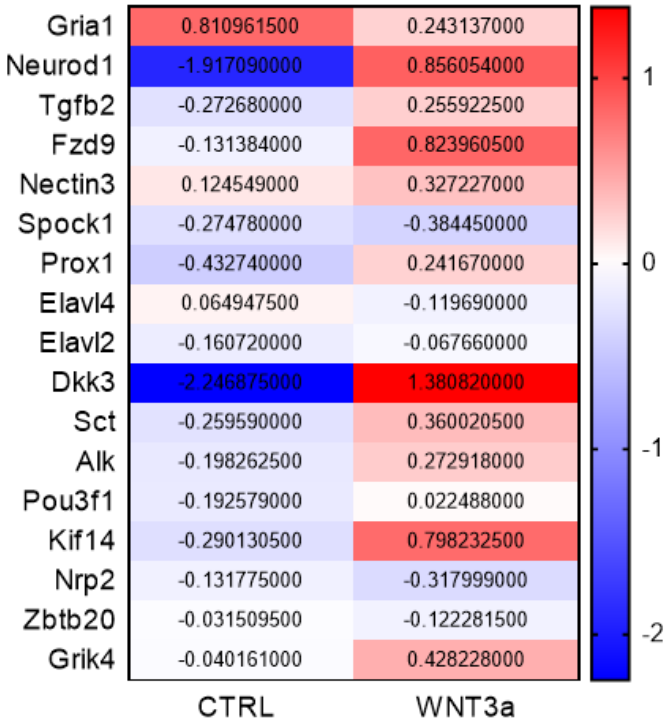

Figure 26: WNT3a factor induces hippocampal patterning. *Heatmap gene expression reporting the log2FoldChange of genes related to the hippocampal signature in control and WNT3a organoids at day 32 (n=3 pool of 6–8 organoids/pool). Data are expressed as log2FoldChange: transcript expression fold-changes estimated for each expressed transcript. Adapted from (Ciarpella et al., 2021).*

Considering the effect of WNT3a supplementation on the hippocampal patterning previously described, we then assessed the impact of WNT3a factor on growth and morphology of brain organoids. We analyzed the maximum diameter of WNT3a organoids at specific time points (day 5, 7, 9, 11, 14, 21 and 32) of the organoid generation protocol and compared the obtained data with those of control organoids ($n \geq 30$/time point). Results showed that the maximum diameter of control and WNT3a organoids similarly increased during the Induction phase reaching a peak of 1.17mm±0.02mm at

day 9 and 1.16±0.03 mm at day 7, respectively, while decreased at a later stage of differentiation (CTRL organoids: 1.08mm±0.02mm at day 11, 1.01mm±0.02 mm at day 14, 1.85mm±0.01mm at day 21, 0.78mm±0.02mm at day 32; WNT3a organoids: 1.11±0.09 mm at day 11, 1.01±0.04 mm at day 14, 0.93±0.04 mm at day 21, 0.80±0.05 mm at day 32, **Figure 27A and B)**. WNT3a supplementation did not significantly impact the morphology of the brain organoids.

Overall, these data indicated that WNT3a organoids developed with consistent size throughout the different phases of the protocol and did not present significant differences from control organoids.

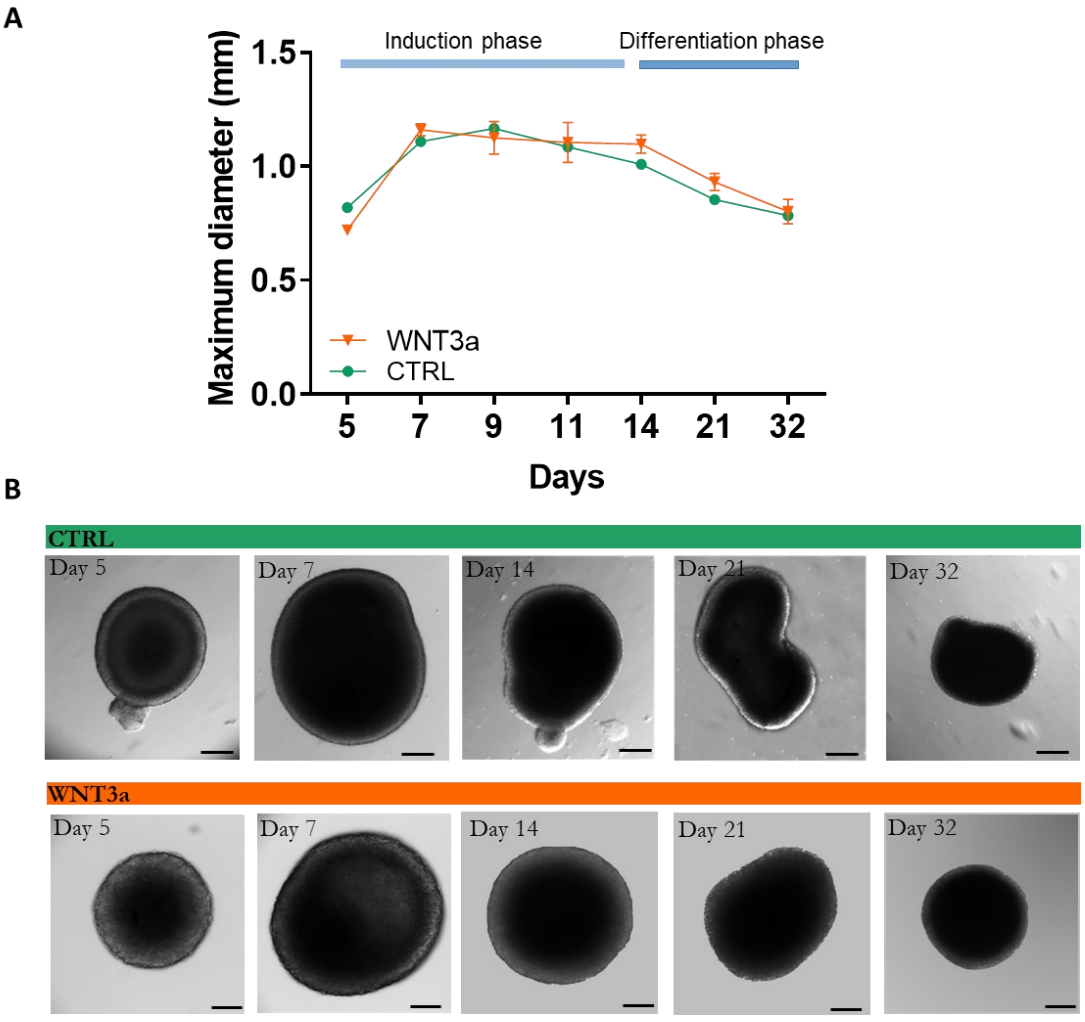

Figure 27: WNT3a organoid growth and morphology during different stages of the protocol. (A) *Graph representing the maximum diameter (mm) of CTRL (green line) and WNT3a (orange line) organoids at specific time points (day 5, 7, 9, 14, 21 and 32) of the organoid generation protocol. Data are expressed as*

mean ± SEM of the maximum diameter (n ≥ 30/time point). ***(B)*** *Representative brightfield images of CTRL and W*NT*3a organoids at different time points (day 5, 7, 14, 21 and 32). Scale bars: 100µm.*

4.3.3 WNT3a organoids show progressive differentiation, maturation and spatial organization

To follow and assess the progressive differentiation, maturation and spatial distribution of WNT3a organoids through the different developmental stages (day 7, 14, 21 and 32), we evaluated the expression and distribution of several markers related to stemness (Vimentin, SOX2), cellular proliferation (Ki67), neuronal progenitors (DCX), immature and mature neurons (TUBB3, MAP2), and glial cells (GFAP) by immunofluorescence analysis **(Figure 28 and 29)**.

At day 7 (end of the Expansion phase), WNT3a organoids showed high number of cells expressing the stemness marker Vimentin which then significantly diminished its expression in the later stages of the organoid development (WNT3a organoids_Vimentin$^+$ cells: 18.73%±1.14% at day 7, n=3; 13.99%±0.79% at day 14, n=3; 9.18%±0.62% at day 21, n=4; 12.27%±0.45% at day 32, n=3; *p<0.05, **p<0.01, **Figure 28A and C**). Moreover, comparing the expression of Vimentin between control and WNT3a organoids, we observed that a day 7 WNT3a organoids showed a significant increase in the number of Vimentin$^+$ cells compared to control organoids (CTRL organoids_Vimentin$^+$ cells: 15.45%±0.51%, n=7 vs WNT3a organoids_Vimentin$^+$ cells: 18.73%±0.63%, n=3, **p<0.01, **Figure 28I**), which significantly decreased at the beginning of the Differentiation phase (day 14) (CTRL organoids_Vimentin$^+$ cells: 23.60%±2.14%, n=6 vs WNT3a organoids_Vimentin$^+$ cells: 13.99%±1.09%, n=3, *p<0.05, **Figure 28I**). No differences were found at later developmental stages (CTRL organoids_Vimentin$^+$ cells: 8.79%±1.02% at day 21, n=4; 7.88%±1.15% at day 32, n=3 vs WNT3a organoids_Vimentin$^+$ cells: 9.18%±0.61% at day 21, n=4; 12.27%±2.40% at day 32, n=3, **Figure 28I**)**.** Similarly, we observed a higher number of cells expressing the stemness marker SOX2 at day 7 which significantly reduced in later stages of development (WNT3a organoids_SOX2$^+$ cells: 91.90%±0.27% at day 7, n=3; 60.96%±2.27% at day 14, n=4; 16.73%±3.03% at day 21, n=3; 27,50%±1.75% at day 32, n=4, **p<0.01, ***p<0.001, ****p<0.0001, **Figure 28B and D**). Qualitative analysis of

SOX2 cellular distribution showed an initial (day 7) widespread localization of $SOX2^+$ NSCs within the entire WNT3a organoid **(Figure 28G)**; its expression maintained an intersperse distribution both in the inner and the external layer until the later stage of differentiation (day 14, day 21 and day 32**, Figure 28G**). Moreover, WNT3a organoids showed a significantly increase in the number of cells expressing the SOX2 marker at day 7 compared to control organoids (CTRL organoids_$SOX2^+$ cells: 79.09%±2.95%, n=6 vs WNT3a organoids_$SOX2^+$ cells: 91.90%±0.33% , n=3, *p<0.05, **Figure 28J**) which remained higher during the induction and differentiation phases (CTRL organoids_$SOX2^+$ cells: 51.69%±1.99% at day 14, n=5; 9.95%±2.42% at day 21, n=5; 10.79%±0.517% at day 32, n=3 vs WNT3a organoids_$SOX2^+$ cells: 60.96%±5.025% at day 14, n=4; 16.73%±4.31% at day 21, n=3; 27,50%±3.01% at day 32, n=4, ***p<0.001, **Figure 28J**). Beside the stemness phenotype, we assessed the cell proliferation within WNT3a organoids by analysing the abundance of the cells-expressing Ki67, a cell-cycle G1/S-G2/M marker. As expected, results showed a higher number of proliferating cells during the Expansion phase (WNT3a organoids_$Ki67^+$: 23.79%±1.01% at day 7, n=3, **Figure 28A and E**), which significantly decreased (****p<0.0001) at the end of the Induction phase (9.66%±1.18% at day 14, n=3, **Figure 28A and E**) and drastically during the Differentiation phase (WNT3a organoids_$Ki67^+$ cells: 0.95%±0.05% at day 21, n=4; 0%±0% at day 32, n=3, ****p<0.0001, **Figure 28A and E**). This data was in line with the morphological analysis showing a reduction in organoid size at later developmental stages (see **Figure 27**). Interestingly, evaluating the different expression of Ki67 proliferating cell marker between control and WNT3a organoids, we showed a significantly increase in the number of $Ki67^+$ cells in WNT3a organoids compared to control organoids during the Expansion (day 7) and Induction (day 14) phases (CTRL organoids_$Ki67^+$ cells: 17.17%±1.03% at day 7, n=5; 1.89%±1.08% at day 14, n=3 vs WNT3a organoids_$Ki67^+$ cells: 23.79%±0.81% at day 7, n=3; 9.666%±0.64% at day 14, n=3, **p<0.01, **Figure 28K**), while a significantly reduction at the end of the differentiation phase (day 32) (CTRL organoids_$Ki67^+$ cells: 0.985%±1.21%, n=4 vs WNT3a organoids_$Ki67^+$ cells: 0%±0%, n=3, ***p< 0.001, **Figure 28K**). Then, we analysed the expression of the neural progenitor marker doublecortin (DCX) in WNT3a organoids. During the initial stages of WNT3a organoid development, we observed an increasing number of DCX^+ cells which significantly decreased during the Differentiation

phase (WNT3a organoids_DCX$^+$ cells: 9.95%±0.33% at day 7, n=3; 28.48%±2.86% at day 14, n=4; 17.58%±0.13% at day 21; 7.36%±2.54% at day 32, n=3, *p<0.05, ***p< 0.001**, Figure 28B and F**), suggesting the advance of the neuronal maturation process. At day 7, the DCX$^+$ cells showed an interspersed distribution within the entire organoid structure. Starting from the Induction phase (day 14), they strongly rearranged to spatially cluster in the external region, forming a dense and thick layer of neuronal precursors cells (**Figure 28H**). Notably, at day 14 and day 21 we observed a significantly increase in the number of DCX$^+$ cells in WNT3a organoids compared to control organoids (CTRL organoids_DCX$^+$ cells: 17.09%±2.83% at day 14, n=5; 5.77%±1.07% at day 21, n=3 vs WNT3a organoids_DCX$^+$ cells: 28.48%±2.86% at day 14, n=4; 17.58%±0.13% at day 21, n=3, *p<0.05, ***p< 0.001, **Figure 28L**).

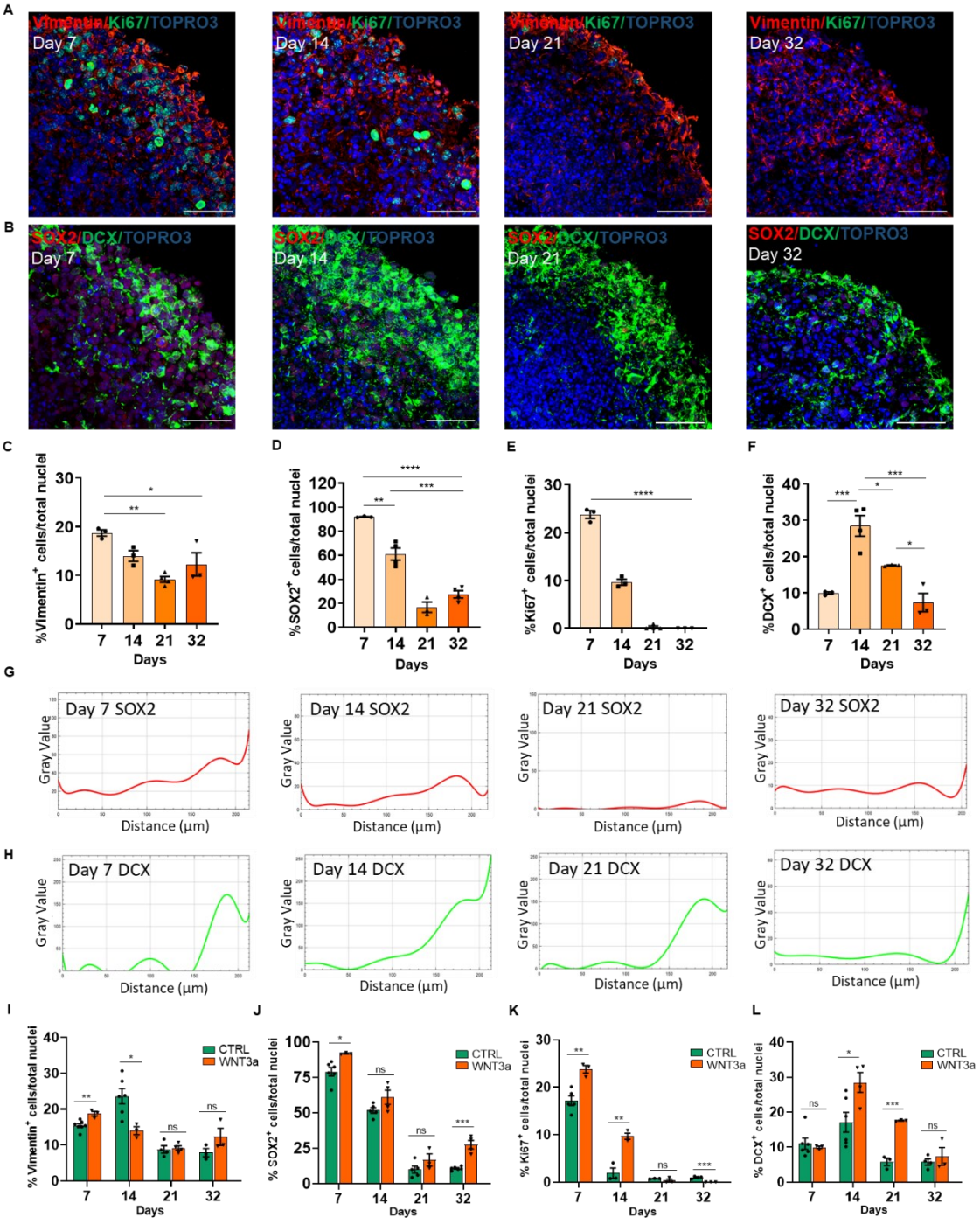

Figure 28: Organization and spatial distribution of stemness and neural progenitor cells in brain organoids after WNT3a supplementation. ***(A)*** *Representative confocal immunofluorescence images of sliced WNT3a organoids at different protocol stages (day 7, 14, 21 and 32) showing Vimentin$^+$ (red) NSCs and Ki67$^+$ (green) proliferating cells. TOPRO3: total nuclei. Scale bar: 50 µm.* ***(B)*** *Representative confocal immunofluorescence images of sliced WNT3a organoids at different protocol stages (day 7, 14, 21 and 32) showing SOX2$^+$ (red) NSCs and DCX$^+$ (green) neuronal progenitors' localization. TOPRO3: total nuclei. Scale bar: 50 µm.* ***(C)*** *Graph representing the quantification of the percentage of Vimentin$^+$ cells*

normalized for the total cell nuclei in WNT3a organoids at different time-points (day 7, 14, 21 and 32). ***(D)*** *Graph representing the quantification of the percentage of $SOX2^+$ cells normalized for the total cell nuclei in WNT3a organoids at different time-points (day 7, 14, 21 and 32).* ***(E)*** *Graph representing the quantification of the percentage of $Ki67^+$ cells normalized for the total cell nuclei in WNT3a organoids at different time-points (day 7, 14, 21 and 32).* ***(F)*** *Graph representing the quantification of the percentage of DCX^+ cells normalized for the total cell nuclei in WNT3a organoids at different time-points (day 7, 14, 21 and 32).* ***(G-H)*** *Fluorescence intensity analysis showing expression of SOX2* ***(G)*** *and DCX* ***(H)*** *plotted versus the distance from the center (left) to the edge (right) of WNT3a organoids at day 7, 14, 21 and 32.* ***(I)*** *Graph representing the quantification of the percentage of $Vimentin^+$ cells normalized for the total cell nuclei in CTRL and WNT3a organoids at different time-points (day 7, 14, 21 and 32).* ***(J)*** *Graph representing the quantification of the percentage of $SOX2^+$ cells normalized for the total cell nuclei in CTRL and WNT3a organoids at different time-points (day 7, 14, 21 and 32).* ***(K)*** *Graph representing the quantification of the percentage of $Ki67^+$ cells normalized for the total cell nuclei in CTRL and WNT3a organoids at different time-points (day 7, 14, 21 and 32).* ***(L)*** *Graph representing the quantification of the percentage of DCX^+ cells normalized for the total cell nuclei in CTRL and WNT3a organoids at different time-points (day 7, 14, 21 and 32). All the images in* ***A*** *and* ***B*** *are maximum intensity projections of z stack confocal acquisitions. Analysis performed on n≥3 different organoids and at least 3 entire section for each organoid. Data in all graphs are expressed as mean ± SEM. Differences between experimental conditions were analyzed ordinary one-way ANOVA followed by Tukey's multiple comparison test and two-tailed unpaired t-test for two datasets (CTRL vs WNT3a). p-value < 0.05 was considered statistically significant. ⁎p< 0.05; ⁎⁎p< 0.01; ⁎⁎⁎p< 0.001; ⁎⁎⁎⁎p< 0.0001. ns: no statistical differences. Adapted from (Ciarpella et al., 2021).*

In order to evaluate the presence of immature neurons in WNT3a organoids, we assessed the expression of the immature neuronal marker TUBB3 by immunofluorescence analysis **(Figure 29A)**. As expected, from day 7 to day 21 we observed a progressive increase of the $TUBB3^+$ neurons amount which remained almost stable in the later differentiation stages (WNT3a organoids_$TUBB3^+$ cells: 11.48%±1.13% at day 7, n=3; 15.82%±1.67% at day 14, n=4; 17.53%±3.39% at day 21, n=4; 16.07%±1.90% at day 32, n=4, **Figure 29C**). At day 7, $TUBB3^+$ immature neurons were found spread within the WNT3a organoid structure and then, during the development, acquiring a progressive spatial organization as an external thick layer **(Figure 29G)**. Notably, starting from the Induction phase (day 14), the $TUBB3^+$ neurons mainly clustered in the external region of the organoid, forming a layer which progressively increased its thickness (day 21 and day 32) **(Figure 29G)**. We also compared the TUBB3 expression in control and WNT3a

organoids and we observed no significant differences between the two groups at all the time point analysed (CTRL organoids_TUBB3$^+$ cells: 7.63%±1.16% at day 7, n=11; 15.85%±2.69% at day 14, n=4; 19.05%±1.65% at day 21, n=7; 17.55%±2.35% at day 32, n=9 vs WNT3a organoids_TUBB3$^+$ cells: 11.48%±1.13% at day 7, n=3; 15.82%±1.67% at day 14, n=4; 17.53%±3.39% at day 21, n=4; 16.07%±1.90% at day 32, n=4, **Figure 29J**). The decay of the immature neuronal population at later time-points was counteracted by the constant increment of mature MAP2$^+$ neurons through the different WNT3a organoid developmental stages (WNT3a organoids_MAP2$^+$ cells: 8.85%±0.34% at day 7, n=11; 12.23%±0.82% at day 14, n=9; 19.91%±1.20% at day 21, n=9; 22.34%±1.46% at day 32, n=8, ****p<0.0001, **Figure 29B and D**). As shown in **Figure 29H**, qualitative analysis of MAP2 cellular distribution showed an initial (day 7) widespread localization of MAP2$^+$ neurons within the entire WNT3a organoid. Starting from the induction phase (day 14), MAP2$^+$ cells progressively rearranged to spatially cluster at the surface of WNT3a organoids, forming at day 32 a dense and structured thick layer characterized by neuronal processes converging toward the formation of a potentially functional neuronal net. The analysis of the MAP2 expression in control and WNT3a organoids revealed a significantly increase of the number of MAP2$^+$ cells in WNT3a organoids at day 14 compared to control organoids (CTRL organoids_MAP2$^+$ cells: 8.34%±0.78%, n=4; vs WNT3a organoids_MAP2$^+$ cells: 12.23%±0.82%, n=9, *p<0.05, **Figure 29K**), while was similar between the two groups at the later developmental stages (CTRL organoids_MAP2$^+$ cells: 16.75%±1.22% at day 21, n=8; 24.40%±2.08% at day 32, n=9 vs WNT3a organoids_MAP2$^+$ cells: 19.91%±1.20% at day 21, n=9; 22.34%±1.46% at day 32, n=8, **Figure 29K**)

Then, in order to assess WNT3a organoid potential to develop neuronal connections, we evaluated the expression of the presynaptic marker synaptophysin (Syn) in MAP2$^+$ neurons at different developmental stages **(Figure 29B)**. Accordingly with the overall increase of MAP2$^+$ neurons during the organoid development **(Figure 29D)**, we observed a significant increment of the synaptic density in the later differentiation phases (WNT3a organoids_Syn$^+$ area/MAP2$^+$ area: 1.40%±0.18% at day 7, n=5; 0.38%±1.34% at day 14, n=3; 26.53%±0.52% at day 21, n=3; 31.64%±4.21% at day 32, n=3, ****p<0.0001, **Figure 29E**). Moreover, the synaptic density was similar in control and WNT3a organoids (CTRL organoids_Syn$^+$ area/MAP2$^+$ area: 0.62%±0.25% at day 7, n=4;

0.12%±0.04% at day 14, n=3; 23.20%±1.20% at day 21, n=4; 34.53%±4.26% at day 32, n=5 vs WNT3a organoids_Syn^+ area/$MAP2^+$ area: 1.40%±0.18% at day 7, n=5; 0.38%±1.34% at day 14, n=3; 26.53%±0.52% at day 21, n=3; 31.64%±4.21% at day 32, n=3, **Figure 29L**).

Then, we evaluated the presence of different cell population in WNT3a organoids, focusing our attention on the analysis of the expression of the specific astrocytes marker, Glial Fibrillary Acid Protein (GFAP) **(Figure 29A)**. Results showed that, while we found a stable 10% of astrocytes in control organoids during organoid development (CTRL organoids_$GFAP^+$ cells: 9.45%±1.88% at day 7, n=3; 12.67%±0.42% at day 14, n=3; 10.27%±0.20% at day 21, n=3; 11.79%±1.18% at day 32, n=7, **Figure 29M**), in WNT3a organoids the $GFAP^+$ cells progressively increased during the different developmental stages (WNT3a organoids_$GFAP^+$ cells: 7.09%±1.63% at day 7; 8.31%±0.95% at day 14; 9.70%±0.25% at day 21; 14.36%±2.60% at day 32, n=3/time point, p= 0.051, **Figure 29F and M**). Notably, qualitative analysis of $GFAP^+$ cells distribution showed a widespread localization within WNT3a organoids **(Figure 29I)**, with the majority of $GFAP^+$ cells closely associated to $TUBB3^+$ neural cells **(Figure 29A)**, suggesting a role in supporting neuronal maturation.

Overall, these data indicated that WNT3a supplementation promoted in NSCs-derived organoids cell differentiation and maturation with a progressive decrease of stemness-related markers together with a progressive increase of differentiation-related markers.

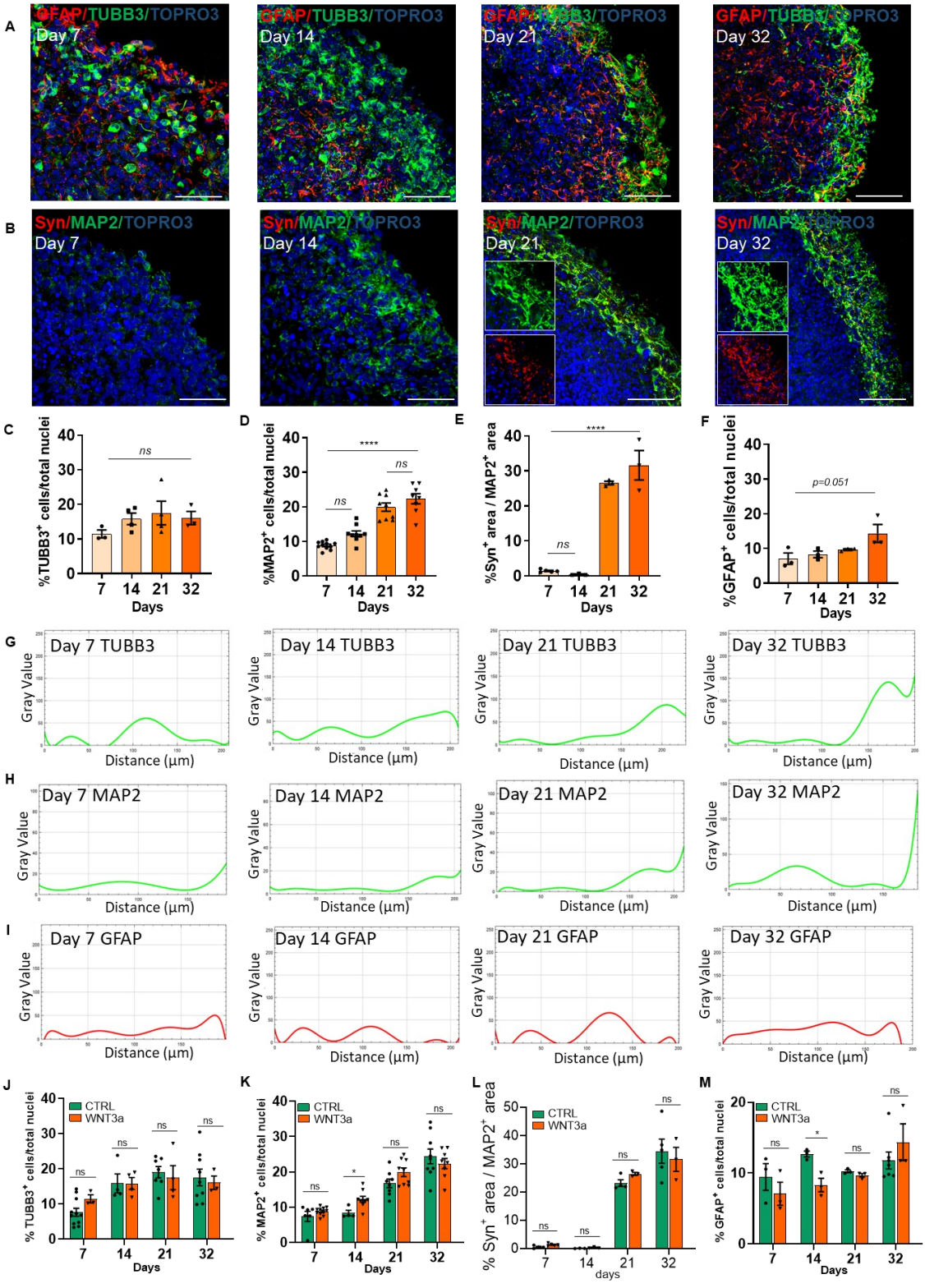

Figure 29: Organization and spatial distribution of immature and mature neurons and astrocytic cells in brain organoids after WNT3a supplementation. ***(A)*** *Representative confocal immunofluorescence images of sliced WNT3a organoids at different protocol stages (day 7, 14, 21 and 32) showing TUBB3$^+$ (green) immature neurons and GFAP$^+$ (red) astrocytes. TOPRO3: total nuclei. Scale bar: 50 µm.* ***(B)***

*Representative confocal immunofluorescence images of sliced W*NT*3a organoids at different time points (day 7, 14, 21 and 32) showing MAP2$^+$ (green) mature neurons and Syn$^+$ (red) pre-synaptic marker colocalization. White boxes show higher magnification of the dense and structured layer of mature neurons (MAP2$^+$) at the surface of the organoid, expressing the Syn marker. Scale bar: 50 μm.* ***(C)*** *Graph representing the quantification of the percentage of TUBB3$^+$ cells normalized for the total cell nuclei in W*NT*3a organoids at different time-points (day 7, 14, 21 and 32).* ***(D)*** *Graph representing the quantification of the percentage of MAP2$^+$ cells normalized for the total cell nuclei in W*NT*3a organoids at different time-points (day 7, 14, 21 and 32).* ***(E)*** *Graph representing the quantification of the percentage of Syn$^+$ area relative to MAP2$^+$ area in W*NT*3a organoids at different time-points (day 7, 14, 21 and 32).* ***(F)*** *Graph representing the quantification of the percentage of GFAP$^+$ cells normalized for the total cell nuclei in W*NT*3a organoids at different time-points (day 7, 14, 21 and 32).* ***(G-I)*** *Fluorescence intensity analysis showing the expression of TUBB3* ***(G),*** *MAP2* ***(H)*** *and GFAP* ***(I)*** *plotted versus the distance from the center (left) to the edge (right) of W*NT*3a organoids at day 7, 14, 21 and 32.* ***(J)*** *Graph representing the quantification of the percentage of TUBB3$^+$ cells normalized for the total cell nuclei in CTRL and W*NT*3a organoids at different time-points (day 7, 14, 21 and 32).* ***(K)*** *Graph representing the quantification of the percentage of MAP2$^+$ cells normalized for the total cell nuclei in CTRL and W*NT*3a organoids at different time-points (day 7, 14, 21 and 32).* ***(L)*** *Graph representing the quantification of the percentage of Syn$^+$ area relative to MAP2$^+$ area normalized for the total cell nuclei in CTRL and W*NT*3a organoids at different time-points (day 7, 14, 21 and 32).* ***(M)*** *Graph representing the quantification of the percentage of GFAP$^+$ cells normalized for the total cell nuclei in CTRL and W*NT*3a organoids at different time-points (day 7, 14, 21 and 32). All the pictures in* ***A*** *and* ***B*** *are maximum intensity projections of z stack confocal acquisitions. Analysis performed on n≥3 different organoids and at least 3 entire section for each organoid. Data in all graphs are expressed as mean ± SEM. Differences between experimental conditions were analyzed using ordinary one-way ANOVA followed by Tukey's multiple comparison test and two-tailed unpaired t-test for two datasets (CTRL vs WNT3a). p-value < 0.05 was considered statistically significant. ⁎p< 0.05, ⁎⁎⁎⁎p< 0.0001. ns=no statistical differences. Adapted from (Ciarpella et al., 2021).*

4.3.4 Brain organoids develop CA3 hippocampal-specific neurons after WNT3a supplementation

To assess whether WNT3a supplementation successfully acted on the cell differentiation promoting the hippocampal specification of the brain organoid, particularly promoting the CA3 hippocampal neurons specification, we evaluated in WNT3a and control organoid the expression of two specific hippocampal markers: the Zinc Finger BTB Domain Containing 20 (ZBTB20) marker and the Kainate Acid 1 (KA1) marker. ZBTB20 is expressed by hippocampal neurons throughout the developmental stages,

instead KA1 identify CA3 pyramidal neurons (Tole et al., 1997; Wisden & Seeburg, 1993). Results showed that mature organoids (day 32) supplemented with WNT3a factor displayed a significantly higher expression of $ZBTB20^+$ cells compared to control organoid (CTRL organoids_$ZBTB20^+$ cells: 1.8%±1.25%, n=3 vs WNT3a organoids_$ZBTB20^+$ cells: 8.24%±0.87%, n=5, **p<0.01, **Figure 30A and B**). Interestingly, evaluating the percentage of $MAP2^+$ cells expressing the ZBTB20 marker normalized for the total $MAP2^+$ neurons, we found that at day 32 mature neurons ($MAP2^+$) in WNT3a organoids showed a significant increased expression of the ZBTB20 marker compared to control organoids (CTRL organoids_$MAP2^+$ $ZBTB20^+$ cells over total $MAP2^+$ cells: 6.59%±2.90%, n=4 vs WNT3a organoids_$MAP2^+$ $ZBTB20^+$ cells over total $MAP2^+$ cells: 48.33%±12.09%, n=3, **p < 0.01, **Figure 30C and D**). We then specifically investigated the presence of CA3 pyramidal neurons. The analysis showed that $KA1^+$ cell content was significantly higher in WNT3a organoids compared to control organoid (CTRL organoids_$KA1^+$ cells: 6.28%±1.11%, n=3 vs WNT3a organoids_$KA1^+$ cells: 14.2%±2.3%, n=5, *p < 0.05, **Figure 30E and F**) and that the percentage of mature pyramidal neurons ($MAP2^+$ $KA1^+$) normalized for the total $MAP2^+$ neurons was also significantly increased in WNT3a organoids compared to control organoids (CTRL organoids_$MAP2^+$ $KA1^+$ cells over total $MAP2^+$ cells: 18.14%±2.45% vs WNT3a organoids_$MAP2^+$ $KA1^+$ cells over total $MAP2^+$ cells: 83.13%±5.45%, n=3/condition, **p < 0.01, **Figure 30G and H**).

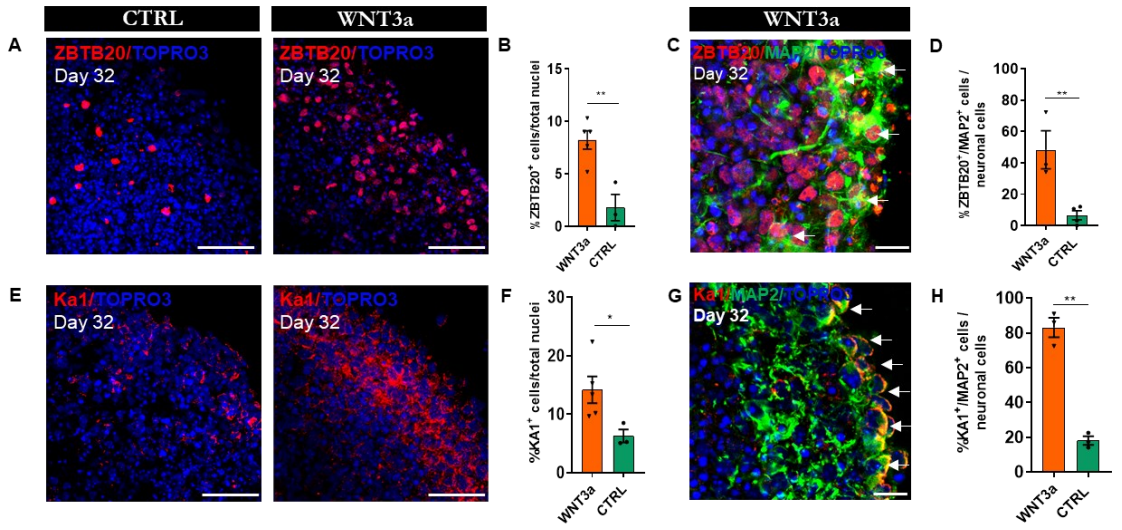

Figure 30: WNT3a organoids show CA3 hippocampal signature. ***(A, E)*** *Representative confocal immunofluorescence images of sliced CTRL and WNT3a organoids, at day 32, showing cells positive for the pan-hippocampal ZBTB20* ***(A****, red)* *and the CA3-specific KA1* ***(E****, red)* *markers. TOPRO3: total nuclei. Scale bar: 50 µm.* ***(B, F)*** *Graphs showing the percentage of ZBTB20* ***(B)*** *and KA1* ***(F)*** *positive cells normalized for the total cell nuclei at day 32 in control and WNT3a organoids.* ***(C, G)*** *Representative confocal immunofluorescence images of sliced WNT3a organoids (day 32), showing double-positive cells (highlighted by white arrows) for ZBTB20 and MAP2 mature neuronal markers* ***(C)*** *and for KA1 and MAP2 mature neuronal markers* ***(G)****. TOPRO3: total nuclei. Scale bar: 20 µm.* ***(D, H)*** *Graphs showing the percentage of ZBTB20$^+$/MAP2$^+$ cells* ***(D)*** *and of KA1$^+$/MAP2$^+$ cells* ***(H)*** *over total neuronal cells in WNT3a and CTRL organoids at day 32. All the images in* ***A, C, E*** *and* ***G*** *are maximum intensity projections of z stack confocal acquisitions. Analysis was performed on n=3 different organoids and at least on 3 entire sections for each organoid. Data in all graphs are expressed as mean ± SEM. Statistical differences between experimental conditions were evaluated by two-tailed unpaired t-test for two datasets (CTRL vs WNT3a) for both markers. p-value < 0.05 was considered statistically significant. *p <0.05, **p<0.01. Adapted from (Ciarpella et al., 2021).*

To further confirm the improved hippocampal signature observed in organoids after WNT3a supplementation, we qualitatively evaluated the expression of the hippocampal CA1/2 region markers (OCT6, FDZ9) and of the dentate gyrus granule neurons (PROX1) in WNT3a organoids at day 32 as in the adult mouse tissue (8 weeks). WNT3a organoids were found to express OCT6 and FDZ9 markers (**Figure 31A and B**). Notably, PROX1 expression was not detectable in WNT3a organoids **(Figure 31C)**, further suggesting that the usage of low WNT3a concentration is able to specifically boost the CA3 (Sarkar et al., 2018) and to a lesser extent CA1/CA2 commitment. Regional identity analysis of the

expression of the choroid plexus (TTR), cerebral cortex region (FOXG1) and ganglionic eminence hallmarks (GSX2 and NKX2.1) markers, further confirmed the specific hippocampal signature of WNT3a organoids at day 32. Indeed, results showed low expression of TTR **(Figure 31D)** and FOXG1 markers **(Figure 31E)** and undetectable level of GSX2 **(Figure 31F)** and NKX2.1 **(Figure 31G)**.

Overall, these data suggested that WNT3a supplementation in brain organoids promoted the acquisition of a hippocampal lineage-commitment and specifically the neuronal signature of the CA3 hippocampus.

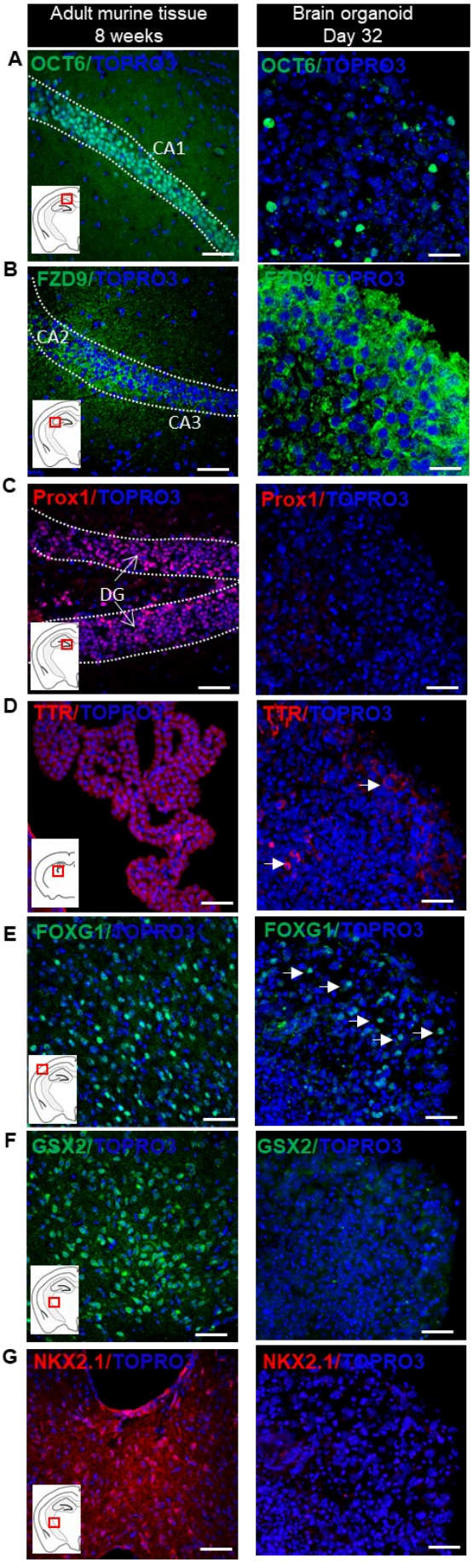
Adult murine tissue
8 weeks
Brain organoid
Day 32
A
OCT6/TOPRO3
CA1
OCT6/TOPRO3
B
FZD9/TOPRO3
CA2
CA3
FZD9/TOPRO3
C
Prox1/TOPRO3
DG
Prox1/TOPRO3
D
TTR/TOPRO3
TTR/TOPRO3
E
FOXG1/TOPRO3
FOXG1/TOPRO3
F
GSX2/TOPRO3
GSX2/TOPRO3
G
NKX2.1/TOPRO3
NKX2.1/TOPRO3

Figure 31: WNT3a organoids express hippocampal regions markers. (A) *Representative confocal immunofluorescence images of sliced adult (8 weeks) murine brain tissue (left panel) and mature WNT3a organoids (day 32, right panel) showing the expression of OCT6-CA1 (green) marker. TOPRO3: total nuclei. Scale bar: 50µm and 20µm.* ***(B)*** *Representative confocal immunofluorescence images of sliced adult (8 weeks) murine brain tissue (left panel) and mature WNT3a organoids (day 32, right panel) showing the expression of FZD9-CA2 (green) marker. TOPRO3: total nuclei. Scale bar: 50µm and 20µm.* ***(C)*** *Representative confocal immunofluorescence images of sliced adult (8 weeks) murine brain tissue (left panel) and mature WNT3a organoids (day 32, right panel) showing the expression of Prox1-DG* ***(****red****)*** *marker. TOPRO3: total nuclei. Scale bar: 50µm and 20µm.* ***(D)*** *Representative confocal immunofluorescence images of sliced adult (8 weeks) murine brain tissue (left panel) and mature WNT3a organoids (day 32, right panel), showing the low expression of TTR-choroid plexus (red) marker. TOPRO3: total nuclei. Scale bar: 50µm and 20µm.* ***(E)*** *Representative confocal immunofluorescence images of sliced adult (8 weeks) murine brain tissue (left panel) and mature WNT3a organoids (day 32, right panel), showing the low expression of FOXG1-cortical (green), marker. TOPRO3: total nuclei. Scale bar: 50µm and 20µm.* ***(F, G)*** *Representative confocal immunofluorescence images of sliced adult (8 weeks) murine brain tissue (left panel) and mature WNT3a organoids (day 32, right panel), showing no expression of GSX2- (green,* ***F****) and NKX2.1- (red,* ***G****) ganglionic eminences markers. TOPRO3: total nuclei. Scale bar: 50µm and 20µm. All the images in* ***A, B, C****,* ***D****,* ***E****,* ***F*** *and* ***G*** *are maximum intensity projections of z stack confocal acquisitions. Adapted from (Ciarpella et al., 2021).*

4.3.5 Mouse hippocampal brain organoids exhibit cell spontaneous activity

Spontaneous neuronal activity is an important step during neuronal development. The first spontaneous electrical activity in the immature brain is driven by intracellular calcium fluctuations (Rosenberg & Spitzer, 2011). Considering the drastically increased in Syn expression in WNT3a-organoids at later stages of development, we then assessed the cellular activity of selected cells within the organoid structure with the live calcium imaging analysis at early (day 7), intermediate (day 14) and mature (day 21 and day 32) time points during the organoid development. Specifically, we evaluated the fluorescence intensity signal of the chemical calcium indicator, Fluo4-AM (Gee et al., 2000). At early stages of the organoid development (day 7), low number of fluorescence intensity peaks were detected within WNT3a organoids (5 active cells/20 evaluated cells, n=2 organoids, n=10 cells/ organoid, **Figure 32A and B**). However, starting from day 14, we observed an increment of the spontaneous activity of cells constituting the WNT3a organoids with 12 cells displaying calcium flux spontaneous oscillations out of a total of 30 analyzed

cells (n=3 organoids, n=10 cells/organoid, **Figure 32A and B**). Notably, at day 21 and day 32, all the selected cells analysed (30 active cells/30 evaluated cells, n=3 organoids, n=10 cells/organoid, *p <0.05, **Figure 32A and B**) displayed calcium flux spontaneous oscillations. By evaluating the mean number of detected peaks per minute of recording per organoids at different time point of the generation protocol (n=3/time point), results showed a significant increase of the mean number of calcium peaks in early mature (day 21: 1.89±0.09 peaks/min, *p <0.05, n=3, **Figure 32C**) and later mature (day 32: 1.88±0.5 peaks/min, *p <0.05, n=3, **Figure 32C**) WNT3a organoids compared to the number of calcium peaks detected in early ones (day 7: 0.08±0.08 peaks/min, n=2, **Figure 32C**). Overall, these data indicated that WNT3a supplementation in brain organoids displayed a progressive increase of the spontaneous calcium activity during the development, suggesting that WNT3a factor promotes the maturation and the functionality of the neurons within WNT3a organoids.

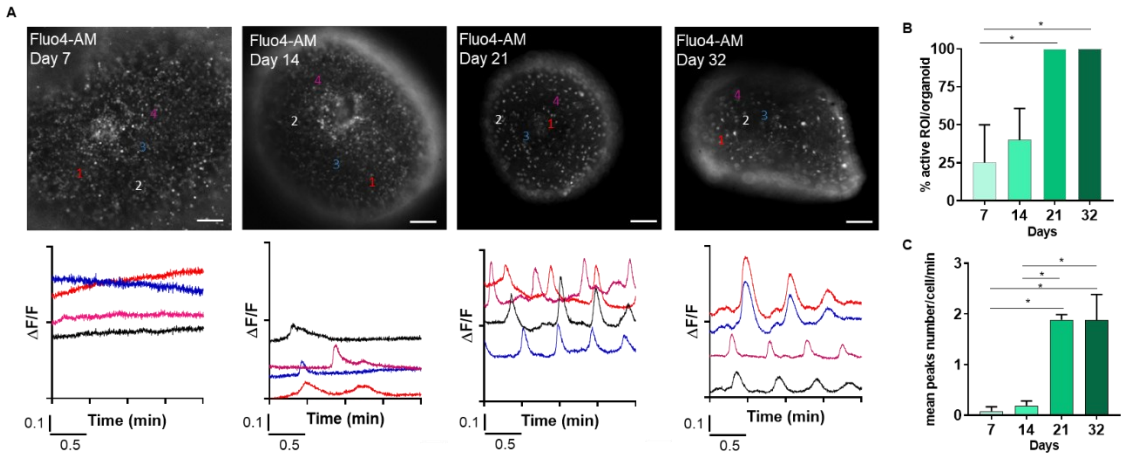

Figure 32: WNT3a organoids display a progressive increase of spontaneous calcium activity during development. (A) *Time-lapse Fluo4-AM calcium imaging on whole mount WNT3a organoids at different time point (day 7, 14, 21 and 32), paired to representative graphs of calcium flux. Note the increasing neural activity over time as well as a major peak synchronization. Scale bars: 200µm.* ***(B)*** *Graph showing the percentage of active cells within the organoids at different time points (day 7, 14, 21 and 32, n=3 organoids/time point; n=10 cells selected in each organoid).* ***(C)*** *Graph representing the average number of the peaks counted for each cell per minute at different time points (day 7, 14, 21 and 32, n=3 organoids/time point; n=10 cells selected in each organoid). Data in all graphs are expressed as mean ± SEM. Statistical differences between experimental conditions were evaluated by ordinary one-way ANOVA. p-value < 0.05 was considered statistically significant. *p<0.05. Adapted from (Ciarpella et al., 2021).*

4.4 *In vivo* transplantation of rat hippocampal-derived NSCs in combination with the v-ECM hydrogel Alginate in the ventral CA3 (vCA3) hippocampus of an epileptic rat model

This PhD thesis is part European Project HERMES that has the ultimate goal to overcome Temporal Lobe Epilepsy (TLE) disorder, an adulthood focal epilepsy frequently refractory to anti-epileptic medications (Blair, 2012), by pursuing self-repair process of dysfunctional brain circuits with the use of bioengineered brain tissue (brain organoids), neuromorphic microelectronics, and artificial intelligence (AI). Here, we first set up the *in vivo* transplantation of rat hippocampal-derived neural stem cells (NSCs) in the ventral CA3 (vCA3) of the hippocampus of a TLE rat and considering the effects of alginate observed in brain organoids *in vitro* (see *Section 4.1*), we resuspended the NSCs in a solution containing the alginate. We isolated NSCs from the hippocampal tissue of rat brain embryos E18.5, expanded in growth media (DMEM/F12-Glutamax, 2% B27, 1% N2 and 1% Pen/Strept) supplemented with 20 ng/mL of epidermal growth factor (EGF) and 20 ng/mL of basic fibroblast growth factor (bFGF). Moreover, in order to allow their identification in the brain following transplantation, the NSCs were transduced with a lentivirus (1.5 MOI) carrying the Green Fluorescent Protein (GFP) reporter, (see *Materials and Methods section*). The TLE rat model and the NSCs transplantation was performed by the Dr. Giulia Curia Lab, University of Modena – Reggio Emilia.

4.4.1 Rat hippocampal NSCs maintain their own neuronal phenotype *in vitro*

Before transplantation in the vCA3, we performed a phenotype characterization, after 4 days in culture, of the NSCs by assessing the expression of markers related to stemness (SOX2), intermediate neuronal progenitors (Doublecortin, DCX), immature neurons (TUBB3), mature neurons (MAP2 and NeuN), cell proliferation (Ki67) and cell apoptosis (Caspase-3) markers. Results showed that the majority of the GFP^+ NSCs expressed the proliferative marker Ki67 (26.56%±4.34%, n=3, **Figure 33A and C**), while only few of them were positive for the Caspase-3 (5.98%±1.04%, n=2, **Figure 33A and C**), highlighting their viability and active proliferative activity. Interestingly, most of the GFP^+ NSCs expressed the stemness marker SOX2 (73.55%±1.25%, n=4, **Figure 33B**

and C). Regarding the expression of markers related to the neuronal lineage, data showed a similar amount of DCX and TUBB3 (DCX: 32.49%±14.5%, n=4; TUBB3: 33.24%±9.74%, n=4, **Figure 33B and C),** while no expression of MAP2 and NeuN was detected (data not shown).

Overall, these results suggested that 4 days after the isolation, cultured GFP^+ NSCs still maintained their own neuronal phenotype *in vitro,* mainly characterized by the expression of proliferative and stemness makers and by neuronal progenitor markers.

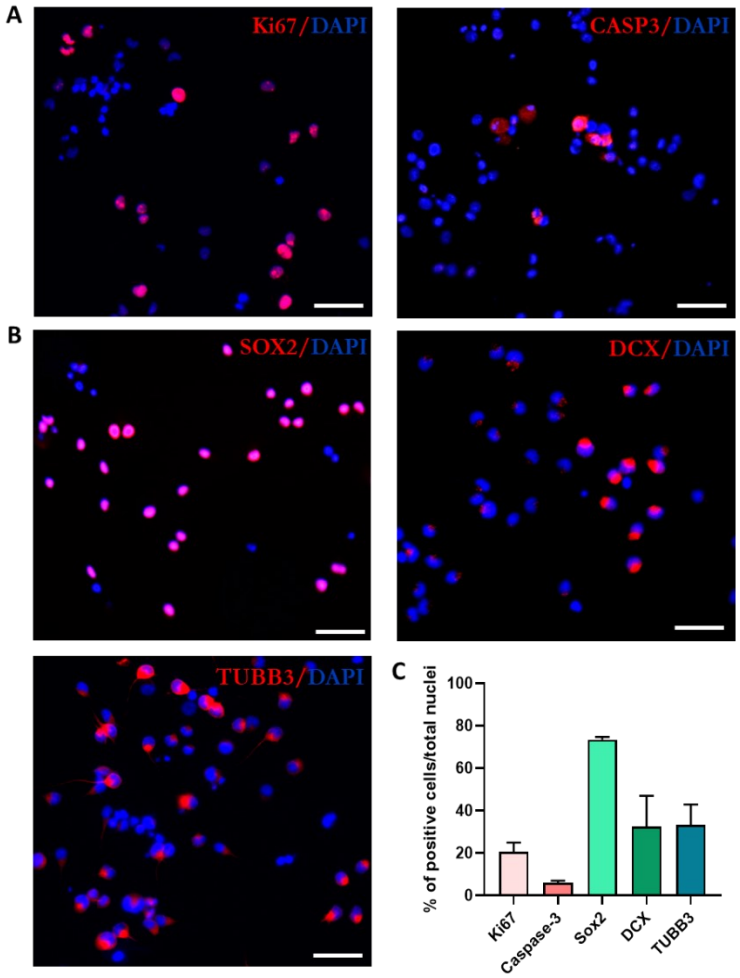

Figure 33: NSCs preserve their own neuronal characteristics in vitro. (A, B) *Representative images of the immunostaining of the proliferative marker Ki67 (red) and apoptotic marker Caspase-3 (red)* ***(A)****, the stemness marker SOX2 (red), neuronal progenitor DCX (red) and immature neuronal TUBB3 (red) markers* ***(B)****. DAPI: total nuclei. Scale bar: 200 µm.* ***(C)*** *Graph showing the percentage of cells belonging to different cell populations over the total cell populations' number.*

4.4.2 Rat hippocampal-derived NSCs in combination with alginate matrix are found in the ventral CA3 of epileptic rats at short and long term post transplantation

In order to set up the rat hippocampal-derived NSCs transplantation in the vCA3, 22 adult male (7-weeks old) Sprague Dawley rats were intraperitoneally treated with pilocarpine (380 mg/kg) to induce status epilepticus (SE), a brain insult leading to TLE (see *Materials and Methods section*). To avoid the increase of the intracranial pressure after cell transplantation, four weeks after SE induction, rats were injected in the vCA3 area of both hemispheres with the cytotoxic agent ibotenic acid (IBO, 1 mg/ml in PBS, 0.3 µl, 1 µl/min), which is known to induce localized brain lesions (Jarrard, 1989). Considering our previous results indicating the capability of alginate to give trophic support to the cells and to preserve organoid structure (see *Section 4.1*), we assess the effect on TLE animal model of a single transplantation in the vCA3 of GFP^+ NSCs alone or in combination with Mg^{2+}-alginate. Alginate forms a hydrogel of variable stiffness following the physical cross-linking with divalent cations, such as Ca^{2+} and Mg^{2+}. As Ca^{2+} overload may induce neuron excitotoxicity (Berliocchi, Bano, & Nicotera, 2005), in order to reduce Ca^{2+} concentration, we combined the alginate with Mg^{2+}, which exerts a neuroprotective effect (McDonald, Silverstein, & Johnston, 1990). Four days after IBO injection, the animals were divided in two groups: the first group underwent a single cell transplantation in both hemispheres of NSCs ($1.5*10^6$ cells, 5µl/injection), while the second group of NSCs in combination with Mg^{2+}-alginate ($1.5*10^6$ cells in 3µl + 2 µl Mg^{2+}-alginate solution, total 5 µl/injection). The transplantation was performed at specific coordinates (right hemisphere above DG: AP -0.55 mm; ML ±0.45 mm; DV 0.35 mm; left hemisphere above HPC: AP -0.55 mm; ML ±0.45 mm; DV -0.15 mm) accordingly with the "The Rat Brain in Stereotaxic Coordinates" (George Paxinos and Charles Watson, Academic Press, 2004) (in collaboration with UNiMORE) (see *Materials and Methods section*). To validate the success of NSCs transplantation in terms of NSC presence and correct localization in the vCA3, animals were sacrificed and perfused at 2 weeks post transplantation (2 wpt, short term) and 9 weeks post transplantation (9 wpt, long term), and brains were dissected and sectioned in order to perform further immunohistochemical and immunofluorescence analysis. GFP expression was used to detect grafted NSCs, while the Mg^{2+}-alginate was visible thanks to the conjugation with the Alexa fluor 568 antibody. Hematoxylin and Eosin staining

showed that the transplantation procedure was successful as indicated by the presence of GFP^+ NSCs and Mg^{2+}-alginate matrix in the vCA3 of TLE rats 2 wpt **(Figure 34A and B)**. Similarly, the immunostaining for GFP marker revealed the presence of GFP^+ NSCs alone and of GFP^+ NSCs + Mg^{2+}-alginate in the vCA3 of the epileptic rats 9 wpt **(Figure 34C)**. Moreover, at both short and long term post transplantation about 70% of the grafted cells were found in the desired area.

These results suggested that the chosen coordinates were optimal to get the cells into the ventral CA3 of epileptic rats and that the GFP^+ NSCs and Mg^{2+}-alginate were found in the desire area at both short and long term post transplantation.

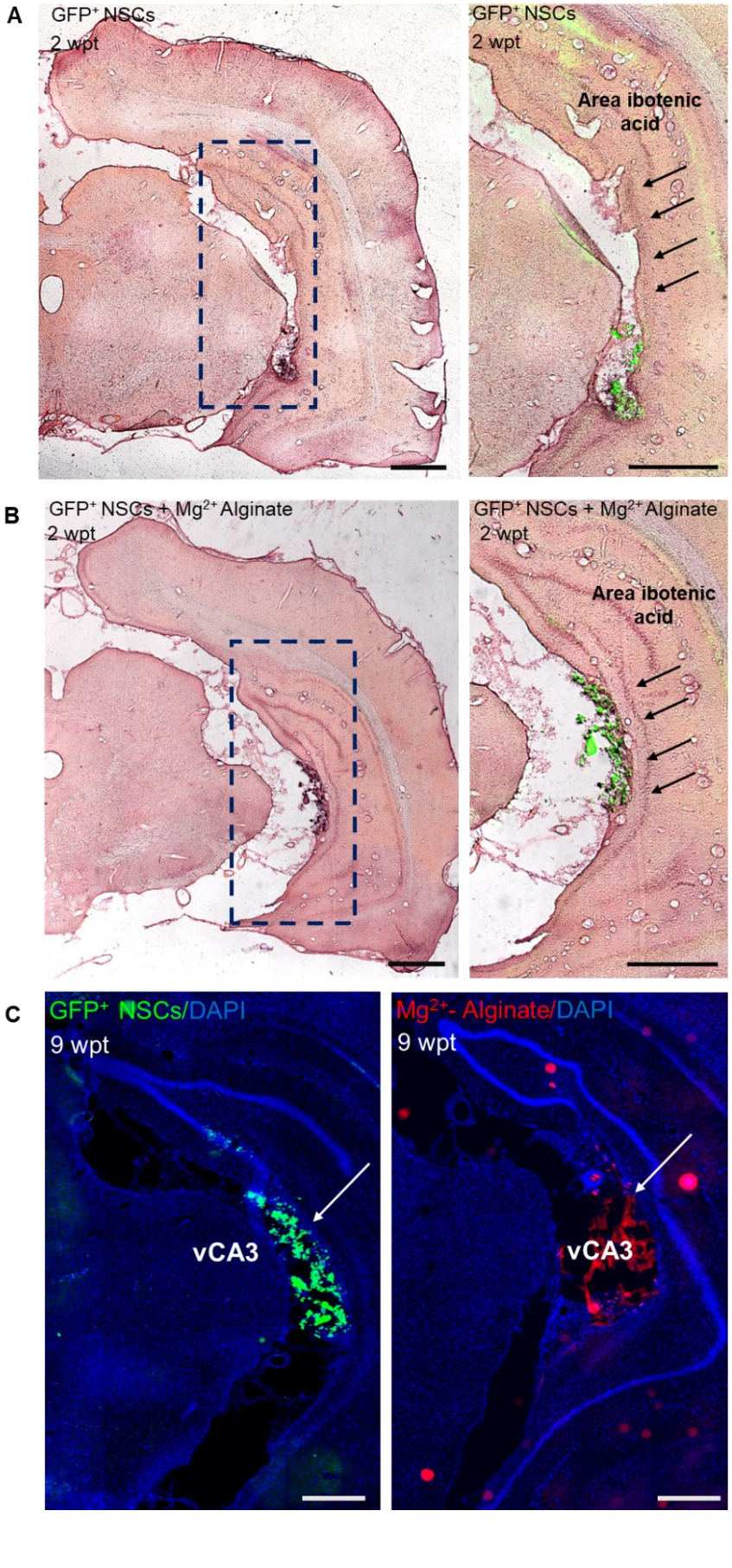
A
GFP+ NSCs
2 wpt
GFP+ NSCs
2 wpt
Area ibotenic acid
B
GFP+ NSCs + Mg2+ Alginate
2 wpt
GFP+ NSCs + Mg2+ Alginate
2 wpt
Area ibotenic acid
C
GFP+ NSCs/DAPI
9 wpt
vCA3
Mg2+- Alginate/DAPI
9 wpt
vCA3

Figure 34: GFP$^+$ NSCs and Mg^{2+}-alginate are found in vCA3 of epileptic rats 2 wpt and 9 wpt. (A, B) *Representative images of the Hematoxylin and Eosin staining of coronal section of epileptic rat brain transplanted with GFP$^+$ NSCs* ***(A)*** *or with GFP$^+$ NSCs + Mg^{2+}-alginate* ***(B)*** *at 2 wpt. GFP$^+$ NSCs are identified with the GFP antibody (green). Red dots indicate the area of lesion induced by ibotenic acid. DAPI: total nuclei. Scale bars: 1 mm (left panels) and 500 µm (right panels).* ***(C)*** *Representative images of the immunostaining of GFP$^+$ NSCs (green) and Mg^{2+}-alginate (red) in the hippocampal vCA3 of epileptic rats at 9 wpt. Scale bars: 200 µm.*

4.4.3 Rat hippocampal NSCs retain stemness until 9 weeks post transplantation

Since we effectively noted the presence of transplanted cells both after 2 and 9 weeks, we then questioned about their survival, differentiation, and maturation and whether the presence of Mg^{2+}-alginate could influence the maturation of the cells at long term post transplantation. To this aim, we performed immunofluorescence analysis for the stemness (SOX2 and Vimentin), for the immature neurons (TUBB3) and for the mature neurons (MAP2 and NeuN) markers. We also assessed the expression of the apoptotic marker Caspase-3. From this qualitative analysis, we found that some GFP^+ NSCs in the vCA3 co-expressed the stemness markers SOX2 and Vimentin in epileptic rats transplanted with NSCs **(Figure 35A)** or with NSCs + Mg^{2+}-alginate **(Figure 35B)**. However, no significant differences were observed in the expression of these markers between the two groups. Moreover, the expression of TUBB3, MAP2 and NeuN neuronal markers was not detected in the GFP^+ cells (data not shown). Interestingly, the absence of Caspasi-3 positivity of GFP^+ cells indicated that the transplanted NSCs survived in the hostile environment (data not shown). Overall, these data suggested that the NSCs after 9 weeks post transplantation persisted in a stemness state, and the presence of the alginate did not affect the differentiation and maturation of the cells. These data suggested that combined approaches should be further investigated in order to improve NSC maturation, differentiation and integration into the host tissue once transplanted. Indeed, we are now performing further studies to improve NSC integration into the host tissue. Experiments have been set up to test the effect of the combination of NSCs with the BDNF factor and the morphogen WNT3a in order to increase their maturation and to allow their hippocampal commitment, respectively, in the hostile environment once transplanted (in collaboration with Dr. Giulia Curia Lab, University of Modena). Moreover, studies

should be performed to evaluate the effects of stem cells transplantation on the occurrence of recurrent seizures and behavioral deficits characterizing the TLE animal model.

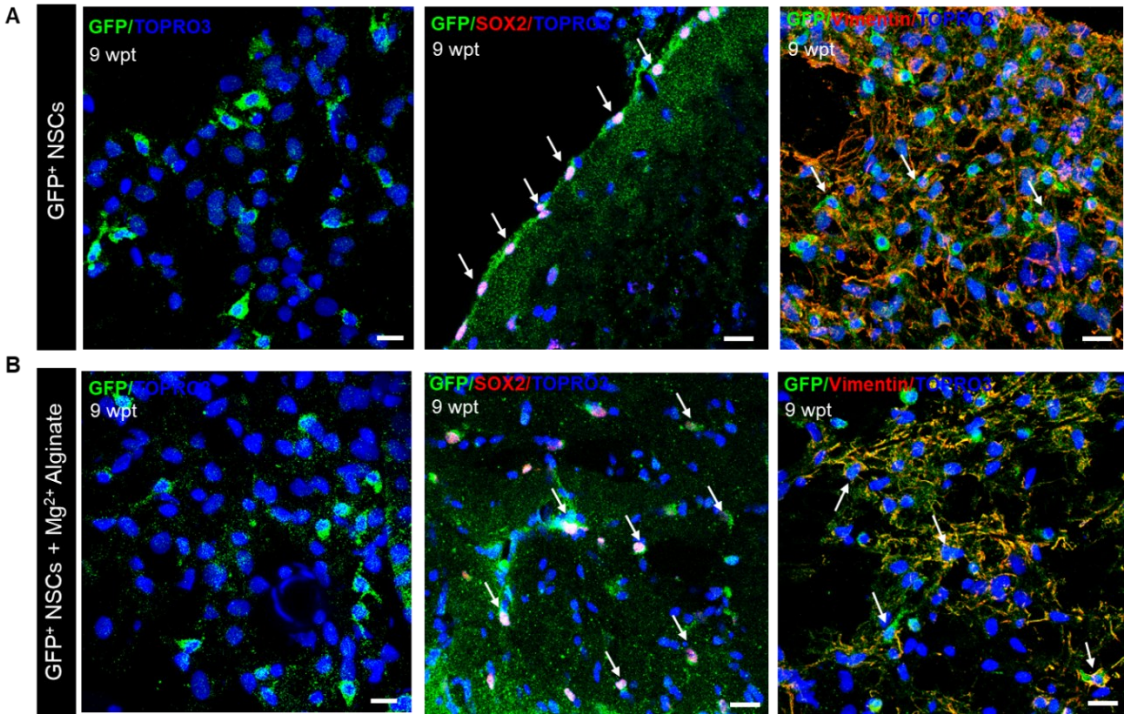

Figure 35: GFP$^+$ NSCs remain in a stemness state 9 weeks post transplantation. ***(A)*** *Representative confocal images of the immunostaining of GFP$^+$ NSCs (green) co-expressing the stemness markers SOX2 (red) and Vimentin (red) in the hippocampal vCA3 of epileptic rats transplanted with GFP$^+$ NSCs 9 wpt. DAPI: total nuclei. Scale bars: 20 µm.* ***(B)*** *Representative images of the immunostaining of GFP$^+$ NSCs (green) co-expressing the stemness markers SOX2 (red) and Vimentin (red) in the hippocampal vCA3 of epileptic rats transplanted with GFP$^+$NSCs + Mg^{2+}-alginate 9 wpt. DAPI: total nuclei. Scale bars: 20 µm. All the images in* ***A*** *and* ***B*** *are maximum intensity projections of z-stack confocal acquisitions.*

5. DISCUSSION

Despite enormous progress in pharmacological research, handling Central Nervous System (CNS) disorders is still challenging. To date, the majority of neurodegenerative diseases lack of effective cure, remission of pathological condition is rather partial and currently available drugs are extremely expensive and own troublesome side effects. This led to a considerable burden on society and to a high economic impact. Therefore, there is an urgent need to develop new effective treatments for the cure of CNS diseases. Recently, *in vitro* three-dimensional (3D) biological systems - organoids - have emerged as the state-of-the-art biotechnology to improve the chance of translatability of drugs for preclinical therapies and mimic the complexity of organs, proposing numerous approaches for human disease modeling, tissue engineering, drug development, large-scale pharmacological studies, diagnosis, and regenerative medicine. In particular, brain organoid technology is emerging as the latest frontier in regenerative medicine as they own the potential to be used as model for brain development (Quadrato et al., 2017), neurological disorders (Lancaster et al., 2013; P. Wang et al., 2017) and as functional grafts to regenerate damaged brain tissue (Mansour et al., 2018; S. N. Wang et al., 2020).

In this context, my PhD thesis was focused on the optimization of the in-house established protocol for the generation of mouse brain organoids in order to **(i)** increase brain organoid maturation and functionality and **(ii)** to promote hippocampal lineage commitment. In a translational prospective, the goal of my thesis project was **(iii)** to apply the organoid technology as new therapeutic strategy for the treatment of Temporal Lobe Epilepsy (TLE) in a rat model.

Increase brain organoid neuronal maturation and functionality

In our lab, we have developed, for the first time, a highly standardized, reproducible, and fast (5 weeks) murine brain organoid model starting from embryonic neural stem cells (Ciarpella et al., 2021). Indeed, given the fast growth rate and short scaling time of mouse brain development, murine brain organoids can be generated in a short time and with low production costs compared to hiPSC-derived brain organoids that require long time and high production cost for their *in vitro* generation that may hinder their potential

application in large-scale studies. In our study we demonstrated that the generated brain organoids showed the presence of neuronal lineage committed cells which progressively mature into neurons during the different organoid developmental stages (Ciarpella et al., 2021). Although we found the presence of synaptic components and spontaneous cellular calcium activity, the low number of neuronal cells and their incomplete neuronal maturation did not allow the formation of a robust neuronal network able to mimic a potential information processing. With these premises, in this work we optimized the in-house established protocol for the generation of brain organoids in order to enhance the organoid neuronal maturation and functionality. We demonstrated that the use of a vegetal extracellular matrix (ECM), the alginate (Palazzolo et al., 2015; Palazzolo et al., 2017) and of a selection of bioenergetic molecules called α5 (Bifari et al., 2020) increased the organoid differentiation, maturation and functionality *in vitro*.

A key aspect for organoid 3D spatial organization is the use of the ECM, a 3D network of extracellular macromolecules, such as collagen and glycoproteins, which provides structural and biochemical support to the cells. Specifically, we embedded neural stem cells (NSCs)-derived organoids with alginate ECM, a highly bio-compatible, low immunogenic algal polysaccharide, cross-linkable via bivalent cations to form a hydrogel (Johnson et al., 1997), and we evaluated its effect on neuronal differentiation and maturation *in vitro*. Mouse brain organoids were generated according to the three-phase protocol established in our lab (Ciarpella et al., 2021) and the alginate embedding was applied at the beginning of the Differentiation phase of the generation protocol. Our results showed that, although the alginate scaffold did not affect the size and morphology of brain organoids during their development, its application determined a significant decrease of both proliferative $Ki67^+$ cells at day 32 and of the number of dead cells at day 40 compared to control organoids. These data were in line with the literature (Palazzolo et al., 2015; Palazzolo et al., 2017). The reduction of Ki67-expressing cell in alginate-embedded organoid compared to control organoid highlighted the capability of the alginate ECM to boost the maturation of the cells constituting the organoid. Moreover, the reduction of cell dead demonstrated the potential of alginate ECM to provide structural and trophic support to the brain organoids. Immunofluorescence analysis revealed the presence of immature ($TUBB3^+$) and mature ($MAP2^+$) neuronal cells with high level of differentiation. Although we observed a lower number of neuronal cells

(TUBB3$^+$ and MAP2$^+$) in alginate-embedded organoids compared to control ones, neurons within the alginate-embedded organoids exhibited increased synaptic density (Syn$^+$ area/MAP2$^+$ area), suggesting a higher neuronal maturation compared to control organoids. Moreover, alginate-embedded organoids showed a higher co-localization of presynaptic (Syn) and postsynaptic (PSD95) punctae compared to control organoid, confirming the capability of alginate ECM to enhance the formation of a potentially functional neuronal networks within organoids. As support of the capability of alginate ECM to promote the neuronal lineage differentiation and maturation, results showed that alginate-embedded organoids significantly decreased the number of astrocytes (GFAP$^+$ cells) compared to control organoid, suggesting that alginate may favor the acquisition of a neuronal rather than an astrocyte phenotype. These data indicated that the use of alginate ECM preserved the organoid structure during the development and maturation, reducing uncontrolled growth typical of undifferentiated cells (Łabowska et al., 2021) and increased neuronal differentiation and maturation in brain organoids compared to control organoids. Our data were in line with the literature, indicating that the combined use of biomaterials with stem cells enhance their therapeutic function and support graft survival upon transplantation in CNS disorder models (Adil et al., 2017; Bible et al., 2012; Jin et al., 2010).

Accordingly with the literature (Bifari et al., 2020; Dolci et al., 2022), cell metabolism could be an attractive target to restore neural cell function and eventually heal pathological conditions. Studies reported that a selection of bioenergetic molecules, including the tricarboxylic acid (TCA) cycle intermediates, essential amino acids (EAAs), branched-chain amino acids (BCAAs), and the cofactors thiamine and pyridoxine, altogether referred to as α5, enhanced NSC neuronal maturation *in vitro*, increasing the total dendritic length, the mean number of branches and the number and maturation of the dendritic spines (Bifari et al., 2020). Specifically, α5 supplementation to the NSCs modulated the cellular metabolism driving the NSC neuronal differentiation and maturation through a metabolic shift towards oxidative phosphorylation (Bifari et al., 2020). In addition, pharmacological modulation of neuronal phenotype and maturation has been proposed as an attractive therapeutic treatment of neurological diseases (Dolci et al., 2022). Based on these observations, we supplemented the organoid differentiation medium with α5 mixture and investigated its effects on mouse brain organoid

differentiation, maturation and functionality. To assess the effects of α5 on the promotion of the brain organoid differentiation and maturation, we evaluated the expression of markers related to stemness ($SOX2^+$), immature ($TUBB3^+$) and mature neurons ($MAP2^+$) throughout the later organoid developmental phases by immunofluorescence analysis. Our results showed that α5 supplementation did not affect the maximum diameter of brain organoid. Notably, data revealed that α5 supplementation, although did not influence the expression of the stemness marker SOX2, significantly increased the expression of immature ($TUBB3^+$) and mature ($MAP2^+$) neuronal cells at the later stages of development. Moreover, accordingly with the increased number of mature neurons, α5 organoids showed a trend of increase of the synaptic density (Syn^+ area/ $MAP2^+$ area), although not significant. These results were in line with the literature (Bifari et al., 2020), highlighting the capability of α5 to improve neuronal maturation *in vitro*. Interestingly, calcium imaging analysis in mature a5 organoids, revealed the potential of α5 mixture to enhance the cell spontaneous calcium activity, suggesting the formation of a cellular network composed by neurons exhibiting potentially functional synaptic connections. Overall, these data suggested that α5 mixture may be a useful approach to enhance neuronal differentiation, maturation and functionality in brain organoids and may be an exploitable therapy to improve neuronal differentiation in neurodegenerative diseases.

WNT3a supplementation promotes hippocampal commitment in brain organoids

To date, although the mechanisms of hippocampal patterning and growth remain unclear, it was shown that a key role in these processes was played by the WNT3a signaling pathway which locally regulates the expansion of the caudomedial cortex from which the hippocampus develop (Lee et al., 2000). The hippocampus is one of the brain regions mostly involved in the pathological progression of many neurodegenerative disorders. An *in vitro* 3D structure able to replicate the hippocampal signature can be extremely useful for regenerative medicine, drug screening and neurodegenerative disease studies. Data regarding the induction of the hippocampal lineage commitment in 3D organoids obtained from murine neural stem cells is still lacking and to date the studies published focused on the generation of 3D organoids starting from human neural progenitor cells or

human induced pluripotent stem cells (iPSCs) (Sakaguchi et al., 2015; Sarkar et al., 2018; Yu et al., 2014). In our lab we previously set up a standardized protocol for the generation of mouse brain organoids (Ciarpella et al., 2021), however their characterization showed only a weak gene expression and patterning related to the hippocampus. To improve the hippocampal lineage commitment in the cultured brain organoids, we optimized the protocol accordingly to the one described by Sarkar and colleagues (Sarkar et al., 2018) which efficiently generated CA3 neurons from human iPSCs. Since WNT pathway is crucial for the hippocampal fate determination (Lie et al., 2005), in order to mimic the *in vivo* gradient of the molecules exerted by the cortical hem during hippocampal development (Grove et al., 1998), and to specifically generate CA3 mouse hippocampal organoids, we specifically supplemented the culture medium, during the Expansion and Induction phases, with the WNT3a factor. In line with studies conducted on WNT3a deficient mice, in which the hippocampus was severely reduced in size or missing (Lee et al., 2000), gene expression qPCR analysis performed both on control and WNT3a organoids confirmed the pivotal role of WNT3a in guiding properly the hippocampal lineage commitment and specification. In WNT3a organoids, the morphogen supplementation, in fact, resulted in a higher expression of key genes (including Grik4, Zbtb20, Sct, Alk) for the CA3 hippocampal development in WNT3a organoids compared to control ones. To assess the effects of WNT3a on the promotion of the brain organoid differentiation and maturation, we evaluated the expression of markers related to stemness ($SOX2^+$, $Vimentin^+$), neuronal progenitors (DCX^+), immature and mature neurons ($TUBB3^+$, $MAP2^+$), and glial cells ($GFAP^+$) throughout the different organoid developmental phases by immunofluorescence analysis. In line with the reduction of the maximum diameter at the later time points analysed, in WNT3a organoids, NSCs and neural precursor amount decreased over time, as well as the $KI67^+$ cell population, reaching the minimum at 32 days. Accordingly to several works supporting the WNT3a factor role in the expansion of the progenitor cell population *in vitro* (Muroyama, Kondoh, & Takada, 2004; Yoshinaga et al., 2010), in brain organoids WNT3a supplementation induced an increased expression of DCX^+ neural progenitors and $TUBB3^+$ immature neurons at the first stages of the organoid development compared to control organoids (Ciarpella et al., 2021). In addition, WNT3a positively affected the "inside-out" cell spatial distribution, as highlighted by the presence of a superficial defined packed DCX^+

and TUBB3$^+$ cell layers compared to the control organoids. The reduction of the number of immature DCX$^+$ and mature TUBB3$^+$ neuronal populations observed at later time-points was accompanied by the contemporaneous increase of the mature MAP2$^+$ neuron amount during the organoid developmental stages. Moreover, WNT3a organoids showed a significant increase of the synaptic density (Syn$^+$ area/MAP2$^+$ area) at later stage of differentiation, demonstrating that differentiated neurons, once mature, gave rise to a 3D heterogeneous and potentially functional synaptic network within the organoids. Synaptic development depends on astrocytes which play a supporting role in the energy and nutritional supply to neurons (Y. Kim, Park, & Choi, 2019). The presence of astrocytes within human brain organoids has been already reported (Pasca et al., 2015; Quadrato et al., 2017), and it has been showed that the addition of astrocytes to the neuronal cultures promotes synapse maturation and spontaneous action potential formation (Allen & Eroglu, 2017). Our results showed that the supplementation of WNT3a in the brain organoid culture media promoted a progressively increase in the astrocytes (GFAP$^+$) number during the different organoid differentiation stages compared to control organoids in which we observed a substantial unchanged percentage of GFAP$^+$ cells during the brain organoid development. In WNT3a organoids the astrocytes were mainly found in close contact with differentiating neuronal cells, suggesting, accordingly with the literature, their involvement in the regular neuronal activity and in the synaptic circuit's development. As confirmation of the results observed in brain organoids, it was well reported in literature that the addition of WNT3a in the culture media of 2D cell cultures of embryonic telencephalon neurospheres can selectively enhance both neuronal and astrocyte differentiation (Muroyama et al., 2004). The use of precise concentration of WNT3a (5ng/ml) allowed us to obtain consistent hippocampal specific neurons, expressing both the pan-hippocampal ZBTB20 marker, which is typical of all hippocampal neurons, and the KA1 marker which is primarily expressed by pyramidal neurons of the CA3 subfield of the hippocampus. Interestingly, a slight expression of other CA hippocampal subfield markers (i.e., OCT6 and FZD9) was found in mature WNT3a organoids while no expression of PROX1, specific for the DG hippocampal region, was detected. Calcium signaling and spontaneous oscillations of the intracellular calcium concentrations in synchronized patterns were found in many types of neural tissues *in vivo* and *in vitro*, including the hippocampus. This calcium activity is crucial to

sustain brain development and function, and play a pivotal role in several aspects of the neuronal growth and differentiation such as synapses maturation and synaptic contact formation (Rosenberg & Spitzer, 2011). By Fluo-4AM calcium imaging analysis, we noted a progressive increase of the cell activity within WNT3a organoids during the several time-points considered, suggesting the possible formation of a cellular network, composed by neurons exhibiting potentially functional synaptic connections. Our data were in line with literature, showing that WNT3a supplementation modulated and enhanced the amplitude of spontaneous calcium fluxes in neurons (Avila et al., 2020). Overall, these data demonstrated the possibility to obtain *in vitro* a complex 3D structure resembling the hippocampal tissue. These findings could pave the way to the use of this technology as platform for the study of hippocampal development in health and disease as well as to be exploited in transplantation procedures for restoring hippocampal disfunctions, such as in epilepsy.

Apply the organoid technology as new therapeutic strategy for the treatment of TLE

Temporal Lobe Epilepsy (TLE) is an adulthood focal epilepsy frequently refractory to anti-epileptic medications (Blair, 2012), and Mesial TLE (MTLE) is its most severe epilepsy condition, mainly characterized by hippocampal sclerosis (Brodie, Barry, Bamagous, Norrie, & Kwan, 2012; Thom, 2014). In TLE hippocampal sclerosis is accompanied by neurogenesis and rewiring, leading to its functional impairment (Cohen, Navarro, Clemenceau, Baulac, & Miles, 2002; Parent et al., 1997) and ultimately to seizure generation; the ventral hippocampus is particularly involved in seizure onset. Current medical treatments for TLE are extremely expensive and have a widespread impact on patients' health-related quality of life. In this context, cell therapy has emerged as novel therapeutic approach for the treatment of this neurological disorder (Bible et al., 2012; Jin et al., 2010; Upadhya et al., 2019). Results obtained *in vitro* from the use of alginate ECM as embedding scaffold of brain organoids, specifically highlighted the role of alginate to give trophic support to the cells and to preserve organoid structure. With these premises, we adopted a pilocarpine rat model of TLE and investigated whether the resuspension of NSCs in a solution with or without alginate ECM could positively impact

their survival, differentiation and maturation in the hostile environment of TLE. The NSC neuronal phenotype was first validated *in vitro,* detecting the expression of both stemness markers (SOX2) and neuronal progenitor markers (DCX, TUBB3). Once transplanted in the hippocampal ventral region of the CA3, NSCs alone or in combination with alginate still showed a stemness phenotype at both short term (2 weeks) and long term (9 weeks) post transplantation, with no differences among the two experimental groups. Thus, our data showed that the presence of the alginate ECM in this experimental condition is not sufficient to support neuronal NSCs differentiation, maturation and integration into the host tissue. The pathological hostile microenvironment of the brain in TLE rat model represents a huge obstacle for the integration and differentiation of the NSCs, leading to a low survival cell rate and a host-tissue reaction after NSCs transplantation and thus in a low therapeutic efficacy (Henriques et al., 2019; Zhao et al., 2021). Therefore, the combination of different approaches, such as the alginate matrix, that could give trophic support to the transplanted NSCs, the morphogen WNT3a which could boost their hippocampal commitment and also the addition to the cell suspension of factors enhancing cellular maturation, like the BDNF, would overcome these problems. Moreover, the advent of the 3D brain organoid technology is emerging as a promising source of transplantable tissues and functional cell types for cell therapy in regenerative medicine. To date, several groups have succeeded in brain organoid grafting reporting that cerebral organoid implanted into lesion sites differentiated into cortical neurons, formed long projections, and reversed deficits in animal model of traumatic brain injury and/or lesioned mouse cortex (Bao et al., 2021; Kitahara et al., 2020; Z. Wang et al., 2020). Interestingly, blood vessels were observed in some of the grafts, reporting successful attempts of organoids vascularization (Daviaud, Friedel, & Zou, 2018; Mansour et al., 2018; Shi et al., 2020) and suggesting the effective integration of the organoids in the physiologic system of the host tissue. Therefore, the direct transplantation of murine-derived brain organoids into rodents could represent a valuable tool to deeply investigate how neuron integrate into the brain circuitry and the effect on the damaged brain tissue in a TLE rat model.

CONCLUSION

In conclusion, my PhD work led to the optimization with different strategies (alginate, α5, WNT3a) of the protocol for the generation of mouse brain organoids in terms of increasing neuronal differentiation, maturation and functionality and promoting hippocampal lineage commitment *in vitro*. The efficacy of alginate matrix, α5 mixture and WNT3a factor in improving the organoid neuronal differentiation and maturation, and the hippocampal patterning, pave the way to explore the combination of these approaches for the development of a brain organoid transplantation protocol to treat CNS disorder, such as TLE. Moreover, the recent ground-breaking demonstration that transplanted brain organoids facilitate the structural and functional development of neuronal networks and their integration into the host brain (Mansour et al., 2018), makes them an interesting alternative to dissociated cell-based therapy.

REFERENCES

Adil, M. M., Vazin, T., Ananthanarayanan, B., Rodrigues, G. M. C., Rao, A. T., Kulkarni, R. U., . . . Schaffer, D. V. (2017). Engineered hydrogels increase the post-transplantation survival of encapsulated hESC-derived midbrain dopaminergic neurons. *Biomaterials, 136*, 1-11. doi:https://doi.org/10.1016/j.biomaterials.2017.05.008

Allen, N. J., & Eroglu, C. (2017). Cell Biology of Astrocyte-Synapse Interactions. *Neuron, 96*(3), 697-708. doi:10.1016/j.neuron.2017.09.056

Alvers, A. L., Fishwick, L. K., Wood, M. S., Hu, D., Chung, H. S., Dunn, W. A., Jr., & Aris, J. P. (2009). Autophagy and amino acid homeostasis are required for chronological longevity in Saccharomyces cerevisiae. *Aging Cell, 8*(4), 353-369. doi:10.1111/j.1474-9726.2009.00469.x

Angevine, J. B., Jr. (1965). Time of neuron origin in the hippocampal region. An autoradiographic study in the mouse. *Exp Neurol Suppl*, Suppl 2:1-70. Retrieved from https://www.ncbi.nlm.nih.gov/pubmed/5838955

Attwell, D., & Laughlin, S. B. (2001). An energy budget for signaling in the grey matter of the brain. *J Cereb Blood Flow Metab, 21*(10), 1133-1145. doi:10.1097/00004647-200110000-00001

Avila, M. E., Sepulveda, F. J., Burgos, C. F., Moraga-Cid, G., Parodi, J., Moon, R. T., . . . De Ferrari, G. V. (2020). Correction: Canonical Wnt3a modulates intracellular calcium and enhances excitatory neurotransmission in hippocampal neurons. *J Biol Chem, 295*(27), 9265. doi:10.1074/jbc.AAC120.014663

Bao, Z., Fang, K., Miao, Z., Li, C., Yang, C., Yu, Q., . . . Ji, J. (2021). Human Cerebral Organoid Implantation Alleviated the Neurological Deficits of Traumatic Brain Injury in Mice. *Oxidative medicine and cellular longevity, 2021*, 6338722-6338722. doi:10.1155/2021/6338722

Barshes, N., Demopoulos, A., & Engelhard, H. H. (2005). Anatomy and physiology of the leptomeninges and CSF space. *Cancer Treat Res, 125*, 1-16. doi:10.1007/0-387-24199-x_1

Bartfeld, S., Bayram, T., van de Wetering, M., Huch, M., Begthel, H., Kujala, P., . . . Clevers, H. (2015). In vitro expansion of human gastric epithelial stem cells and

their responses to bacterial infection. *Gastroenterology, 148*(1), 126-136.e126. doi:10.1053/j.gastro.2014.09.042

Bartolomei, F., Khalil, M., Wendling, F., Sontheimer, A., Regis, J., Ranjeva, J. P., . . . Chauvel, P. (2005). Entorhinal cortex involvement in human mesial temporal lobe epilepsy: an electrophysiologic and volumetric study. *Epilepsia, 46*(5), 677-687. doi:10.1111/j.1528-1167.2005.43804.x

Bayer, S. A. (1980). Development of the hippocampal region in the rat. II. Morphogenesis during embryonic and early postnatal life. *J Comp Neurol, 190*(1), 115-134. doi:10.1002/cne.901900108

Beckinghausen, J., & Sillitoe, R. V. (2019). Insights into cerebellar development and connectivity. *Neurosci Lett, 688*, 2-13. doi:10.1016/j.neulet.2018.05.013

Beghi, E., Giussani, G., Nichols, E., Abd-Allah, F., Abdela, J., Abdelalim, A., . . . Murray, C. J. L. (2019). Global, regional, and national burden of epilepsy, 1990–2016: a systematic analysis for the Global Burden of Disease Study 2016. *The Lancet Neurology, 18*(4), 357-375. doi:https://doi.org/10.1016/S1474-4422(18)30454-X

Ben-Ari, Y., & Lagowska, J. (1978). [Epileptogenic action of intra-amygdaloid injection of kainic acid]. *C R Acad Hebd Seances Acad Sci D, 287*(8), 813-816. Retrieved from https://www.ncbi.nlm.nih.gov/pubmed/103652

Ben-Ari, Y., Lagowska, J., Tremblay, E., & Le Gal La Salle, G. (1979). A new model of focal status epilepticus: intra-amygdaloid application of kainic acid elicits repetitive secondarily generalized convulsive seizures. *Brain Res, 163*(1), 176-179. doi:10.1016/0006-8993(79)90163-x

Ben-Ari, Y., Tremblay, E., Riche, D., Ghilini, G., & Naquet, R. (1981). Electrographic, clinical and pathological alterations following systemic administration of kainic acid, bicuculline or pentetrazole: metabolic mapping using the deoxyglucose method with special reference to the pathology of epilepsy. *Neuroscience, 6*(7), 1361-1391. doi:10.1016/0306-4522(81)90193-7

Benghanem, S., Mazeraud, A., Azabou, E., Chhor, V., Shinotsuka, C. R., Claassen, J., . . . Sharshar, T. (2020). Brainstem dysfunction in critically ill patients. *Crit Care, 24*(1), 5. doi:10.1186/s13054-019-2718-9

Berliocchi, L., Bano, D., & Nicotera, P. (2005). Ca2+ signals and death programmes in neurons. *Philos Trans R Soc Lond B Biol Sci, 360*(1464), 2255-2258. doi:10.1098/rstb.2005.1765

Bershteyn, M., Nowakowski, T. J., Pollen, A. A., Di Lullo, E., Nene, A., Wynshaw-Boris, A., & Kriegstein, A. R. (2017). Human iPSC-Derived Cerebral Organoids Model Cellular Features of Lissencephaly and Reveal Prolonged Mitosis of Outer Radial Glia. *Cell Stem Cell, 20*(4), 435-449 e434. doi:10.1016/j.stem.2016.12.007

Best, P. J., & White, A. M. (1999). Placing hippocampal single-unit studies in a historical context. *Hippocampus, 9*(4), 346-351. doi:10.1002/(SICI)1098-1063(1999)9:4<346::AID-HIPO2>3.0.CO;2-3

Bible, E., Dell'Acqua, F., Solanky, B., Balducci, A., Crapo, P. M., Badylak, S. F., . . . Modo, M. (2012). Non-invasive imaging of transplanted human neural stem cells and ECM scaffold remodeling in the stroke-damaged rat brain by (19)F- and diffusion-MRI. *Biomaterials, 33*(10), 2858-2871. doi:10.1016/j.biomaterials.2011.12.033

Bifari, F., Decimo, I., Chiamulera, C., Bersan, E., Malpeli, G., Johansson, J., . . . Krampera, M. (2009). Novel stem/progenitor cells with neuronal differentiation potential reside in the leptomeningeal niche. *J Cell Mol Med, 13*(9B), 3195-3208. doi:10.1111/j.1582-4934.2009.00706.x

Bifari, F., Dolci, S., Bottani, E., Pino, A., Di Chio, M., Zorzin, S., . . . Decimo, I. (2020). Complete neural stem cell (NSC) neuronal differentiation requires a branched chain amino acids-induced persistent metabolic shift towards energy metabolism. *Pharmacological Research, 158*, 104863. doi:10.1016/j.phrs.2020.104863

Bjornsson, C. S., Apostolopoulou, M., Tian, Y., & Temple, S. (2015). It takes a village: constructing the neurogenic niche. *Dev Cell, 32*(4), 435-446. doi:10.1016/j.devcel.2015.01.010

Blackstad, T. W. (1956). Commissural connections of the hippocampal region in the rat, with special reference to their mode of termination. *J Comp Neurol, 105*(3), 417-537. doi:10.1002/cne.901050305

Blair, R. D. (2012). Temporal lobe epilepsy semiology. *Epilepsy Res Treat, 2012*, 751510. doi:10.1155/2012/751510

Blurton-Jones, M., Kitazawa, M., Martinez-Coria, H., Castello, N. A., Müller, F. J., Loring, J. F., . . . LaFerla, F. M. (2009). Neural stem cells improve cognition via BDNF in a transgenic model of Alzheimer disease. *Proc Natl Acad Sci U S A, 106*(32), 13594-13599. doi:10.1073/pnas.0901402106

Boisvert, M. M., Erikson, G. A., Shokhirev, M. N., & Allen, N. J. (2018). The Aging Astrocyte Transcriptome from Multiple Regions of the Mouse Brain. *Cell Rep, 22*(1), 269-285. doi:10.1016/j.celrep.2017.12.039

Boj, S. F., Hwang, C. I., Baker, L. A., Chio, II, Engle, D. D., Corbo, V., . . . Tuveson, D. A. (2015). Organoid models of human and mouse ductal pancreatic cancer. *Cell, 160*(1-2), 324-338. doi:10.1016/j.cell.2014.12.021

Brodie, M. J., Barry, S. J., Bamagous, G. A., Norrie, J. D., & Kwan, P. (2012). Patterns of treatment response in newly diagnosed epilepsy. *Neurology, 78*(20), 1548-1554. doi:10.1212/WNL.0b013e3182563b19

Bulchand, S., Grove, E. A., Porter, F. D., & Tole, S. (2001). LIM-homeodomain gene Lhx2 regulates the formation of the cortical hem. *Mech Dev, 100*(2), 165-175. doi:10.1016/s0925-4773(00)00515-3

Cahoy, J. D., Emery, B., Kaushal, A., Foo, L. C., Zamanian, J. L., Christopherson, K. S., . . . Barres, B. A. (2008). A transcriptome database for astrocytes, neurons, and oligodendrocytes: a new resource for understanding brain development and function. *J Neurosci, 28*(1), 264-278. doi:10.1523/JNEUROSCI.4178-07.2008

Cano, A., Fonseca, E., Ettcheto, M., Sanchez-Lopez, E., de Rojas, I., Alonso-Lana, S., . . . Ruiz, A. (2021). Epilepsy in Neurodegenerative Diseases: Related Drugs and Molecular Pathways. *Pharmaceuticals (Basel), 14*(10). doi:10.3390/ph14101057

Cao, Y., Lv, G., Wang, Y. S., Fan, Z. K., Bi, Y. L., Zhao, L., & Guo, Z. P. (2013). Mitochondrial fusion and fission after spinal sacord injury in rats. *Brain Res, 1522*, 59-66. doi:10.1016/j.brainres.2013.05.033

Caronia-Brown, G., Yoshida, M., Gulden, F., Assimacopoulos, S., & Grove, E. A. (2014). The cortical hem regulates the size and patterning of neocortex. *Development, 141*(14), 2855-2865. doi:10.1242/dev.106914

Cavalheiro, E. A., Leite, J. P., Bortolotto, Z. A., Turski, W. A., Ikonomidou, C., & Turski, L. (1991). Long-term effects of pilocarpine in rats: structural damage of the brain

triggers kindling and spontaneous recurrent seizures. *Epilepsia, 32*(6), 778-782. doi:10.1111/j.1528-1157.1991.tb05533.x

Chang, B. S., & Lowenstein, D. H. (2003). Epilepsy. *N Engl J Med, 349*(13), 1257-1266. doi:10.1056/NEJMra022308

Chauhan, P., Jethwa, K., Rathawa, A., Chauhan, G., & Mehra, S. (2021). The Anatomy of the Hippocampus. In R. Pluta (Ed.), *Cerebral Ischemia*. Brisbane (AU).

Ciarpella, F., Zamfir, R. G., Campanelli, A., Ren, E., Pedrotti, G., Bottani, E., . . . Decimo, I. (2021). Murine cerebral organoids develop network of functional neurons and hippocampal brain region identity. *iScience, 24*(12), 103438. doi:10.1016/j.isci.2021.103438

Cohen, I., Navarro, V., Clemenceau, S., Baulac, M., & Miles, R. (2002). On the origin of interictal activity in human temporal lobe epilepsy in vitro. *Science, 298*(5597), 1418-1421. doi:10.1126/science.1076510

Cole, J. T., Mitala, C. M., Kundu, S., Verma, A., Elkind, J. A., Nissim, I., & Cohen, A. S. (2010). Dietary branched chain amino acids ameliorate injury-induced cognitive impairment. *Proc Natl Acad Sci U S A, 107*(1), 366-371. doi:10.1073/pnas.0910280107

Conover, J. C., & Notti, R. Q. (2008). The neural stem cell niche. *Cell and Tissue Research, 331*(1), 211-224. doi:10.1007/s00441-007-0503-6

Curia, G., Longo, D., Biagini, G., Jones, R. S., & Avoli, M. (2008). The pilocarpine model of temporal lobe epilepsy. *J Neurosci Methods, 172*(2), 143-157. doi:10.1016/j.jneumeth.2008.04.019

D'Antona, G., Ragni, M., Cardile, A., Tedesco, L., Dossena, M., Bruttini, F., . . . Nisoli, E. (2010). Branched-chain amino acid supplementation promotes survival and supports cardiac and skeletal muscle mitochondrial biogenesis in middle-aged mice. *Cell Metab, 12*(4), 362-372. doi:10.1016/j.cmet.2010.08.016

Danglot, L., Triller, A., & Marty, S. (2006). The development of hippocampal interneurons in rodents. *Hippocampus, 16*(12), 1032-1060. doi:10.1002/hipo.20225

Datson, N. A., Meijer, L., Steenbergen, P. J., Morsink, M. C., van der Laan, S., Meijer, O. C., & de Kloet, E. R. (2004). Expression profiling in laser-microdissected hippocampal subregions in rat brain reveals large subregion-specific differences

in expression. *Eur J Neurosci, 20*(10), 2541-2554. doi:10.1111/j.1460-9568.2004.03738.x

Daviaud, N., Friedel, R. H., & Zou, H. (2018). Vascularization and Engraftment of Transplanted Human Cerebral Organoids in Mouse Cortex. *eneuro, 5*(6), ENEURO.0219-0218.2018. doi:10.1523/eneuro.0219-18.2018

De Bandt, J. P., & Cynober, L. (2006). Therapeutic use of branched-chain amino acids in burn, trauma, and sepsis. *J Nutr, 136*(1 Suppl), 308s-313s. doi:10.1093/jn/136.1.308S

Decimo, I., Bifari, F., Rodriguez, F. J., Malpeli, G., Dolci, S., Lavarini, V., . . . Fumagalli, G. (2011). Nestin- and doublecortin-positive cells reside in adult spinal cord meninges and participate in injury-induced parenchymal reaction. *Stem Cells, 29*(12), 2062-2076. doi:10.1002/stem.766

Decimo, I., Fumagalli, G., Berton, V., Krampera, M., & Bifari, F. (2012). Meninges: from protective membrane to stem cell niche. *Am J Stem Cells, 1*(2), 92-105. Retrieved from https://www.ncbi.nlm.nih.gov/pubmed/23671802

Dekkers, J. F., Berkers, G., Kruisselbrink, E., Vonk, A., de Jonge, H. R., Janssens, H. M., . . . Beekman, J. M. (2016). Characterizing responses to CFTR-modulating drugs using rectal organoids derived from subjects with cystic fibrosis. *Sci Transl Med, 8*(344), 344ra384. doi:10.1126/scitranslmed.aad8278

del Río, J. A., Martínez, A., Fonseca, M., Auladell, C., & Soriano, E. (1995). Glutamate-like immunoreactivity and fate of Cajal-Retzius cells in the murine cortex as identified with calretinin antibody. *Cereb Cortex, 5*(1), 13-21. doi:10.1093/cercor/5.1.13

Dhikav, V., & Anand, K. (2007). Hippocampal atrophy may be a predictor of seizures in Alzheimer's disease. *Med Hypotheses, 69*(1), 234-235. doi:10.1016/j.mehy.2006.11.031

Dhikav, V., & Anand, K. S. (2007). Glucocorticoids may initiate Alzheimer's disease: a potential therapeutic role for mifepristone (RU-486). *Med Hypotheses, 68*(5), 1088-1092. doi:10.1016/j.mehy.2006.09.038

Dolci, S., Mannino, L., Bottani, E., Campanelli, A., Di Chio, M., Zorzin, S., . . . Decimo, I. (2022). Therapeutic induction of energy metabolism reduces neural tissue

damage and increases microglia activation in severe spinal cord injury. *Pharmacological Research, 178*, 106149. doi:10.1016/j.phrs.2022.106149

Dolci, S., Pino, A., Berton, V., Gonzalez, P., Braga, A., Fumagalli, M., . . . Decimo, I. (2017). High Yield of Adult Oligodendrocyte Lineage Cells Obtained from Meningeal Biopsy. *Front Pharmacol, 8*, 703. doi:10.3389/fphar.2017.00703

Dontu, G., Abdallah, W. M., Foley, J. M., Jackson, K. W., Clarke, M. F., Kawamura, M. J., & Wicha, M. S. (2003). In vitro propagation and transcriptional profiling of human mammary stem/progenitor cells. *Genes Dev, 17*(10), 1253-1270. doi:10.1101/gad.1061803

Eiraku, M., & Sasai, Y. (2011). Mouse embryonic stem cell culture for generation of three-dimensional retinal and cortical tissues. *Nat Protoc, 7*(1), 69-79. doi:10.1038/nprot.2011.429

Eiraku, M., Takata, N., Ishibashi, H., Kawada, M., Sakakura, E., Okuda, S., . . . Sasai, Y. (2011). Self-organizing optic-cup morphogenesis in three-dimensional culture. *Nature, 472*(7341), 51-56. doi:10.1038/nature09941

Etchevers, H. C., Couly, G., Vincent, C., & Le Douarin, N. M. (1999). Anterior cephalic neural crest is required for forebrain viability. *Development, 126*(16), 3533-3543. doi:10.1242/dev.126.16.3533

Fisher, R. S., Cross, J. H., French, J. A., Higurashi, N., Hirsch, E., Jansen, F. E., . . . Zuberi, S. M. (2017). Operational classification of seizure types by the International League Against Epilepsy: Position Paper of the ILAE Commission for Classification and Terminology. *Epilepsia, 58*(4), 522-530. doi:10.1111/epi.13670

Gao, D., Vela, I., Sboner, A., Iaquinta, P. J., Karthaus, W. R., Gopalan, A., . . . Chen, Y. (2014). Organoid cultures derived from patients with advanced prostate cancer. *Cell, 159*(1), 176-187. doi:10.1016/j.cell.2014.08.016

Gee, K. R., Brown, K. A., Chen, W. N., Bishop-Stewart, J., Gray, D., & Johnson, I. (2000). Chemical and physiological characterization of fluo-4 Ca(2+)-indicator dyes. *Cell Calcium, 27*(2), 97-106. doi:10.1054/ceca.1999.0095

Ghannam, J. Y., & Al Kharazi, K. A. (2022). Neuroanatomy, Cranial Meninges. In *StatPearls*. Treasure Island (FL).

Gomes, A. R., Fernandes, T. G., Vaz, S. H., Silva, T. P., Bekman, E. P., Xapelli, S., . . . Diogo, M. M. (2020). Modeling Rett Syndrome With Human Patient-Specific Forebrain Organoids. *Front Cell Dev Biol, 8*, 610427. doi:10.3389/fcell.2020.610427

Gonzalez, C., Armijo, E., Bravo-Alegria, J., Becerra-Calixto, A., Mays, C. E., & Soto, C. (2018). Modeling amyloid beta and tau pathology in human cerebral organoids. *Mol Psychiatry, 23*(12), 2363-2374. doi:10.1038/s41380-018-0229-8

Gronholm, M., Feodoroff, M., Antignani, G., Martins, B., Hamdan, F., & Cerullo, V. (2021). Patient-Derived Organoids for Precision Cancer Immunotherapy. *Cancer Res, 81*(12), 3149-3155. doi:10.1158/0008-5472.CAN-20-4026

Grove, E. A., Tole, S., Limon, J., Yip, L., & Ragsdale, C. W. (1998). The hem of the embryonic cerebral cortex is defined by the expression of multiple Wnt genes and is compromised in Gli3-deficient mice. *Development, 125*(12), 2315-2325. doi:10.1242/dev.125.12.2315

Hallermann, S., de Kock, C. P., Stuart, G. J., & Kole, M. H. (2012). State and location dependence of action potential metabolic cost in cortical pyramidal neurons. *Nat Neurosci, 15*(7), 1007-1014. doi:10.1038/nn.3132

Hamilton, L. W. (1976). The Limbic System Defined. In L. W. Hamilton (Ed.), *Basic Limbic System Anatomy of the Rat* (pp. 25-32). Boston, MA: Springer US.

Hampson, R. E., Jarrard, L. E., & Deadwyler, S. A. (1999). Effects of ibotenate hippocampal and extrahippocampal destruction on delayed-match and -nonmatch-to-sample behavior in rats. *J Neurosci, 19*(4), 1492-1507. doi:10.1523/jneurosci.19-04-01492.1999

Hattiangady, B., Rao, M. S., Zaman, V., & Shetty, A. K. (2006). Incorporation of embryonic CA3 cell grafts into the adult hippocampus at 4-months after injury: effects of combined neurotrophic supplementation and caspase inhibition. *Neuroscience, 139*(4), 1369-1383. doi:10.1016/j.neuroscience.2006.01.058

Hayamizu, T. F., Mangan, M., Corradi, J. P., Kadin, J. A., & Ringwald, M. (2005). The Adult Mouse Anatomical Dictionary: a tool for annotating and integrating data. *Genome Biol, 6*(3), R29. doi:10.1186/gb-2005-6-3-r29

Hedlund, E., & Perlmann, T. (2009). Neuronal cell replacement in Parkinson's disease. *J Intern Med, 266*(4), 358-371. doi:10.1111/j.1365-2796.2009.02155.x

Henriques, D., Moreira, R., Schwamborn, J., Pereira de Almeida, L., & Mendonça, L. S. (2019). Successes and Hurdles in Stem Cells Application and Production for Brain Transplantation. *Frontiers in Neuroscience, 13*, 1194-1194. doi:10.3389/fnins.2019.01194

Hirsch, W. L., Kemp, S. S., Martinez, A. J., Curtin, H., Latchaw, R. E., & Wolf, G. (1989). Anatomy of the brainstem: correlation of in vitro MR images with histologic sections. *AJNR Am J Neuroradiol, 10*(5), 923-928. Retrieved from https://www.ncbi.nlm.nih.gov/pubmed/2505535

Ho, B. X., Pek, N. M. Q., & Soh, B. S. (2018). Disease Modeling Using 3D Organoids Derived from Human Induced Pluripotent Stem Cells. *Int J Mol Sci, 19*(4). doi:10.3390/ijms19040936

Huch, M., Gehart, H., van Boxtel, R., Hamer, K., Blokzijl, F., Verstegen, M. M., . . . Clevers, H. (2015). Long-term culture of genome-stable bipotent stem cells from adult human liver. *Cell, 160*(1-2), 299-312. doi:10.1016/j.cell.2014.11.050

Hunt, R. F., Girskis, K. M., Rubenstein, J. L., Alvarez-Buylla, A., & Baraban, S. C. (2013). GABA progenitors grafted into the adult epileptic brain control seizures and abnormal behavior. *Nat Neurosci, 16*(6), 692-697. doi:10.1038/nn.3392

Idowu, S., Bertrand, P. P., & Walduck, A. K. (2022). Homeostasis and Cancer Initiation: Organoids as Models to Study the Initiation of Gastric Cancer. *International journal of molecular sciences, 23*(5), 2790. doi:10.3390/ijms23052790

Itopa, E. A. (2020). Anatomy of the hippocampus and its emerging roles in modulating emotion-dependent autonomic activities. *Italian Journal of Anatomy and Embryology, 124*(3). doi:10.13128/ijae-11663

Jackson, J. H. (1890). The Lumleian Lectures on Convulsive Seizures. *Br Med J, 1*(1527), 765-771. doi:10.1136/bmj.1.1527.765

Jarrard, L. E. (1989). On the use of ibotenic acid to lesion selectively different components of the hippocampal formation. *J Neurosci Methods, 29*(3), 251-259. doi:10.1016/0165-0270(89)90149-0

Jernigan, T. L., & Stiles, J. (2017). Construction of the human forebrain. *Wiley Interdiscip Rev Cogn Sci, 8*(1-2). doi:10.1002/wcs.1409

Jiajia, L., Shinghung, M., Jiacheng, Z., Jialing, W., Dilin, X., Shengquan, H., . . . Wei, C. (2017). Assessment of Neuronal Viability Using Fluorescein Diacetate-

Propidium Iodide Double Staining in Cerebellar Granule Neuron Culture. *J Vis Exp*(123). doi:10.3791/55442

Jin, K., Mao, X., Xie, L., Galvan, V., Lai, B., Wang, Y., . . . Greenberg, D. A. (2010). Transplantation of human neural precursor cells in Matrigel scaffolding improves outcome from focal cerebral ischemia after delayed postischemic treatment in rats. *J Cereb Blood Flow Metab, 30*(3), 534-544. doi:10.1038/jcbfm.2009.219

Johnson, F. A., Craig, D. Q., & Mercer, A. D. (1997). Characterization of the block structure and molecular weight of sodium alginates. *J Pharm Pharmacol, 49*(7), 639-643. doi:10.1111/j.2042-7158.1997.tb06085.x

Khalaf-Nazzal, R., & Francis, F. (2013). Hippocampal development - old and new findings. *Neuroscience, 248*, 225-242. doi:10.1016/j.neuroscience.2013.05.061

Kim, J., Koo, B.-K., & Knoblich, J. A. (2020). Human organoids: model systems for human biology and medicine. *Nature Reviews Molecular Cell Biology, 21*(10), 571-584. doi:10.1038/s41580-020-0259-3

Kim, Y., Park, J., & Choi, Y. K. (2019). The Role of Astrocytes in the Central Nervous System Focused on BK Channel and Heme Oxygenase Metabolites: A Review. *Antioxidants (Basel), 8*(5). doi:10.3390/antiox8050121

Kitahara, T., Sakaguchi, H., Morizane, A., Kikuchi, T., Miyamoto, S., & Takahashi, J. (2020). Axonal Extensions along Corticospinal Tracts from Transplanted Human Cerebral Organoids. *Stem Cell Reports, 15*(2), 467-481. doi:10.1016/j.stemcr.2020.06.016

Knierim, J. J. (2015). The hippocampus. *Curr Biol, 25*(23), R1116-1121. doi:10.1016/j.cub.2015.10.049

Korinek, V., Barker, N., Moerer, P., van Donselaar, E., Huls, G., Peters, P. J., & Clevers, H. (1998). Depletion of epithelial stem-cell compartments in the small intestine of mice lacking Tcf-4. *Nature Genetics, 19*(4), 379-383. doi:10.1038/1270

Kretschmann, H. J., & Wingert, F. (1968). [On the quantitative development of hippocampal formation in the albino rat]. *J Hirnforsch, 10*(6), 471-486. Retrieved from https://www.ncbi.nlm.nih.gov/pubmed/5733522

Łabowska, M. B., Cierluk, K., Jankowska, A. M., Kulbacka, J., Detyna, J., & Michalak, I. (2021). A Review on the Adaption of Alginate-Gelatin Hydrogels for 3D Cultures and Bioprinting. *Materials (Basel), 14*(4). doi:10.3390/ma14040858

Lancaster, M. A., & Knoblich, J. A. (2014a). Generation of cerebral organoids from human pluripotent stem cells. *Nat Protoc, 9*(10), 2329-2340. doi:10.1038/nprot.2014.158

Lancaster, M. A., & Knoblich, J. A. (2014b). Organogenesis in a dish: modeling development and disease using organoid technologies. *Science, 345*(6194), 1247125. doi:10.1126/science.1247125

Lancaster, M. A., Renner, M., Martin, C. A., Wenzel, D., Bicknell, L. S., Hurles, M. E., . . . Knoblich, J. A. (2013). Cerebral organoids model human brain development and microcephaly. *Nature, 501*(7467), 373-379. doi:10.1038/nature12517

Laughlin, S. B., de Ruyter van Steveninck, R. R., & Anderson, J. C. (1998). The metabolic cost of neural information. *Nat Neurosci, 1*(1), 36-41. doi:10.1038/236

Lee, H., Yun, S., Kim, I.-S., Lee, I.-S., Shin, J. E., Park, S. C., . . . Park, K. I. (2014). Human Fetal Brain-Derived Neural Stem/Progenitor Cells Grafted into the Adult Epileptic Brain Restrain Seizures in Rat Models of Temporal Lobe Epilepsy. *PLoS One, 9*(8), e104092. doi:10.1371/journal.pone.0104092

Lee, J. H., Bhang, D. H., Beede, A., Huang, T. L., Stripp, B. R., Bloch, K. D., . . . Kim, C. F. (2014). Lung stem cell differentiation in mice directed by endothelial cells via a BMP4-NFATc1-thrombospondin-1 axis. *Cell, 156*(3), 440-455. doi:10.1016/j.cell.2013.12.039

Lee, S. M., Tole, S., Grove, E., & McMahon, A. P. (2000). A local Wnt-3a signal is required for development of the mammalian hippocampus. *Development, 127*(3), 457-467. doi:10.1242/dev.127.3.457

Lein, E. S., Zhao, X., & Gage, F. H. (2004). Defining a molecular atlas of the hippocampus using DNA microarrays and high-throughput in situ hybridization. *J Neurosci, 24*(15), 3879-3889. doi:10.1523/JNEUROSCI.4710-03.2004

Levesque, M., Avoli, M., & Bernard, C. (2016). Animal models of temporal lobe epilepsy following systemic chemoconvulsant administration. *J Neurosci Methods, 260*, 45-52. doi:10.1016/j.jneumeth.2015.03.009

Li, G., & Pleasure, S. J. (2014). The development of hippocampal cellular assemblies. *Wiley Interdiscip Rev Dev Biol, 3*(2), 165-177. doi:10.1002/wdev.127

Li, M., & Izpisua Belmonte, J. C. (2019). Organoids - Preclinical Models of Human Disease. *N Engl J Med, 380*(6), 569-579. doi:10.1056/NEJMra1806175

Li, X., Liu, T., Song, K., Yao, L., Ge, D., Bao, C., . . . Cui, Z. (2006). Culture of neural stem cells in calcium alginate beads. *Biotechnol Prog, 22*(6), 1683-1689. doi:10.1021/bp060185z

Lie, D. C., Colamarino, S. A., Song, H. J., Desire, L., Mira, H., Consiglio, A., . . . Gage, F. H. (2005). Wnt signalling regulates adult hippocampal neurogenesis. *Nature, 437*(7063), 1370-1375. doi:10.1038/nature04108

LoPachin, R. M., Gaughan, C. L., Lehning, E. J., Kaneko, Y., Kelly, T. M., & Blight, A. (1999). Experimental spinal cord injury: spatiotemporal characterization of elemental concentrations and water contents in axons and neuroglia. *J Neurophysiol, 82*(5), 2143-2153. doi:10.1152/jn.1999.82.5.2143

Lorente De Nó, R. (1934). Studies on the structure of the cerebral cortex. II. Continuation of the study of the ammonic system. *Journal für Psychologie und Neurologie, 46*, 113-177.

Maclean, P. D. (1952). Some psychiatric implications of physiological studies on frontotemporal portion of limbic system (visceral brain). *Electroencephalogr Clin Neurophysiol, 4*(4), 407-418. doi:10.1016/0013-4694(52)90073-4

Maillard, L., Vignal, J. P., Gavaret, M., Guye, M., Biraben, A., McGonigal, A., . . . Bartolomei, F. (2004). Semiologic and electrophysiologic correlations in temporal lobe seizure subtypes. *Epilepsia, 45*(12), 1590-1599. doi:10.1111/j.0013-9580.2004.09704.x

Mangale, V. S., Hirokawa, K. E., Satyaki, P. R., Gokulchandran, N., Chikbire, S., Subramanian, L., . . . Monuki, E. S. (2008). Lhx2 selector activity specifies cortical identity and suppresses hippocampal organizer fate. *Science, 319*(5861), 304-309. doi:10.1126/science.1151695

Mansour, A. A., Goncalves, J. T., Bloyd, C. W., Li, H., Fernandes, S., Quang, D., . . . Gage, F. H. (2018). An in vivo model of functional and vascularized human brain organoids. *Nat Biotechnol, 36*(5), 432-441. doi:10.1038/nbt.4127

Marchesini, G., Bianchi, G., Merli, M., Amodio, P., Panella, C., Loguercio, C., . . . Italian, B. S. G. (2003). Nutritional supplementation with branched-chain amino acids in advanced cirrhosis: a double-blind, randomized trial. *Gastroenterology, 124*(7), 1792-1801. doi:10.1016/s0016-5085(03)00323-8

Mariani, J., Coppola, G., Zhang, P., Abyzov, A., Provini, L., Tomasini, L., . . . Vaccarino, F. M. (2015). FOXG1-Dependent Dysregulation of GABA/Glutamate Neuron Differentiation in Autism Spectrum Disorders. *Cell, 162*(2), 375-390. doi:10.1016/j.cell.2015.06.034

Mathern, G. W., Kuhlman, P. A., Mendoza, D., & Pretorius, J. K. (1997). Human fascia dentata anatomy and hippocampal neuron densities differ depending on the epileptic syndrome and age at first seizure. *J Neuropathol Exp Neurol, 56*(2), 199-212. doi:10.1097/00005072-199702000-00011

Mattson, M. P. (2008). Glutamate and neurotrophic factors in neuronal plasticity and disease. *Ann N Y Acad Sci, 1144*, 97-112. doi:10.1196/annals.1418.005

McDonald, J. W., Silverstein, F. S., & Johnston, M. V. (1990). Magnesium reduces N-methyl-D-aspartate (NMDA)-mediated brain injury in perinatal rats. *Neurosci Lett, 109*(1-2), 234-238. doi:10.1016/0304-3940(90)90569-u

Morizane, R., & Bonventre, J. V. (2017). Generation of nephron progenitor cells and kidney organoids from human pluripotent stem cells. *Nat Protoc, 12*(1), 195-207. doi:10.1038/nprot.2016.170

Moshiri, A., Close, J., & Reh, T. A. (2004). Retinal stem cells and regeneration. *Int J Dev Biol, 48*(8-9), 1003-1014. doi:10.1387/ijdb.041870am

Muroyama, Y., Kondoh, H., & Takada, S. (2004). Wnt proteins promote neuronal differentiation in neural stem cell culture. *Biochem Biophys Res Commun, 313*(4), 915-921. doi:10.1016/j.bbrc.2003.12.023

Nantasanti, S., de Bruin, A., Rothuizen, J., Penning, L. C., & Schotanus, B. A. (2016). Concise Review: Organoids Are a Powerful Tool for the Study of Liver Disease and Personalized Treatment Design in Humans and Animals. *Stem Cells Transl Med, 5*(3), 325-330. doi:10.5966/sctm.2015-0152

Nicolas, J., Magli, S., Rabbachin, L., Sampaolesi, S., Nicotra, F., & Russo, L. (2020). 3D Extracellular Matrix Mimics: Fundamental Concepts and Role of Materials Chemistry to Influence Stem Cell Fate. *Biomacromolecules, 21*(6), 1968-1994. doi:10.1021/acs.biomac.0c00045

O'Keefe, J., & Dostrovsky, J. (1971). The hippocampus as a spatial map. Preliminary evidence from unit activity in the freely-moving rat. *Brain Res, 34*(1), 171-175. doi:10.1016/0006-8993(71)90358-1

O'Keefe, J., & Nadel, L. (1979). Précis of O'Keefe & Nadel's The hippocampus as a cognitive map. *Behavioral and Brain Sciences, 2*(4), 487-494. doi:10.1017/S0140525X00063949

O'Keefe, J., Nadel, L., Keightley, S., & Kill, D. (1975). Fornix lesions selectively abolish place learning in the rat. *Exp Neurol, 48*(1), 152-166. doi:10.1016/0014-4886(75)90230-7

O'Rahilly, R., & Muller, F. (1986). The meninges in human development. *J Neuropathol Exp Neurol, 45*(5), 588-608. Retrieved from https://www.ncbi.nlm.nih.gov/pubmed/3746345

Palazzolo, G., Broguiere, N., Cenciarelli, O., Dermutz, H., & Zenobi-Wong, M. (2015). Ultrasoft Alginate Hydrogels Support Long-Term Three-Dimensional Functional Neuronal Networks. *Tissue Eng Part A, 21*(15-16), 2177-2185. doi:10.1089/ten.TEA.2014.0518

Palazzolo, G., Moroni, M., Soloperto, A., Aletti, G., Naldi, G., Vassalli, M., . . . Difato, F. (2017). Fast wide-volume functional imaging of engineered in vitro brain tissues. *Sci Rep, 7*(1), 8499. doi:10.1038/s41598-017-08979-8

Palmer, T. D., Takahashi, J., & Gage, F. H. (1997). The adult rat hippocampus contains primordial neural stem cells. *Mol Cell Neurosci, 8*(6), 389-404. doi:10.1006/mcne.1996.0595

Parent, J. M., Yu, T. W., Leibowitz, R. T., Geschwind, D. H., Sloviter, R. S., & Lowenstein, D. H. (1997). Dentate granule cell neurogenesis is increased by seizures and contributes to aberrant network reorganization in the adult rat hippocampus. *J Neurosci, 17*(10), 3727-3738. doi:10.1523/jneurosci.17-10-03727.1997

Park, D., Yang, Y. H., Bae, D. K., Lee, S. H., Yang, G., Kyung, J., . . . Kim, Y. B. (2013). Improvement of cognitive function and physical activity of aging mice by human neural stem cells over-expressing choline acetyltransferase. *Neurobiol Aging, 34*(11), 2639-2646. doi:10.1016/j.neurobiolaging.2013.04.026

Park, J. C., Jang, S. Y., Lee, D., Lee, J., Kang, U., Chang, H., . . . Mook-Jung, I. (2021). A logical network-based drug-screening platform for Alzheimer's disease representing pathological features of human brain organoids. *Nat Commun, 12*(1), 280. doi:10.1038/s41467-020-20440-5

Pasca, A. M., Sloan, S. A., Clarke, L. E., Tian, Y., Makinson, C. D., Huber, N., . . . Pasca, S. P. (2015). Functional cortical neurons and astrocytes from human pluripotent stem cells in 3D culture. *Nat Methods, 12*(7), 671-678. doi:10.1038/nmeth.3415

Patel, S. P., Sullivan, P. G., Lyttle, T. S., & Rabchevsky, A. G. (2010). Acetyl-L-carnitine ameliorates mitochondrial dysfunction following contusion spinal cord injury. *J Neurochem, 114*(1), 291-301. doi:10.1111/j.1471-4159.2010.06764.x

Paz, J. T., & Huguenard, J. R. (2015). Microcircuits and their interactions in epilepsy: is the focus out of focus? *Nature neuroscience, 18*(3), 351-359. doi:10.1038/nn.3950

Pino, A., Fumagalli, G., Bifari, F., & Decimo, I. (2017). New neurons in adult brain: distribution, molecular mechanisms and therapies. *Biochem Pharmacol, 141*, 4-22. doi:10.1016/j.bcp.2017.07.003

Quadrato, G., Nguyen, T., Macosko, E. Z., Sherwood, J. L., Min Yang, S., Berger, D. R., . . . Arlotta, P. (2017). Cell diversity and network dynamics in photosensitive human brain organoids. *Nature, 545*(7652), 48-53. doi:10.1038/nature22047

Racine, R. J. (1972). Modification of seizure activity by electrical stimulation. II. Motor seizure. *Electroencephalogr Clin Neurophysiol, 32*(3), 281-294. doi:10.1016/0013-4694(72)90177-0

Rao, M. S., Hattiangady, B., Rai, K. S., & Shetty, A. K. (2007). Strategies for promoting anti-seizure effects of hippocampal fetal cells grafted into the hippocampus of rats exhibiting chronic temporal lobe epilepsy. *Neurobiol Dis, 27*(2), 117-132. doi:10.1016/j.nbd.2007.03.016

Revah, O., Gore, F., Kelley, K. W., Andersen, J., Sakai, N., Chen, X., . . . Pașca, S. P. (2022). Maturation and circuit integration of transplanted human cortical organoids. *Nature, 610*(7931), 319-326. doi:10.1038/s41586-022-05277-w

Richtsmeier, J. T., & Flaherty, K. (2013). Hand in glove: brain and skull in development and dysmorphogenesis. *Acta Neuropathol, 125*(4), 469-489. doi:10.1007/s00401-013-1104-y

Rosenberg, S. S., & Spitzer, N. C. (2011). Calcium signaling in neuronal development. *Cold Spring Harb Perspect Biol, 3*(10), a004259. doi:10.1101/cshperspect.a004259

Saboori, P., & Sadegh, A. (2015). Histology and Morphology of the Brain Subarachnoid Trabeculae. *Anat Res Int, 2015*, 279814. doi:10.1155/2015/279814

Sakaguchi, H., Kadoshima, T., Soen, M., Narii, N., Ishida, Y., Ohgushi, M., . . . Sasai, Y. (2015). Generation of functional hippocampal neurons from self-organizing human embryonic stem cell-derived dorsomedial telencephalic tissue. *Nat Commun, 6*, 8896. doi:10.1038/ncomms9896

Sakthiswary, R., & Raymond, A. A. (2012). Stem cell therapy in neurodegenerative diseases: From principles to practice. *Neural Regen Res, 7*(23), 1822-1831. doi:10.3969/j.issn.1673-5374.2012.23.009

Sarkar, A., Mei, A., Paquola, A. C. M., Stern, S., Bardy, C., Klug, J. R., . . . Gage, F. H. (2018). Efficient Generation of CA3 Neurons from Human Pluripotent Stem Cells Enables Modeling of Hippocampal Connectivity In Vitro. *Cell Stem Cell, 22*(5), 684-697 e689. doi:10.1016/j.stem.2018.04.009

Scheffer, I. E., Berkovic, S., Capovilla, G., Connolly, M. B., French, J., Guilhoto, L., . . . Zuberi, S. M. (2017). ILAE classification of the epilepsies: Position paper of the ILAE Commission for Classification and Terminology. *Epilepsia, 58*(4), 512-521. doi:10.1111/epi.13709

Sciacca, S., Lynch, J., Davagnanam, I., & Barker, R. (2019). Midbrain, Pons, and Medulla: Anatomy and Syndromes. *Radiographics, 39*(4), 1110-1125. doi:10.1148/rg.2019180126

Scoville, W. B., & Milner, B. (1957). Loss of recent memory after bilateral hippocampal lesions. *J Neurol Neurosurg Psychiatry, 20*(1), 11-21. doi:10.1136/jnnp.20.1.11

Sharma, B., Lawrence, D. W., & Hutchison, M. G. (2018). Branched Chain Amino Acids (BCAAs) and Traumatic Brain Injury: A Systematic Review. *J Head Trauma Rehabil, 33*(1), 33-45. doi:10.1097/HTR.0000000000000280

Sharma, T. P., Wiley, L. A., Whitmore, S. S., Anfinson, K. R., Cranston, C. M., Oppedal, D. J., . . . Stone, E. M. (2017). Patient-specific induced pluripotent stem cells to evaluate the pathophysiology of TRNT1-associated Retinitis pigmentosa. *Stem Cell Res, 21*, 58-70. doi:10.1016/j.scr.2017.03.005

Shen, Q., Wang, Y., Kokovay, E., Lin, G., Chuang, S. M., Goderie, S. K., . . . Temple, S. (2008). Adult SVZ stem cells lie in a vascular niche: a quantitative analysis of niche cell-cell interactions. *Cell Stem Cell, 3*(3), 289-300. doi:10.1016/j.stem.2008.07.026

Shetty, A. K. (2011). Progress in cell grafting therapy for temporal lobe epilepsy. *Neurotherapeutics, 8*(4), 721-735. doi:10.1007/s13311-011-0064-y

Shetty, A. K., & Turner, D. A. (2000). Fetal hippocampal grafts containing CA3 cells restore host hippocampal glutamate decarboxylase-positive interneuron numbers in a rat model of temporal lobe epilepsy. *J Neurosci, 20*(23), 8788-8801. doi:10.1523/JNEUROSCI.20-23-08788.2000

Shetty, A. K., Zaman, V., & Turner, D. A. (2000). Pattern of long-distance projections from fetal hippocampal field CA3 and CA1 cell grafts in lesioned CA3 of adult hippocampus follows intrinsic character of respective donor cells. *Neuroscience, 99*(2), 243-255. doi:10.1016/s0306-4522(00)00178-0

Shi, Y., Sun, L., Wang, M., Liu, J., Zhong, S., Li, R., . . . Wang, X. (2020). Vascularized human cortical organoids (vOrganoids) model cortical development in vivo. *PLOS Biology, 18*(5), e3000705. doi:10.1371/journal.pbio.3000705

Shin, M. K., Bang, J. S., Lee, J. E., Tran, H. D., Park, G., Lee, D. R., & Jo, J. (2022). Generation of Skeletal Muscle Organoids from Human Pluripotent Stem Cells to Model Myogenesis and Muscle Regeneration. *Int J Mol Sci, 23*(9). doi:10.3390/ijms23095108

Silva, A., Pereira, J., Oliveira, C. R., Relvas, J. B., & Rego, A. C. (2009). BDNF and extracellular matrix regulate differentiation of mice neurosphere-derived cells into a GABAergic neuronal phenotype. *Journal of neuroscience research, 87*(9), 1986-1996. doi:10.1002/jnr.22041

Silva, T. P., Cotovio, J. P., Bekman, E., Carmo-Fonseca, M., Cabral, J. M. S., & Fernandes, T. G. (2019). Design Principles for Pluripotent Stem Cell-Derived Organoid Engineering. *Stem Cells Int, 2019*, 4508470. doi:10.1155/2019/4508470

Solstad, T., Boccara, C. N., Kropff, E., Moser, M. B., & Moser, E. I. (2008). Representation of geometric borders in the entorhinal cortex. *Science, 322*(5909), 1865-1868. doi:10.1126/science.1166466

Soudry, Y., Lemogne, C., Malinvaud, D., Consoli, S. M., & Bonfils, P. (2011). Olfactory system and emotion: common substrates. *Eur Ann Otorhinolaryngol Head Neck Dis, 128*(1), 18-23. doi:10.1016/j.anorl.2010.09.007

Stanfield, B. B., & Cowan, W. M. (1979). The development of the hippocampus and dentate gyrus in normal and reeler mice. *J Comp Neurol, 185*(3), 423-459. doi:10.1002/cne.901850303

Subramanian, L., & Tole, S. (2009). Mechanisms underlying the specification, positional regulation, and function of the cortical hem. *Cereb Cortex, 19 Suppl 1*, i90-95. doi:10.1093/cercor/bhp031

Sweeney, M. D., Zhao, Z., Montagne, A., Nelson, A. R., & Zlokovic, B. V. (2019). Blood-Brain Barrier: From Physiology to Disease and Back. *Physiol Rev, 99*(1), 21-78. doi:10.1152/physrev.00050.2017

Tabata, H., & Nakajima, K. (2003). Multipolar migration: the third mode of radial neuronal migration in the developing cerebral cortex. *J Neurosci, 23*(31), 9996-10001. Retrieved from https://www.ncbi.nlm.nih.gov/pubmed/14602813

Tamanna, N., & Mahmood, N. (2014). Emerging Roles of Branched-Chain Amino Acid Supplementation in Human Diseases. *Int Sch Res Notices, 2014*, 235619. doi:10.1155/2014/235619

Thom, M. (2014). Review: Hippocampal sclerosis in epilepsy: a neuropathology review. *Neuropathol Appl Neurobiol, 40*(5), 520-543. doi:10.1111/nan.12150

Tole, S., Christian, C., & Grove, E. A. (1997). Early specification and autonomous development of cortical fields in the mouse hippocampus. *Development, 124*(24), 4959-4970. doi:10.1242/dev.124.24.4959

Trinka, E., Cock, H., Hesdorffer, D., Rossetti, A. O., Scheffer, I. E., Shinnar, S., . . . Lowenstein, D. H. (2015). A definition and classification of status epilepticus--Report of the ILAE Task Force on Classification of Status Epilepticus. *Epilepsia, 56*(10), 1515-1523. doi:10.1111/epi.13121

Turner, D. A., & Shetty, A. K. (2003). Clinical prospects for neural grafting therapy for hippocampal lesions and epilepsy. *Neurosurgery, 52*(3), 632-644; discussion 641-634. doi:10.1227/01.neu.0000047825.91205.e6

Turski, W. A., Cavalheiro, E. A., Schwarz, M., Czuczwar, S. J., Kleinrok, Z., & Turski, L. (1983). Limbic seizures produced by pilocarpine in rats: behavioural, electroencephalographic and neuropathological study. *Behav Brain Res, 9*(3), 315-335. doi:10.1016/0166-4328(83)90136-5

Ubink, I., Bolhaqueiro, A. C. F., Elias, S. G., Raats, D. A. E., Constantinides, A., Peters, N. A., . . . Kranenburg, O. (2019). Organoids from colorectal peritoneal metastases as a platform for improving hyperthermic intraperitoneal chemotherapy. *Br J Surg, 106*(10), 1404-1414. doi:10.1002/bjs.11206

Upadhya, D., Attaluri, S., Liu, Y., Hattiangady, B., Castro, O. W., Shuai, B., . . . Shetty, A. K. (2022). Grafted hPSC-derived GABA-ergic interneurons regulate seizures and specific cognitive function in temporal lobe epilepsy. *npj Regenerative Medicine, 7*(1), 38. doi:10.1038/s41536-022-00234-7

Upadhya, D., Hattiangady, B., Castro, O. W., Shuai, B., Kodali, M., Attaluri, S., . . . Shetty, A. K. (2019). Human induced pluripotent stem cell-derived MGE cell grafting after status epilepticus attenuates chronic epilepsy and comorbidities via synaptic integration. *Proceedings of the National Academy of Sciences, 116*(1), 287-296. doi:doi:10.1073/pnas.1814185115

Waldau, B., Hattiangady, B., Kuruba, R., & Shetty, A. K. (2010). Medial Ganglionic Eminence-Derived Neural Stem Cell Grafts Ease Spontaneous Seizures and Restore GDNF Expression in a Rat Model of Chronic Temporal Lobe Epilepsy. *Stem Cells, 28*(7), 1153-1164. doi:https://doi.org/10.1002/stem.446

Wang, P., Mokhtari, R., Pedrosa, E., Kirschenbaum, M., Bayrak, C., Zheng, D., & Lachman, H. M. (2017). CRISPR/Cas9-mediated heterozygous knockout of the autism gene CHD8 and characterization of its transcriptional networks in cerebral organoids derived from iPS cells. *Mol Autism, 8*, 11. doi:10.1186/s13229-017-0124-1

Wang, S. N., Wang, Z., Xu, T. Y., Cheng, M. H., Li, W. L., & Miao, C. Y. (2020). Cerebral Organoids Repair Ischemic Stroke Brain Injury. *Transl Stroke Res, 11*(5), 983-1000. doi:10.1007/s12975-019-00773-0

Wang, Z., Wang, S.-N., Xu, T.-Y., Hong, C., Cheng, M.-H., Zhu, P.-X., . . . Miao, C.-Y. (2020). Cerebral organoids transplantation improves neurological motor function in rat brain injury. *CNS neuroscience & therapeutics, 26*(7), 682-697. doi:10.1111/cns.13286

Wang, Z., Wang, S. N., Xu, T. Y., Miao, Z. W., Su, D. F., & Miao, C. Y. (2017). Organoid technology for brain and therapeutics research. *CNS Neurosci Ther, 23*(10), 771-778. doi:10.1111/cns.12754

Wheeler, D. W., White, C. M., Rees, C. L., Komendantov, A. O., Hamilton, D. J., & Ascoli, G. A. (2015). Hippocampome.org: a knowledge base of neuron types in the rodent hippocampus. *Elife, 4*. doi:10.7554/eLife.09960

Williamson, P. D., French, J. A., Thadani, V. M., Kim, J. H., Novelly, R. A., Spencer, S. S., . . . Mattson, R. H. (1993). Characteristics of medial temporal lobe epilepsy: II. Interictal and ictal scalp electroencephalography, neuropsychological testing, neuroimaging, surgical results, and pathology. *Ann Neurol, 34*(6), 781-787. doi:10.1002/ana.410340605

Wisden, W., & Seeburg, P. H. (1993). A complex mosaic of high-affinity kainate receptors in rat brain. *J Neurosci, 13*(8), 3582-3598. Retrieved from https://www.ncbi.nlm.nih.gov/pubmed/8393486

Ye, F., Kang, E., Yu, C., Qian, X., Jacob, F., Yu, C., . . . Zhang, M. (2017). DISC1 Regulates Neurogenesis via Modulating Kinetochore Attachment of Ndel1/Nde1 during Mitosis. *Neuron, 96*(5), 1204. doi:10.1016/j.neuron.2017.11.034

Yoshinaga, Y., Kagawa, T., Shimizu, T., Inoue, T., Takada, S., Kuratsu, J., & Taga, T. (2010). Wnt3a promotes hippocampal neurogenesis by shortening cell cycle duration of neural progenitor cells. *Cell Mol Neurobiol, 30*(7), 1049-1058. doi:10.1007/s10571-010-9536-6

Yu, D. X., Di Giorgio, F. P., Yao, J., Marchetto, M. C., Brennand, K., Wright, R., . . . Gage, F. H. (2014). Modeling hippocampal neurogenesis using human pluripotent stem cells. *Stem Cell Reports, 2*(3), 295-310. doi:10.1016/j.stemcr.2014.01.009

Zhang, Y., & Bhavnani, B. R. (2006). Glutamate-induced apoptosis in neuronal cells is mediated via caspase-dependent and independent mechanisms involving calpain and caspase-3 proteases as well as apoptosis inducing factor (AIF) and this process is inhibited by equine estrogens. *BMC neuroscience, 7*, 49-49. doi:10.1186/1471-2202-7-49

Zhang, Y., Chen, K., Sloan, S. A., Bennett, M. L., Scholze, A. R., O'Keeffe, S., . . . Wu, J. Q. (2014). An RNA-sequencing transcriptome and splicing database of glia, neurons, and vascular cells of the cerebral cortex. *J Neurosci, 34*(36), 11929-11947. doi:10.1523/JNEUROSCI.1860-14.2014

Zhao, Y., Wang, M., Liang, F., & Li, J. (2021). Recent strategies for enhancing the therapeutic efficacy of stem cells in wound healing. *Stem Cell Research & Therapy, 12*(1), 588. doi:10.1186/s13287-021-02657-3

Zhou, T., Tan, L., Cederquist, G. Y., Fan, Y., Hartley, B. J., Mukherjee, S., . . . Chen, S. (2017). High-Content Screening in hPSC-Neural Progenitors Identifies Drug Candidates that Inhibit Zika Virus Infection in Fetal-like Organoids and Adult Brain. *Cell Stem Cell, 21*(2), 274-283.e275. doi:10.1016/j.stem.2017.06.017